Abstracts

The 27th Hiroshima International Symposium on Synchrotron Radiation

Materials Science using VUV-SX Synchrotron Radiation : Towards the future HiSOR-II project

March 9- 10, 2023

Faculty Club, Hiroshima University

Hiroshima Synchrotron Radiation Center, Hiroshima University

Supported by

The Japanese Society for Synchrotron Radiation Research

Particle Accelerator Society of Japan

The 27th Hiroshima International Symposium

on Synchrotron Radiation

Materials Science using VUV-SX Synchrotron Radiation : Towards the future HiSOR-II project

March 9 – 10, 2023
Hiroshima University Faculty Club

March 9 (Thursday)

08:45 – 09:30	Arrival and Registration
	Opening Chairperson: S. Ideta
09:30 – 09:35	Greeting Shuhei HAYASHI (Deputy Director, Research Environment Division, Science and Technology Policy Bureau, Ministry of Education, Culture, Sports, Science and Technology (MEXT))
09:30 – 09:35	Greeting Shinji KANEKO (Executive Vice President(Global Initiatives), Executive Vice President (Research and Academia-Government-Community Collaboration), Hiroshima University, Japan)
09:40 – 10:10	Overview of HiSOR Activities and Future Plan Kenya Shimada *Director, Synchrotron Radiation Center, Hiroshima University, Japan*
10:10 – 10:30	Symposium Photo
10:30 – 10:45	Coffee break
	Oral Session 1 Chairperson: H. Sato
10:45 – 11:20	O 01 Teppei YOSHIDA *Kyoto University, Japan* "Electron-phonon coupling in correlated electron systems revealed by angle-resolved photoemission spectroscopy"

11:20 – 11:55 O 02 Yuita FUJISAWA

Okinawa Institute of Science and Technology Graduate University, Japan

"Laboratory-based in-situ photoemission spectroscopies of quantum material epitaxial films"

11:55 – 12:30 O 03 Meng WANG

RIKEN, Japan

"XAS study of spin-state related percolative dynamics in magnetic cobaltites"

12:30 – 13:40 Lunch

Poster Session

Chairperson: M. Sawada

13:40 – 14:40 Student Short Oral Session (1-2 min/each)

14:40 – 16:30

※Best Student Poster Award※

We will present the Best Student Poster Award. The winner will be announced during the welcome reception.

Oral Session 2

Chairperson: K. Matsuo and M. Ibrahim

16:30 – 17:05 O04 Martin ANDERSSON

Chalmers University of Technology, Sweden

"Engineering the Biology-Material Interface for Safer Medical Devices"

17:05 – 17:40 O 05 Marie-Christine AVERLANT-PETIT

LCPM, Lorraine University, France

"Self-Assembling of Peptide-Based Gels : A Multiscale Structural Analysis"

Chairperson: H. Namatame

18:00 – 20:00 Welcome Reception

LA Bohème(Faculty Club)

March 11 (Friday)

Oral Session 3 HiSOR-II Special Session
Chairperson: K. Miyamoto

09:30 – 09:45 O 06 Masahiro KATOH
Hiroshima University, Japan
"Design of HiSOR-II"

09:45 – 10:20 O 07 Akira MOCHIHASHI
The Karlsruhe Institute of Technology, Garmany
"KIT – Status of Test Facilities KARA and FLUTE"

10:20 – 10:55 O 08 Shan QIAO
Shanghai Institute of Microsystem and Information Technology, China
"The progress of spin-resolved photoelectron spectroscopy in Shanghai"

10:55 – 11:30 O 09 Dongang ZHANG
Shanghai Jiao Tong University, China
"THz-enhanced ultrafast electron diffraction"

11:30 – 13:00 Lunch

Oral Session 4 HiSOR-II Special Session
Chairperson: M. Katoh

13:00 – 13:35 O 10 Hirofumi YANAGISAWA
University of Tokyo, Japan
"Subnanometric optical control of electron emission sites"

13:35 – 14:10 O 11 Takayuki ICHIKAWA
Hiroshima University, Japan
"Material Science toward achieving Carbon Neutrality"

Closing
Chairperson: Ideta

14:10 – 14:25 Student Award Ceremony
14:25 – 14:30 Closing Remarks
15:00 – 15:30 HiSOR Tour (English)
15:30 – 16:00 HiSOR Tour (Japanese)

Oral Session

-Oral Session-

O01 Electron-phonon coupling in correlated electron systems revealed by angle-resolved photoemission spectroscopy

Teppei YOSHIDA

Graduate School of Human and Environmental Studies, Kyoto University, Japan

O02 Laboratory-based in-situ photoemission spectroscopies of quantum material epitaxial films

Yuita FUJISAWA, Anjana Krishnadas and Yoshinori Okada

Quantum Material Science Unit, Okinawa Institute of Science and Technology, Japan

O03 XAS study of spin-state related percolative dynamics in magnetic cobaltites

Meng WANG

RIKEN Center for Emergent Matter Science (CEMS), Japan

O04 Engineering the Biology-Material Interface for Safer Medical Devices

Martin ANDERSSON

Dept. Chemistry and Chemical Engineering, Applied Chemistry, Chalmers University of Technology, Sweden

O05 Self-Assembling of Peptide-Based Gels : A Multiscale Structural Analysis

Loïc Stefan[a], Guillaume Pickaert[a], Mohamed Ibrahim[b] and Marie-Christine Averlant-Petit[a]

[a]Laboratoire de Chimie Physique Macromoléculaire (LCPM), Université de Lorraine, France.
[b]Hiroshima Synchrotron Radiation Center (HiSOR), Hiroshima University, Japan.

O06 Design of HiSOR-II

Masahiro Katoh[a,b]

[a]Hiroshima University, Japan
[b]Institute for Molecular Science, National Institutes of Natural Sciences, Japan

O07 KIT – Status of Test Facilities KARA and FLUTE

Akira MOCHIHASHI

Karlsruhe Institute of Technology (KIT), Institute for Beam Physics and Technology (IBPT), Germany

O08 The progress of spin-resolved photoelectron spectroscopy in Shanghai

Shan QIAO

Shanghai Institute of Microsystem and Information Technology, China

O09 THz-enhanced ultrafast electron diffraction

Dongang ZHANG

School of Physics and Astronomy, Shanghai Jiao Tong University, China

O10 Subnanometric optical control of electron emission sites

Hirofumi YANAGISAWA[a-d]

[a]*Japan Science and Technology Agency, Japan*
[b]*The University of Tokyo, Japan*
[c]*Ludwig-Maximilians-Universität Munich, Germany*
[d]*Max Planck Institute of Quantum Optics, Germany*

O11 Material Science toward achieving Carbon Neutrality

Takayuki ICHIKAWA

Graduate School of Advanced Science and Engineering, Hiroshima University, Japan

Electron-phonon coupling in the correlated electron systems revealed by angle-resolved photoemission spectroscopy

Teppei Yoshida

Graduate School of Human and Environmental Studies, Kyoto University, Kyoto 606-8501, Japan

Electron-phonon coupling is one of the fundamental many-body interactions and has been discussed as the key to the enhancement of the superconducting temperature T_c in a wide variety of materials such as A-15 compounds, high-T_c cuprates, iron pnictides/chalcogenides, and hydrogen sulfide. The signature of electron-phonon interactions appears in the kink and spectral linewidth of the quasiparticle dispersion and can be investigated by angle-resolved photoemission spectroscopy.

Here we present the signature of electron-phonon coupling observed in the electronic states of $Ca_{2-x}Sr_xRuO_4$ (CSRO) [1] and $BaIr_2Ge_7$ [2]. CSRO shows a metal-insulator transition with a structural phase transition. In the region of small x, the bulk of CSRO is in the insulating phase at low temperatures. We have performed angle-resolved photoemission spectroscopy (ARPES) of CSRO (x = 0.06) and revealed that the surface is in a metallic state while the bulk is in an insulating state. The observed band dispersion of the surface metallic state exhibits kink structures with the energy scales of 35 and 60 meV. The distinct kink structures suggest a strong electron–phonon coupling compared with Sr_2RuO_4.

We also performed ARPES on $BaIr_2Ge_7$ with cage structures and observed the temperature dependence of the ARPES spectra near the Fermi level. We found that the width of the spectral peak shows a concave-downward behavior with temperature similar to the electrical resistivity. Considering the effect of anharmonic phonon modes, this behavior was well reproduced in our simulations. Our results suggest the existence of the weak anharmonic phonon modes in $BaIr_2Ge_7$.

REFERENCES

1. D. Ootsuki, A. Hishikawa, T. Ishida, D. Shibata,Y. Takasuka, M. Kitamura, K. Horiba, Y. Takagi, A. Yasui, C. Sow, S. Yonezawa, Y. Maeno, and T. Yoshida, J. Phys. Soc. Jpn. **91**, 114704 (2022).
2. T. Ishida, D. Ootsuki, S. Ishida, M. Kitamura, K. Horiba, Y. Takagi, A. Yasui, E. Ikenaga, K. Kawashima, Y. Yanagi, A. Iyo, H. Eisaki, and T. Yoshida, Phys. Rev. B **107**, 045116 (2023).

Laboratory-based *in-situ* photoemission spectroscopy of quantum material epitaxial films

Yuita Fujisawa, Anjana Krishnadas, & Yoshinori Okada

Quantum Material Science Unit, Okinawa Institute of Science and Technology, 1919-1 Tancha, Onna, Kunigami-gun, Okinawa, 904-0495, Japan

Epitaxial film technology allows us to design and control the physical properties of quantum materials beyond the bulk properties. It also makes it possible to investigate materials that have been difficult to synthesize their bulk single crystals by such as angle-resolved photoemission spectroscopy (ARPES). To reveal the electronic states of exotic quantum material epitaxial films, we have constructed a so-called vacuum cluster system where a pulsed laser deposition (PLD) system and an APRES system are connected under ultra-high-vacuum (see **Figure 1a**)[1,2]. In this talk, I'd like to introduce one of the recent studies on an oxide superconductor, $LiTi_2O_4$ (LTO).

LTO is a unique spinel oxide with a high superconducting transition temperature of 13 K (see **Figure 1b**). While it is expected to have intimate relation between superconductivity and orbital degree of freedom, less is understood about this material because large size single crystal has not been available. Recently, epitaxial film growth using PLD has been reported [3]. However, direct observation of the electronic structure by APRES has not been accomplished.

This work presents the first observation of the band structure of LTO (111) thin films grown by PLD. The hexagonal Fermi surface with corners on the Brillouin zone corner implies that a saddle point exists near the Fermi energy (E_F). The band dispersion shows a distinct kink structure at 50 meV below E_F, suggesting the enhanced many-body effects. Its temperature dependence reveals a phase transition around 150 K accompanied by the disappearance of the kink. We will discuss the origin in detail.

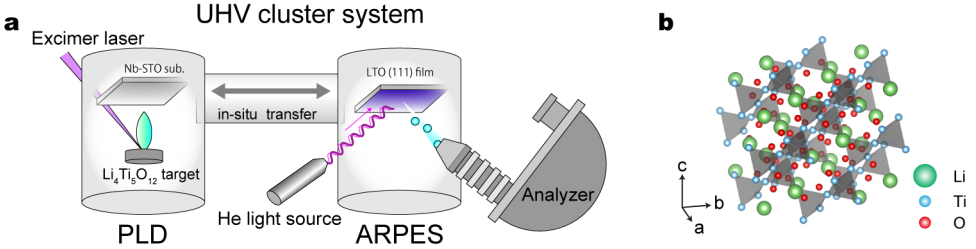

FIGURE 1. (a) Schematics of our UHV cluster system connecting the PLD and the ARPES systems under ultra-high vacuum. (b) Crystal structure of the spinel oxide superconductor $LiTi_2O_4$.

REFERENCES

1. Y. Fujisawa *et al.,* Adv. Mat. **2207121**, 1-11 (2023).
2. T. Kawamoto *et al.,* Phys. Rev. Mat. **7**, 024001 (2023).
3. Y. Okada *et al.,* Nat. Commun. **8**, 15975 (2017).

XAS study of spin-state related percolative dynamics in magnetic cobaltites

Meng Wang [a]

[a]*RIKEN Center for Emergent Matter Science (CEMS), Wako 351-0198, Japan*

Mixed-valent cobaltite is a double-exchange ferromagnetic system, as analogous to the double-exchange manganite. However, the colossal magnetoresistance (CMR) associated with a magnetic-field-driven insulator-metal transition (IMT) at the phase boundary has not yet been reported in cobaltite. Combining magnetic transport, magnetization, magnetic-force-microscopy (MFM), and X-ray absorption spectroscopy (XAS) measurements, we conducted a systematic research on the $La_{0.7}AE_{0.3}CoO_3$ (AE = Ca, Sr, and Ba) films and unveiled the hidden mechanisms that dominate the phase transition dynamics in cobaltite. First, in contrast to utilizing the bulk crystal, we fabricated films on a $SrTiO_3$ substrate with tensile strain to drive it to the insulator-metal phase boundary. All films exhibit a ferromagnetic and non-ferromagnetic phase separation, which is robust against an isothermal magnetic field sweeping, while a percolation induced insulator-to-metal transition can be achieved by a field-cooling process. Such a thermodynamic-history-dependent properties signify a nonergodic feature associated with the dynamics of magnetic domains. By further comparing the nonergodic properties and the spin-sates among $La_{0.7}AE_{0.3}CoO_3$ films by the transport and XAS measurements, respectively, we reveal that the mixed low-spin Co^{3+} forms a key factor to enhance the energy barrier for domain-wall motions during domain percolation. Such a spin-state degree of freedom is absent in manganites, probably resulting in the large difference of the phase evolution kinetics in the magnetic-field-induced IMT between cobaltite and manganite. [1]

REFERENCES

1. M. Wang,† K. Matsuura, M. Nakamura, M. Sawada, M. Kawasaki, and F. Kagawa, “Magnetic field control of insulator-metal crossover in cobaltite films via thermally activated percolation”. *Phy. Rev. B* **106**, 155135 (2022).

Engineering the Biology-Material Interface for Safer Medical Devices

Martin Andersson

Dept. Chemistry and Chemical Engineering, Applied Chemistry, Chalmers University of Technology
SE-412 96 Gothenburg, Sweden

In this presentation, two different concepts of engineering the interface between artificial materials and biology will be demonstrated. The first example is an attempt to form synthetic bone materials, intended for use in medical devices as well as a model system to study bone mineralization, to shed light on *in vivo* bone formation mechanisms. In the second example, controlled surface topography and its impact on protein interaction with surfaces is in focus. Specifically, topographical alterations on similar length scale as proteins has shown to largely affect the interactions, giving us a tool to regulate how foreign materials are integrated with living tissue. This is for example of great interest in the development of medical devices, such as implants, and how they are accepted in the human body.

A novel synthetic approach, highly inspired by the architecture of natural bone, to design mechanically stable nanocomposites incorporating aligned apatite nanocrystals will be demonstrated.[1] To mimic the nanostructure of natural bone, we first combine molecular self-assembly and intermolecular crosslinking to create resilient polymeric matrices with long-range periodicity; then we employ compartmentalized mineral growth via a transient amorphous phase for the biomimetic formation of bone-like apatite. The nano-domains and their alignment has been investigated using 3D small angle X-ray scattering (3D-SAXS)[2] and the crystallization process has been studied using transmission electron microscopy (TEM).[3]

By using silica nanoparticles of various sizes immobilized onto surfaces, the nanotopographical effect on the classical immune complement activation through adsorption of IgG and the following binding of C1q, was examined.[4] In another example, using silica nanoparticles deposited as a gradient in nanostructure density on a surface, the initial attachment of bacteria with or without the presence of human fibrinogen was examined.[5] By using a parallel plate laminar flow chamber, we found a near-linear positive correlation between the adhesion of S. epidermidis with increasing nanoparticle density. However, if the nanostructured gradient was precoated with human fibrinogen the opposite relationship was observed, although the adsorbed amount of fibrinogen was found to be higher on nanostructured than on smooth surfaces. This latter observation correlated well with protein conformation studies using circular dichroism (CD), where the nanostructured surfaces preserved the protein secondary structure, similar to in solution, as compared to the smooth surfaces.

REFERENCES

1. AK Rajasekharan, R Bordes, C Sandström, M Ekh, M Andersson, Small 13 (28), 1700550
2. AK Rajasekharan, A Lotsari et al. Adv. healthcare Mater. 2018 7 (18), 18004663.
3. A Lotsari, AK Rajasekharan, M Halvarsson, M Andersson Nature Comm. 2018, 9 (1), 4170
4. Emma Westas Janco, Mats Hulander, Martin Andersson Acta Biomaterialia, 2018, 74, 112-120
5. M. Hulander, H. Valen-Rukke, G. Sundell, M. Andersson, ACS Biomater. Sci. Eng. 2019, 9, 4323

Self-Assembling of Peptide-Based Gels: A Multiscale Structural Analysis

Loïc Stefan[a], Guillaume Pickaert[a], Mohamed Ibrahim[b] and Marie-Christine Averlant-Petit[a]

[a]*Laboratoire de Chimie Physique Macromoléculaire (LCPM), Université de Lorraine, France.*
[b]*Hiroshima Synchrotron Radiation Center (HiSOR), Hiroshima University, Japan.*

Supramolecular hydrogels have drawn much attention in the past years especially because of their broad range of applications from material science to medical science domains. Peptide-based gels have been developed lately [1, 2], mainly thanks to their higher modularity and possibilities of functionalization compared to polymer gels [3, 4]. Mechanisms of forming peptides hydrogels are starting to be examined: first is the gelation of nanofibrous peptides assemblies and is observed predominantly with oligopeptide precursors. Gel formation in such systems involves supramolecular assembly of precursors into nanofibers, -tapes, -tubes, or -ribbons that entangle and form nonspecific.

The capability of peptides and proteins to form gels is long time known, as gelatine used in cooking. But the development of gel materials was mostly built on serendipity. Moreover, only a few publications are found on relationships between the mechanical properties of the gel materials and their self-assembling [5-7], although the mechanical properties are very important for the applications. As a mesh has a different appearance depending on whether the knitting is tight or loose, there is a correlation between morphology and number of fibrils and mechanical properties of the obtained material. But so far, no rules were found that can predict which peptide sequence, or peptide modification leads to self-assembling in a gel and what kind of soft material it will give. This observation is the starting point of our project.

The assumption is the following: the self-assembling process and the interactions involved in the first stages has an impact on the size, morphology, number of fibrils and, subsequently, on the material properties. study the interactions from the inter-molecular level to supra-molecular, meso-level, and macroscopic properties, to investigate the relationships between self-assembling of the peptide-based molecules and the resulting mechanical properties of gels. In the Laboratoire de Chimie Physique Macromoléculaire, we associate synthesis of gelling molecules, physical chemistry analysis, structural and 3D conformational modelling studies, imaging, and rheology experiments to evaluate correlation between the structural and self-assembling to mechanical properties of the resulting soft material.

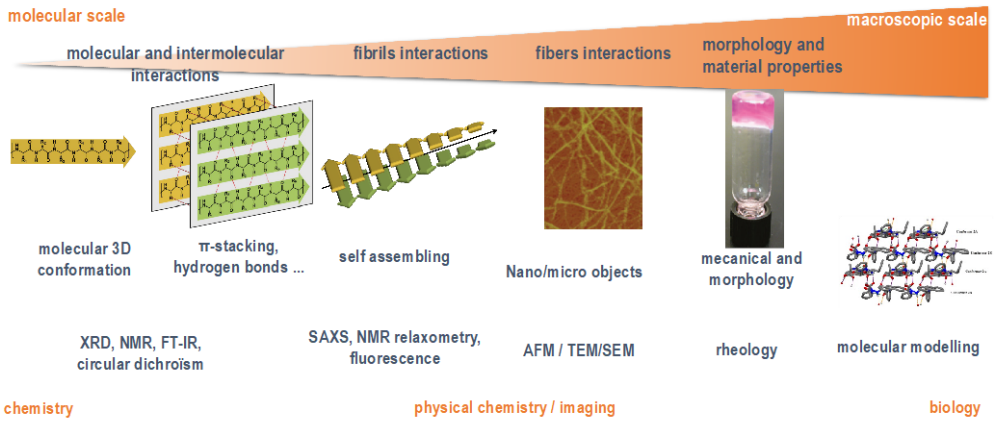

FIGURE 1. Multiscale structural analysis of self-assembling peptide-based gels.

To that end, a multiscale approach has been undertaken from molecular scale to macroscopic scale the interactions involved in the materials (Figure 1) to decipher their influence on the soft material formation and guide chemists to the next generation of gelling molecules.

REFERENCES

[1] M. Piatkowski, *et al. eXPRESS Polymer Letters,* 12, 2018: 100.
[2] M. Sánchez, *et al*. *Frontiers in Bioengineering and Biotechnology,* 8, 2020: 776.
[3] S. Mondal, *et al*. *Soft matter,* 16(6), 2020: 1404.
[4] D. Farahani, *et al. ChemPhysChem,* 20, 2019: 972.
[5] T. Giraud, *et al*. *Nanoscale* 12, 2020: 19905.
[6] X. Wang, *et al*. *Polymers,* 9, 2017: 401.
[7] H. Awada, *et al.* Journal of Organic Chemistry, 82, 2017: 4819.

Design of HiSOR-2

Masahiro Katoh[a,b]

[a]*Hiroshima University,1-3-1 Kagamiyama, Higashi-Hiroshima 739-8526, Japan*
[b]*Institute for Molecular Science, National Institutes of Natural Sciences, 38 Nishigo-Naka, Myodaiji, Okazaki, 444-8585, Japan*

Keywords: Synchrotron light source, electron storage ring.

HiSOR, a low energy and compact synchrotron light source in Hiroshima University, has been operational since the middle of 1990's. It equipped with two undulators which produce high-brightness light in the vacuum ultraviolet range. It has two normal conducting bending magnets with high field strength of 2.7 T, which produce synchrotron radiation in a wide range including tender X-rays even with the low electron energy, 700MeV. On the other hand, the emittance is 400 nm, which is larger by two orders of magnitudes than the 3rd generation sources and results in the low brightness. This large emittance is caused by the simple lattice structure which consists of two 180 degree bending magnets. To make the beam injection system simple and compact, the injection is made at the energy of 150 MeV. Consequently, the ring cannot be operated in the top-up mode, which has become a standard operation mode in modern light sources. Since the HiSOR electron storage ring has a rational design without redundancy, it is difficult to make a major modification to improve the performance or introduce new technologies. This is in contrast with other light sources in Japan, such as Photon Factory [1], UVSOR [2] and SPring-8 [3], which already made or is planning major upgrades.

For the future plan of HiSOR, we designed a completely new ring, HiSOR-2 [4]. The circumference is about 50 m, the electron energy 500 MeV and the emittance around 10nm. It has six straight sections and four of them can be used for undulators. The small emittance gives much higher brightness of undulator radiation by two orders of magnitudes than the present one. It would have a new full energy injector to realize the top-up operation, which consists of a linear accelerator and a booster synchrotron. Such a completely new facility is ideal for further developing the researches based on the high brightness undulator radiation in the vacuum ultraviolet range. However, we have to prepare responding flexibly to changes in the environment surrounding synchrotron radiation science in Japan. As leaving this plan as one candidate, we have started designing alternative plan, which is more compact and hopefully can be realized with less budget [5].

An example of the design is shown in Fig. 1. The circumference is about 30 m and the electron energy is 500 MeV. The emittance is 17 nm. The ring has six 2.2 m straight sections, four of which can be used for undulators. To realize such a simple lattice, we have to develop combined function multipole magnets. Another example has similar lattice structure as in Ref. [4] but is more compact with the circumference of about 40m and the emittance of about 10 nm. An example of the accelerator layout with this second design is shown in Fig. 2, which requires construction of a new building for the storage ring and experimental hall but the full-energy booster synchrotron would be constructed in the present injector room.

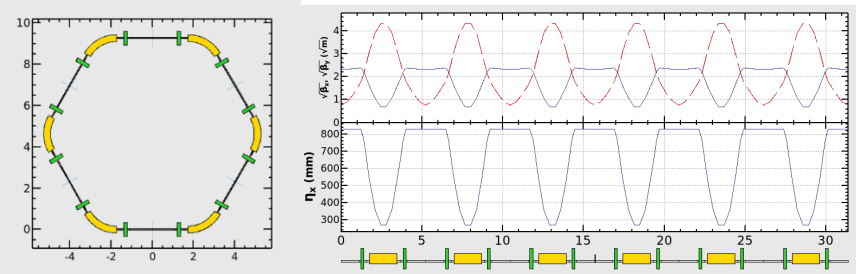

FIGURE 1. Magnetic lattice (left) and optical functions (right) of the new lattice design for HiSOR-2.

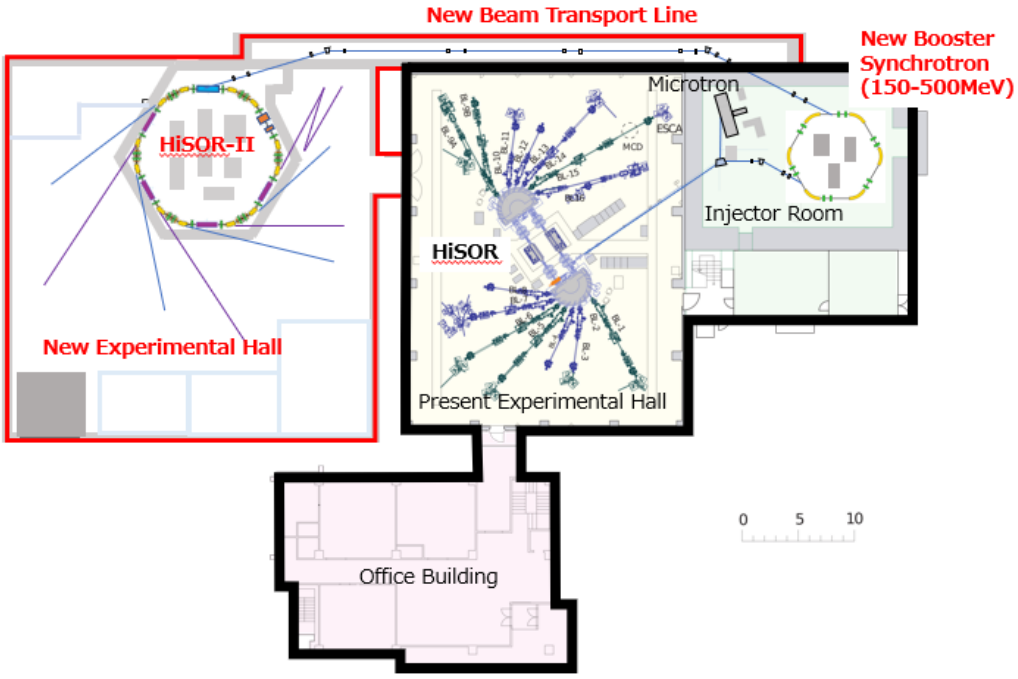

FIGURE 2. An example of the layout of the facility with a design of HiSOR-2 storage ring with 40 m circumference.

It should be noted that, in HiSOR-2, the bending magnets will be normal conducting and have ordinary field strengths such as around 1 T. In addition, the electron energy is lower than the present HiSOR. The bending radiation will not cover the X-ray range. This may strongly limit the application fields of new facility. The accelerator layout shown in Fig. 2 enables us to operate the present HiSOR even after the construction of HiSOR-2.

REFERENCES

1. M. Katoh *et al*., *J. SYNCHROTRON RAD.* 5(3) 366 - 368 (1998).
2. M. Katoh *et al*., *Nucl. Instr. Meth. A*. 467, 68 - 71 (2001).
3. http://rsc.riken.jp/pdf/SPring-8-II.pdf.
4. S. Matsuba *et al., J. Phys. Conf. Ser*. 1350 012015-1~5 (2019).
5. Y. Lu *et al*., in these proceedings

KIT – Status of Test Facilities KARA and FLUTE

Akira Mochihashi[a], on behalf of the accelerator team at KIT IBPT

[a] *Karlsruhe Institute of Technology (KIT), Institute for Beam Physics and Technology (IBPT), Hermann-von-Helmholtz-Platz 1, 76344 Eggenstein-Leopoldshafen, Germany*

In the Institute for Beam Physics and Technology (IBPT) [1] at the Karlsruhe Institute of Technology (KIT) in Germany, the accelerator complexes KARA and FLUTE are in operation as test facilities where various scientific activities for accelerator physics and technology take place now. The Karlsruhe Research Accelerator (KARA) is a high-energy electron storage ring, which provides electron beams with an energy range between 500 MeV to 2.5 GeV and a synchrotron radiation source, the KIT Light Source. The FLUTE (Ferninfrarot Linac- und Test- Experiment) facility serves as an accelerator test facility for various accelerator physics studies, whose core consists of a femtosecond chirped laser-driven RF photo injector, a linear accelerator, and an electron bunch compressor to provide ultra-short electron bunches for THz generation studies and non-linear physics investigations.

As test facilities, KARA and FLUTE and other research infrastructures within the Accelerator Technology Platform (ATP) [2] at KIT support the R&D of technologies for tomorrow's accelerators and detectors. Access to KIT-based accelerators via IBPT is augmented by European Transnational Access via several international projects such as EURO-LABS [3]. ATP provides a single point of contact (SPOC) and central access point for large-scale accelerator projects to the accelerators (KARA and FLUTE) and know-how located at KIT institutes.

IBPT provides an educational and hands-on environment for students and the next generation of accelerator scientists at KIT. Doctor and master candidates and bachelor students are currently engaged in research and development for the projects at KARA and FLUTE and other projects, where the latest frontiers of accelerator physics are promoted enthusiastically.

Following an introduction to KIT and IBPT, the presentation introduces the status of our accelerator complexes, KARA and FLUTE and current research topics and ongoing projects. The international projects associated with the activities are introduced in the context of the research topics at KARA and FLUTE. The educational environment and related outcoming products, such as theses and presentations at international conferences, are shown in the presentation.

REFERENCES

1. IBPT website: https://www.ibpt.kit.edu/index.php
2. ATP website: https://www.ibpt.kit.edu/atp.php
3. EURO-LABS website: https://www.ibpt.kit.edu/project_EURO_LABS.php

The Progress of Spin-Resolved Photoelectron Spectroscopy in Shanghai

Shan Qiao[a]

[a]*Shanghai Institute of microsystem and information techonology, Chinese Academy of Sciences 863 Changning Road, Shanghai, China*

Keywords: spin polarimeter, laser

The performances of two new image type VLEED spin polarimeters and 21 eV laser will be reported. The energy resolution of second version with permanent magnets and quadrupole lenses achieves 12 meV. The possibility to use 45 degree reflection for VLEED spin measurements was also checked and a higher efficiency was obtained at 3.5 eV. This type polarimeter with simple structure can achieve small aberration and have the ability to measure the three dimensional spin polarization. The construction of a time of flight spin polarimeter will also be reported.

Generating a laser with a short wavelength is a bottleneck problem in laser technology. The current applicable extreme ultraviolet (EUV) lasers generated by the multi-photon process, with low efficiency and the record short wavelength of 113.8 nm, do not meet some actual needs. we will report the development of a practical 58.4 nm laser by a single-photon-excitation related anti-Stokes Raman scattering (ASRS). The conversion efficiency is much higher than that of high harmonic generation (HHG). The almost same divergence of 1.9 mrad as that of excitation laser indicates its coherent and stimulating characters. Our results show an applicable path towards up-conversion by a single-photon process to generate intense EUV lasers.

The spin-resolved photoelectron measurements on some systems showing the ability of image type spin polarimeter will also be reported.

THz-enhanced ultrafast electron diffraction

Dongfang Zhang

School of Physics and Astronomy, Shanghai Jiao Tong University, Shanghai 200240, China

Ultrafast electron diffraction (UED) has gained tremendous interest in the ultrafast community in the last decades because of the ability to provide atomic-level material structure information on the femtosecond time scale. Terahertz laser-based accelerators are prominent candidates for driving next-generation compact light sources, promising high-brightness, ultrashort x-ray and electron pulses. Here, I will present on the development of key components in the development of THz based electron sources. Different THz based devices that are capable of performing multiple high-field operations on the 6D-phase-space of ultrashort electron bunches will be introduced, that includes electron acceleration, compression, focusing and streaking [1,2].

The first application with THz-powered electron source in ultrafast electron diffraction will be discussed [3]. In proof-of-principle experiments, we leverage high-field THz pulses to compress the electron bunches by 10x to ~180 fs. The high-quality diffraction patterns and enhanced temporal resolution are benchmarked using ultrafast structural dynamics measurements of silicon. We show that optimization of this technology may enable temporal resolution in the few-fs regime.

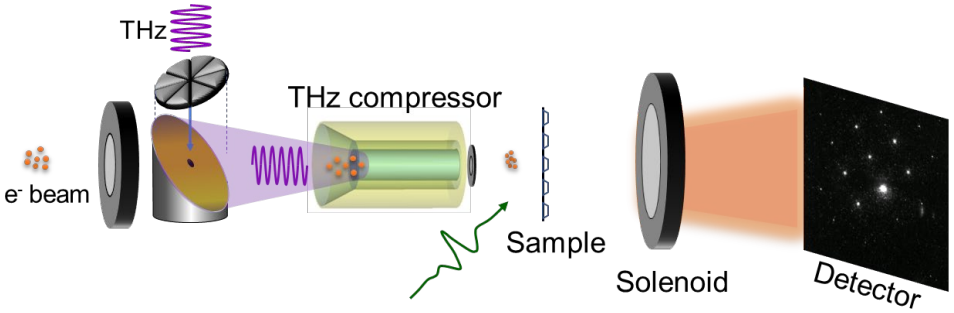

FIGURE 1. THz-enhanced UED setup. A small fraction of the 1030 nm infrared optical beam is converted to 257 nm based on two-stage second harmonic generation. The 257 nm UV pulse is directed onto a gold photocathode generating electron pulses, which are accelerated to 53 keV by the DC electric field. The same infrared laser also drives a multicycle THz generation stage, two single-cycle THz stages, and pump laser for the electron manipulator, the streaker, and sample excitation, respectively. The streaker and the sample are on the same manipulator which can be exchanged for checking the pulse duration at the sample position or performing the ultrafast electron diffraction experiment.

REFERENCES

1. D. Zhang, A. Fallahi, M. Hemmer, X. Wu, M. Fakhari, Y. Hua, H. Cankaya, A.-L. Calendron, L. E. Zapata, N. H. Matlis, and F. X. Kärtner, *Nature Photonics* 12, 336-342 (2018)
2. D. Zhang, M. Fakhari, H. Cankaya, A.-L. Calendron, N. H. Matlis, and F. X. Kärtner, *Physical Review X* 10, 011067 (2020)
3. D. Zhang, T. Kroh, F. Ritzkowsky, T. Rohwer, M. Fakhari, H. Cankaya, A.-L. Calendron, N. H. Matlis, and F. X. Kärtner, *Ultrafast Science* 2021, 1-7 (2021).

Subnanometric optical control of electron emission sites

Hirofumi Yanagisawa[a-d]

[a]*Japan Science and Technology Agency (JP-332-0012 Saitama, Japan)*
[b]*The University of Tokyo (JP-277-8581 Chiba, Japan)*
[c]*Ludwig-Maximilians-Universität Munich (D-85748 Garching, Germany)*
[d]*Max Planck Institute of Quantum Optics (D-85748 Garching, Germany)*

In this presentation, we will provide an overview of our recent development of the optical control of electron emission sites.

By irradiating a sharp metallic needle with femtosecond light pulses, optical fields can be concentrated on the needle's apex, and these localized optical fields then generate electron emissions from the apex [1], as shown schematically in Figure 1(a). Such electron emissions can be used as optically-controlled ultrafast switches that are three to six orders of magnitude faster than current switching devices in modern computers. Concurrent plasmonic effects can spatially control the electron emission at its source on a scale of a few tens of nanometers [2]. For example, one can select emission sites A or B, as shown in Figure 1(b). The optical control of emission sites yields a device equivalent to multiple switches integrated into a nano-object, whose corresponding electronic circuit is shown in the right panel of Figure 1(b). Further acceleration of such a switch would be possible with advances in laser technology. However, further miniaturization of such a spatially controllable electron source is fundamentally difficult via plasmonics, and a paradigm shift is required.

Here, we realized that paradigm shift by employing a recently identified single-molecule electron source that generates electron emissions from individual fullerene molecules deposited on a metallic needle [3], as shown schematically in Figure 2. By illuminating the molecules with light, we discovered that largely modulated emission patterns appeared from a single molecule, approximately one nanometer in size [4]. These are quantum-mechanical phenomena that use variations of molecular orbitals. This scenario is well supported by simulations using density functional theory, which also explains the physics of electron emission patterns from single molecules via DC electric fields—an intractable question for

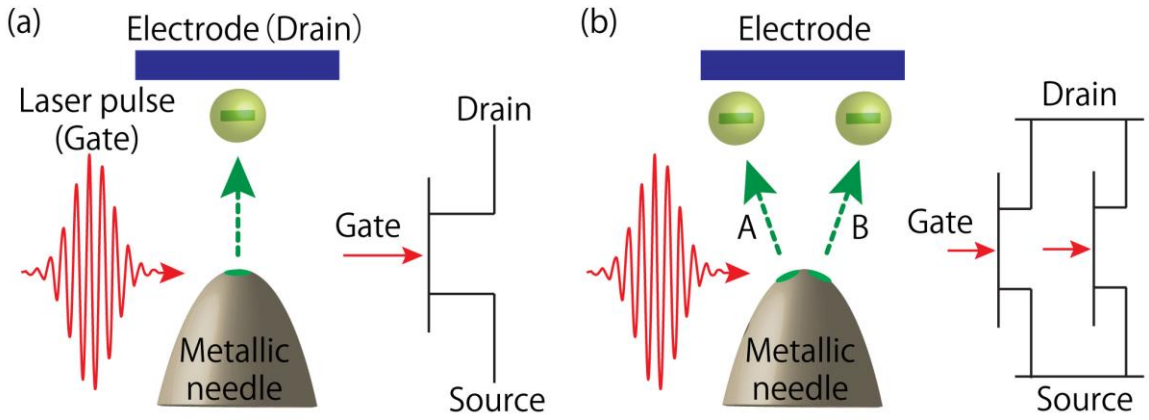

FIGURE 1. Conceptual diagram of how to induce ultrafast electron emission from a nano-object by irradiating a light pulse (a) and optical control of emission sites (b). Electronic circuits equivalent to these electron sources are drawn alongside the figures.

more than seven decades. In addition, we will further discuss optical controllability over emission sites at a single molecule. Our work will open the door to multiple ultrafast switches integrated into a single molecule.

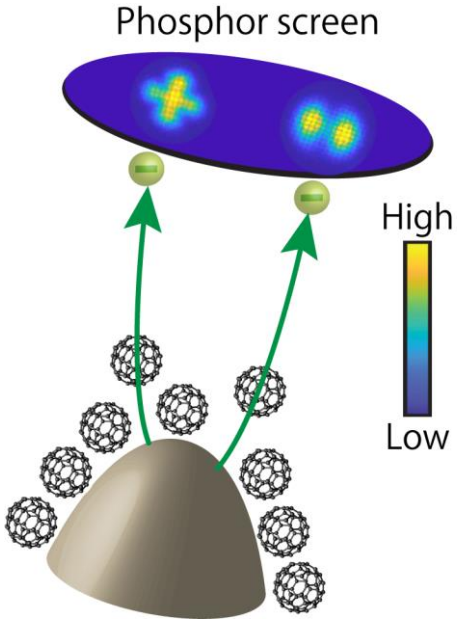

FIGURE 2. Schematic diagram of electron emissions from single fullerene molecules.

REFERENCES

1. P. Hommelhoff, Y. Sortais, A. Aghajani-Talesh, and M. A. Kasevich, Field Emission Tip as a Nanometer Source of Free Electron Femtosecond Pulses. *Phys. Rev. Lett.* **96**, 077401 (2006).
2. H. Yanagisawa, C. Hafner, P. Doná, M. Klöckner, D. Leuenberger, T. Greber, M. Hengsberger, and J. Osterwalder, Optical Control of Field-Emission Sites by Femtosecond Laser Pulses, *Phys. Rev. Lett.* **103**, 257603 (2009).
3. H. Yanagisawa, M. Bohn, F. Goschin, A. P. Seitsonen, and M. F. Kling, Field emission microscopy for a single fullerene molecule, Sci. Rep. **12**, 2174 (2022).
4. H. Yanagisawa, M. Bohn, H. Kitoh, Florian Goschin and M. Kling, Light-induced subnanometric modulation of a single-molecule electron source**,** Phys. Rev. Lett. (in press)

Material Science toward achieving Carbon Neutrality

Takayuki Ichikawa

Graduate School of Advanced Science and Engineering, Hiroshima University, 1-4-1 Kagamiyama Higashi-Hiroshima, 739-8527, Japan

Growing global energy demand and exhaustion of fossil fuels are gradually becoming a big concern for all the people on the Earth. Meanwhile, the deteriorating environmental pollution and global warming with the emergence of recent extreme weather make us re-recognize the importance of the usage of renewable resources with carbon-free emission and energy storage with high efficiency. A secondary battery to store the fluctuating renewable energy attracts a lot of attention and seems to fulfill the requirements of human beings. Since these battery technologies are only suitable for short-term energy storage daily or weekly due to their high cost, and cannot be used for leveling seasonal fluctuations. Due to economic requirement, it is important to establish hydrogen utilization technology as a countermeasure against long-term fluctuations in renewable energy. Therefore, in order to achieve carbon neutrality, it is impossible to avoid the development of high-performance secondary batteries and the establishment of a hydrogen-utilizing society.

Our group has so far focused on various kind of metal hydrides and focused on exploring their functions to solve the above problems. As an example, metal hydrides are considered to be a potential anode material for all-solid-state Li-ion batteries, because of its high theoretical Li storage capacity, relatively low volume expansion, and suitable working potential with very small polarization by the “hydride conversion reaction”. On the other hand, as characteristic properties related to hydrogen gas, not only for high capacity hydrogen storage but also for obtaining high pressure H_2, producing heat by control of H_2 pressure, and absorbing NH_3 with relatively low pressure, we focused on various kinds of hydrides related materials, such as MgH_2, TiFe intermetallic compound, TiH_2, and $LiBH_4$. And then, for high performance properties, “nano-composite techniques” played an important role. Of course, material modification to achieve required performance can only be accelerated by precise and accurate characterizations based on materials science.

The synthesis of hydrogen gas from renewable energies is also quite important technology to be developed with a reasonable cost (in Japan, target cost for hydrogen production is about 2 USD/kg). To achieve this economic requirement, thermochemical method to produce hydrogen is attracting a significant attention. The reaction cycles for water-splitting based on redox reactions of metallic phase of Na are focused in our group, which is composed of three reactions, that is hydrogen generation by solid-liquid reaction, metal separation by thermolysis, and oxygen generation by hydrolysis, where we are able to expect to have the effect of mass production. As is well known that sodium oxides, Na_2O and Na_2O_2 show highly reactive properties to any kind of metals and ceramics at high temperature conditions around 500 °C, it is quite difficult to control the target reaction, which lead to serious corrosion of the vessel materials. In this work, thermodynamic analyses are performed by using the parameters such as operating temperature and partial pressures of the products obtained by the experiments to determine that the Na metal redox cycle is potential hydrogen production technique as thermochemical energy storage. And some suitable way to control this promising reaction by minimizing the corrosion effect would be demonstrated.

Poster Session

-Poster Session-

The poster number with "S" is eligible for the Best Student Poster Award nomination.

P01 Realization of Practical Eightfold Fermions and Fourfold van Hove Singularity in $TaCo_2Te_2$

H. Rong[1*], Z. Huang[1,7*], X. Zhang[2,8*], S. Kumar[3*], F. Zhang[1], C. Zhang[1], Y. Wang[1], Z. Hao[1], Y. Cai[1], L. Wang[1], C. Liu[1], X. Ma[1], S. Guo[1], B. Shen[4], Y. Liu[5], S. Cui[5], K. Shimada[3], Q. Wu[6,10], J. Lin[1], Y. Yao[2,8], Z. Wang[2,8,9#], H. Xu[1#], C. Chen[1#]

1 Shenzhen Institute for Quantum Science and Engineering (SIQSE) and Department of Physics, Southern University of Science and Technology (SUSTech), China.
2 Centre for Quantum Physics, Key Laboratory of Advanced Optoelectronic Quantum Architecture and Measurement, School of Physics, Beijing Institute of Technology, China.
3 Hiroshima Synchrotron Radiation Centre, Hiroshima University, Higashi-Hiroshima, Japan.
4 School of Physics, Sun Yat-Sen University, China.
5 National Synchrotron Radiation Laboratory, University of Science and Technology of China, China.
6 Beijing National Laboratory for Condensed Matter Physics, and Institute of Physics, Chinese Academy of Sciences, China.
7 Department of Physics, The Hong Kong University of Science and Technology, Clear Water Bay, Hong Kong, China.
8 Beijing Key Lab of Nanophotonics and Ultrafifine Optoelectronic Systems, Beijing Institute of Technology, China.
9 Material Science Center, Yangtze Delta Region Academy of Beijing Institute of Technology, China.
10 University of Chinese Academy of Sciences, China.

P02S Evolution of Electronic States in Epitaxial YBCO Thin Films with Calcium Doping by Angle-Resolved Photoemission Spectroscopy

A. Krishnadas[1], Y. Fujisawa[1], M. Pardo-Almanza[1], K. Yamagami[1,2], Y. Obata[1], Y. Okada[1]

1 Quantum Materials Science Unit, Okinawa Institute of Science and Technology (OIST), Japan.
2 Japan Synchrotron Radiation Research Institute, Japan

P03S Symmetry reduction in the electronic structure of heavily overdoped Pb-Bi2201 detected by ARPES

Y. Miyai[1], T. Kurosawa[2], M. Oda[3], M. Arita[4], S. Ideta[4], K. Shimada[4]

1 Graduate School of Science, Hiroshima University, Japan
2 Fuculty of Science and Engineearing, Muroran Institute of Technology, Japan
3 Department of Physics, Hokkaido University, Japan
4 Hiroshima Synchrotron Radiation Center, Hiroshima University, Japan

P04 Recent upgrades and activities of HiSOR BL-1

S. Ideta[1,2], S. Kumar[1], Y. Miyai[2], Y. Kumar[2], A. Kumar[2], M. Arita[1], H. Iwasawa[3], K. Shimada[1,2]

1 Hiroshima Synchrotron Radiation Center (HiSOR), Hiroshima Univ., Japan
2 Graduate School of Advanced Science and Engineering, Hiroshima Univ., Japan
3 National Institutes for Quantum Science and Technology (QST), Japan

-Poster Session-

The poster number with "S" is eligible for the Best Student Poster Award nomination.

P05S Re-examination of the phase diagram of the high-T_c cuprate superconductor $Bi_2Sr_2CaCu_2O_{8+\delta}$ studied by ARPES

Y. Tsubota[1], Y. Miyai[2], S. Kumar[2], K. Tanaka[3], S. Ishida[4], H. Eisaki[4], S. Nakagawa[5], T. Kashiwagi[5], M. Arita[2], K. Shimada[2], S. Ideta[2]

1 Graduate School of Advanced Science and Engineering, Hiroshima Univ. Japan
2 Hiroshima Synchrotron Radiation Center (HiSOR), Hiroshima Univ., Japan
3 UVSOR-Ⅲ Synchrotron, Institute for Molecular Science, Japan
4 National Institute of Advanced Industrial Science and Technology (AIST), Japan
5 Division of Materials Science, Tsukuba University, Japan

P06S Exploration of Novel Topological Semimetal and Evolution of the Electronic Structure Using High-Resolution ARPES

Y. Kumar[1], S. Kumar[2], K. Shimada[1,2]

1 Graduate School of Advanced Science and Engineering, Hiroshima University, Japan
2 Hiroshima Synchrotron Radiation Centre (HiSOR), Hiroshima University, Japan

P07S Development of ARPES analysis method using Bayesian Inference and application to cuprates

K. Ishiba[1], Y. Miyai[1], S. Kumar[2], T. Kurosawa[3], M. Oda[4], S. Ideta[2], K. Shimada[2]

1 Graduate School of Advanced Science and Engineering, Hiroshima Univ., Japan
2 Hiroshima Synchrotron Radiation Center, Hiroshima Univ., Japan
3 Faculty of Science and Engineering, Muroran Institute of Technology, Japan
4 Department of Science, Hokkaido Univ., Japan

P08S Momentum dependence of the spectral weight in the single layer high-Tc cuprate $Bi_2Sr_2CuO_{6+\delta}$ studied by ARPES

Y. Onishi[1], Y. Miyai[1], Y. Tsubota[1], S. Kumar[2], M. Atira[2], H. Eisaki[3], S. Ishida[3], K. Shimda[1,2], S. Ideta[1,2]

1 Graduate School of Advanced Science and Engineering, Hiroshima Univ., Japan
2 Hiroshima Synchrotron Radiation Center (HiSOR), Hiroshima Univ., Japan
3 National Institute of Advanced Industrial Science and Technology (AIST), Japan

P09 Characterization of amorphous carbon films by X-ray magnetic circular dichroism

Y. Muraoka[1], T. Kanayama[1], S. Enomoto[1], T. Wakita[1], M. Sawada[2]

1 Research Institute for Interdisciplinary Science, Okayama University, Japan
2 Hiroshima Synchrotron Radiation Center, Hiroshima University, Japan

P10 Photoemission spectroscopy measurements for phase-separated TiO2-VO2 films on mica substrates

Y. Muraoka[1], T. Wakita[1], T. Yokoya[1]

1 Research Institute for Interdisciplinary Science, Okayama University, Japan

P11 Current activities of research and education on BL-5 (FY2022)

T. Yokoya[1,2], T. Wakita[2], Y. Muraoka[1,2]

1 Research Institute for Interdisciplinary Science, Okayama University, Japan
2 Research Laboratory for Surface Science, Okayama University, Japan

-Poster Session-

The poster number with "S" is eligible for the Best Student Poster Award nomination.

P12 Visualization of boron distributions on inorganic and organic material surfaces by PEEM

T. Wakita[1], K. Igawa[3], M. Kaneda[2], N. Ikeda[2], H. Terato4, Y. Muraoka[1,2], T. Yokoya[1,2]

1 Research Institute for Interdisciplinary Science, Okayama University, Japan
2 Graduate School of Natural Science and Technology, Okayama University, Japan
3 Neutron Therapy Research Center, Okayama University, Japan
4 Advanced Science Research Center, Okayama University, Japan

P13 X-ray absorption spectroscopy of photodamaged polyimide film

O. Takahashi[1,4], T. Ohnishi[1,4], R. Yamamura[1,4], E. Kobayashi[2], K. Kubo[3,4], M. Okazaki[3,4], Y. Horikawa[3,4], M. Oura[4], H. Yoshida[1,5]

1 Basic Chemistry Program, Graduate School of Advanced Science and Engineering, Hiroshima University, Japan
2 Kyushu Synchrotron Light Research Center, Japan
3 Department of Physics and Information Science, Japan
4 RIKEN SPring-8 Center, Japan
5 Hiroshima Synchrotron Radiation Center, Hiroshima University, Japan

P14S Investigating the possibility of creating a "pure" p-type Bi_2Se_3

Y. Higuchi[1], R. Itaya[1], M. Tomita[1], H. Saito[2], K. Suzuki[2], H. Sato[3], K. Sato[2,4], K. Sakamoto[1,4]

1 Department of Applied Physics, Osaka University, Japan
2 Division of Materials and Manufacturing Science, Osaka University, Japan
3 Hiroshima Synchrotron Radiation Center, Hiroshima University, Japan
4 Spintronics Research Network Division, OTRI, Osaka University, Japan

P15S Observation of electron structure of chiral magnet $Yb(Ni_{1-x}Cu_x)_3Al_9$ by ARPES

Y. Tanimoto[1], M. Sugimoto[2], R. Kamimori[1], H. Sato[3], M. Arita[3], S. Kumar[3], K. Shimada[3], S. Nakamura[4], S. Ohara[4]

1 Graduate School of Advanced Science and Engineering, Hiroshima University, Japan
2 Faculty of Science, Hiroshima University, Japan
3 Hiroshima Synchrotron Radiation Center, Hiroshima University, Japan
4 Graduate School of Engineering, Nagoya Institute of Technology, Japan

P16 Changes in Electronic States in Gd-TM metallic glasses Rejuvenated by Temperature Cycling

S. Hosokawa[1], K. Kobayashi[1]

1 Institute of Industrial Nanomaterials, Kumamoto University, Japan

P17 Spiral band structure hidden in the bulk chiral crystal $NbSi_2$

C. Zhang[1], K. Miyamoto[1], T. Shishidou[2], R. Amano[3], T. Sayo[3], C. Shimada[3], Y. Kousaka[3], M.I Weinert[2], Y. Togawa[3], T. Okuda[1]

1 Hiroshima Synchrotron Radiation Center, Hiroshima University, Japan
2 Department of Physics, University of Wisconsin-Milwaukee, USA
3 Deparment of Physics and Electronics, Osaka Metropolitan University, Japan

P18S Investigation of Perpendicular Anisotropy in FeCo Alloy Films Covered with Oxygen for Development of Multi Spin Detecting Target

K. Kunitomo[1], K. Miyamoto[2], T. Okuda[2]

1 Graduate School of Advanced Science and Engneering Hiroshima University, Japan
2 Hiroshima Synchrotron Radiation Center (HSRC), Hiroshima University, Japan

-Poster Session-

The poster number with "S" is eligible for the Best Student Poster Award nomination.

P19 Cluster Distortions in Amorphous Organotin Sulfide Compounds by EXAFS Measurements

J. R. Stellhorn[1,2], S. Hayakawa[2], B. Paulus[3], J. L. Vasco[3], B. D. Klee[4], S. Dehnen[3], W. Pilgrim[3]

1 Department of Physics, Nagoya University, Japan
2 Department of Applied Chemistry, Graduate School of Advanced Science and Engineering, Hiroshima University, Japan
3 Department of Chemistry, Philipps University of Marburg, Germany
4 Complex Fluid Research Department, Wigner Research Centre for Physics, Hungary

P20S First results of phase transformation from vaterite to calcite observed by Ca K-edge XAFS and XRD.

Y. Ma[1], J. R. Stellhorn[1,3], N. Kawata[2], S. Hayakawa[1]

1 Graduate School of Advanced Science and Engineering, Hiroshima University, Japan
2 Natural Science Center for Basic Research and Development, Hiroshima University, Japan
3 Department of Physics, Nagoya University, Japan

P21S Hydration Structure of Acetone Studied with Concentration-Dependent Absorption Spectra in the Ultraviolet Region

C. Sugahara[1], K. Matsuo[2], K. Okada[1,2]

1 Graduate School of Advanced Science and Engineering, Hiroshima University, Japan
2 Hiroshima Synchrotron Radiation Center, Hiroshima University, Japan

P22S Dynamic Observation of Interaction Process between β-Lactoglobulin and Membrane by Time-Resolved Vacuum-Ultraviolet Circular Dichroism

S. Hashimoto[1], K. Matsuo[2]

1 Graduate School of Advanced Science and Engineering, Hiroshima University, Japan
2 Hiroshima Synchrotron Radiation Center, Hiroshima University, Japan

P23 Optical Activity Measurement of Amino-acid Films Irradiated with Circularly Polarized Lyman-α Light

J. Takahashi[1], M. Kobayashi[2], G. Fujimori[1], K. Kobayashi[1], H. Ota[3], K. Matsuo[4], M. Katoh[3,4], Y. Kebukawa[1], S. Yoshimura[2], H. Nakamura[2]

1 Faculty of Engineering, Yokohama National University, Japan
2 Department of Helical Plasma Research, National Institute for Fusion Science, Japan
3 UVSOR Facility, Institute for Molecular Science, Japan
4 Hiroshima Synchrotron Radiation Center, Hiroshima University, Japan

P24S Interaction Mechanism between the Antimicrobial Peptide Magainin2 and Lipid Membrane Revealed by Synchrotron-Radiation Circular- and Linear-Dichroism Spectroscopy

R. Tsuji[1], M. Kumashiro[2], K. Matsuo[3]

1 Graduate School of Advanced Science and Engineering, Hiroshima University, Japan
2 Institute of Advanced Medical Sciences, Tokushima University, Japan
3 Hiroshima Synchrotron Radiation Center, Hiroshima University, Japan

-Poster Session-

The poster number with "S" is eligible for the Best Student Poster Award nomination.

P25S Membrane-bound conformation of the non-amyloid-β component of α-synuclein characterized by vacuum-ultraviolet circular dichroism and molecular-dynamics simulation

R. Imaura[1], K. Matsuo[2]
1 Graduate School of Advanced Science and Engineering, Hiroshima University, Japan
2 Hiroshima Synchrotron Radiation Center, Hiroshima University, Japan

P26 Torsional Angle Dependence of Ultrafast Charge Transfer in Biphenyl Monolayers

K. Yoshioka[1], J. Yamada[1], A. Niozu[1], S. Wada[1,2]
1 Department of Physical Science, Hiroshima University, Japan
2 Hiroshima Synchrotron Radiation Center, Hiroshima University, Japan

P27 Measurements of Work Functions of Organic Monolayers Adsorbed on Gold Surfaces

J. Yamad[1], K. Yoshiok[1], A. Niozu[1,2], S. Wada[1,2,3]
1 Faculty of Science, Hiroshima University, Japan
2 Graduate School of Advanced Science and Technology, Hiroshima University, Japan
3 Hiroshima Synchrotron Radiation Center, Hiroshima University, Japan

P28S Magnetic properties of Co ultrathin films intercalated underneath monolayer h-BN grown on Ni(111) probed by soft X-ray magnetic circular dichroism

W. Nishizawa[1], M. Sawada[2]
1 Graduate School of Science, Hiroshima University Japan
2 Hiroshima Synchrotron Radiation Center, Hiroshima University Japan

P29 Design Study on HiSOR-II

Y. Lu[1], M. Shimada[3,1], H. Miyauchi[3,1], M. Katoh[1,2]
1 Hiroshima Synchrotron Radiation Center, Hiroshima University, Japan
2 Institute for Molecular Science, Japan
3 High Energy Accelerator Research Organization, Japan

22BG011 BL-1

Realization of Practical Eightfold Fermions and Fourfold van Hove Singularity in $TaCo_2Te_2$

Hongtao Rong[1*], Zhenqiao Huang[1,7*], Xin Zhang[2,8*], Shiv Kumar[3*], Fayuang Zhang[1], Chengcheng Zhang[1], Yuan Wang[1], Zhanyang Hao[1], Yongqing Cai[1], Le Wang[1], Cai Liu[1], Xiao-Ming Ma[1], Shu Guo[1], Bing Shen[4], Yi Liu[5], Shengtao Cui[5], Kenya Shimada[3], Quansheng Wu[6,10], Junhao Lin[1], Yugui Yao[2,8], Zhiwei Wang[2,8,9#], Hu Xu[1#], and Chaoyu Chen[1#]

[1] *Shenzhen Institute for Quantum Science and Engineering (SIQSE) and Department of Physics, Southern University of Science and Technology (SUSTech), Shenzhen 518055, China.*

[2] *Centre for Quantum Physics, Key Laboratory of Advanced Optoelectronic Quantum Architecture and Measurement, School of Physics, Beijing Institute of Technology, Beijing 100081, China.*

[3] *Hiroshima Synchrotron Radiation Centre, Hiroshima University, Higashi-Hiroshima, Hiroshima 739-0046, Japan.*

[4] *School of Physics, Sun Yat-Sen University, Guangzhou 510275, China.*

[5] *National Synchrotron Radiation Laboratory, University of Science and Technology of China, Hefei, Anhui 230029, China.*

[6] *Beijing National Laboratory for Condensed Matter Physics, and Institute of Physics, Chinese Academy of Sciences, Beijing 100190, China.*

[7] *Department of Physics, The Hong Kong University of Science and Technology, Clear Water Bay, Hong Kong, China.*

[8] *Beijing Key Lab of Nanophotonics and Ultrafifine Optoelectronic Systems, Beijing Institute of Technology, Beijing 100081, China.*

[9] *Material Science Center, Yangtze Delta Region Academy of Beijing Institute of Technology, Jiaxing 314011, China.*

[10] *University of Chinese Academy of Sciences, Beijing 100049, China.*

Keywords: Topological states, eightfold fermions, fourfold van Hove singularity, hourglass fermion

Searching for new elementary excitation/quasiparticles is a key pursuit of condensed matter physics. In the past decades, Weyl and Dirac type low-energy quasiparticles, in analog to relativistic massless Weyl and Dirac fermions in high-energy physics, have been realized based on materials such as graphene, topological insulator, and Weyl/Dirac semimetal. Moreover, the 230 space groups in condensed matter physics impose fewer constraints on the allowed types of fermions. New fermionic quasiparticles beyond high-energy physics, including threefold, sixfold, and eightfold fermions, can emerge. So far, while Weyl (twofold), threefold, Dirac (fourfold), and sixfold quasiparticles have been observed in quantum materials[1-12], eightfold fermions remain to be realized. Based on a nonsymmorphic crystal $TaCo_2Te_2$, we provide a clear spectroscopic signature of eightfold degenerate fermions protected by the combination of crystalline and time-reversal symmetry.

We establish $TaCo_2Te_2$ as a conjoint topological and quantum critical platform with handful stimuli available to tune its physical properties. Chemical substitution or applying strain may introduce long range magnetic order and magnetic quantum critical point is expected. The negligible SOC leads to the practical realization of eightfold fermions, which, according to theoretical analysis, serves as a topological quantum critical point. Symmetry breaking via magnetic field or uniaxial strain may lead to various topologically trivial or nontrivial phases such as Dirac point, Weyl point or nodal lines. Consequently, our findings will stimulate broad research interest from subfields of condensed matter physics such as quantum transport, strong correlation, material synthesis and topological states of matter.

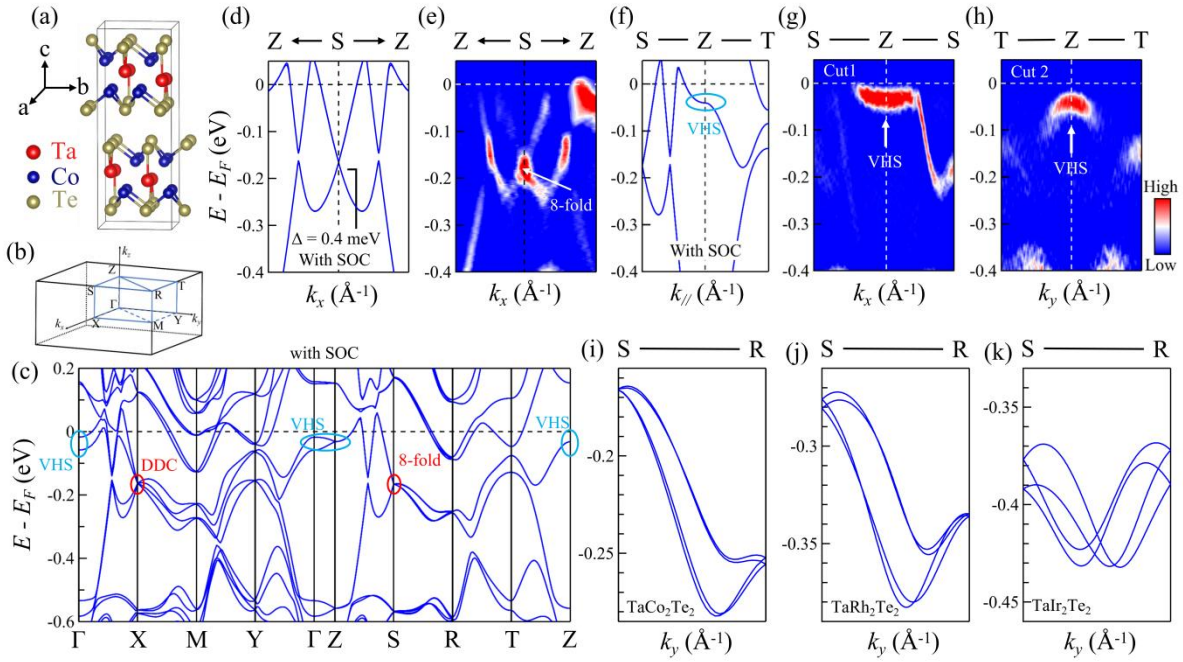

FIGURE 1. Crystal structure, eightfold fermion, fourfold van Hove singularity and hourglass in $TaCo_2Te_2$. (a) Crystal structure. (b) 3D bulk BZ. (c) DFT calculated dispersions along the high-symmetry path with considering SOC. (d, e) DFT calculated dispersions and ARPES dispersion around eightfold fermion. (f-h) DFT calculated dispersions and ARPES dispersion around van Hove singularity. (i-k) DFT predicted hourglass fermions in TaT_2Te_2 (T= Co, Rh and Ir).

REFERENCES

1. A. Alexandradinata, Zhijun Wang & B. Andrei Bernevig. *Physical Review X* **6**, 021008 (2016)
2. B. Bradlyn, J. Cano, Z. Wang, M. G. Vergniory, C. Felser, R. J. Cava & B. A. Bernevig. *Science* **353**, 5037 (2016)
3. S. M. Huang, S. Y. Xu, I. Belopolski, C. C. Lee, G. Chang, T. R. Chang, B. Wang, N. Alidoust, G. Bian, M. Neupane, D. Sanchez, H. Zheng, H. T. Jeng, A. Bansil, T. Neupert, H. Lin & M. Z. Hasan. *Proc Natl Acad Sci USA* **113**, 1180-1185 (2016)
4. Z. Wang, A. Alexandradinata, R. J. Cava & B. A. Bernevig. *Nature* **532**, 189-194 (2016)
5. Hongming Weng, Chen Fang, Zhong Fang & Xi Dai. *Physical Review B* **93**, 241202 (2016)
6. B. J. Wieder, Y. Kim, A. M. Rappe & C. L. Kane. *Phys Rev Lett* **116**, 186402 (2016)
7. Ziming Zhu, Georg W. Winkler, QuanSheng Wu, Ju Li & Alexey A. Soluyanov. *Physical Review X* **6**, 031003 (2016)
8. Qihang Liu & Alex Zunger. *Physical Review X* **7**, 021019 (2017)
9. Benjamin J. Wieder, Barry Bradlyn, Zhijun Wang, Jennifer Cano, Youngkuk Kim, Hyeong-Seok D. Kim, Andrew M. Rappe, C. L. Kane & B. Andrei Bernevig. *Science* **361**, 246-251 (2018)
10. Weikang Wu, Zhi-Ming Yu, Xiaoting Zhou, Y. X. Zhao & Shengyuan A. Yang. *Physical Review B* **101**, 205134 (2020)
11. P. J. Guo, Y. W. Wei, K. Liu, Z. X. Liu & Z. Y. Lu. *Phys Rev Lett* **127**, 176401 (2021)
12. Jennifer Cano, Barry Bradlyn & M. G. Vergniory. *APL Materials* **7**, 101125 (2019)

P02S

Evolution of Electronic States in Epitaxial YBCO Thin Films with Calcium Doping by Angle-Resolved Photoemission Spectroscopy

Anjana Krishnadas[a], Yuita. Fujisawa[a], Markel Pardo-Almanza[a], Kohei Yamagami[a,b], Yukiko Obata[a], Yoshinori. Okada[a]

[a]*Quantum Materials Science Unit, Okinawa Institute of Science and Technology (OIST), Okinawa 904-0495, Japan.*

[b]*Japan Synchrotron Radiation Research Institute, Hyogo, 679–5198, Japan.*

Keywords: High temperature superconductors, ARPES, epitaxial thin film growth, heterostructures.

Abstract

Cuprates are among the most intriguing strongly correlated systems, exhibiting a variety of complex electronic phases. Studies on the nature of the Fermi surface (FS) and the electronic properties of HTSCs such as $YBa_2Cu_3O_{7-d}$ (YBCO) have also gained attention thanks to powerful experimental technologies [1,2] and advances in thin film growth [3,4]. The development of film-based heterostructures is a new major challenge.

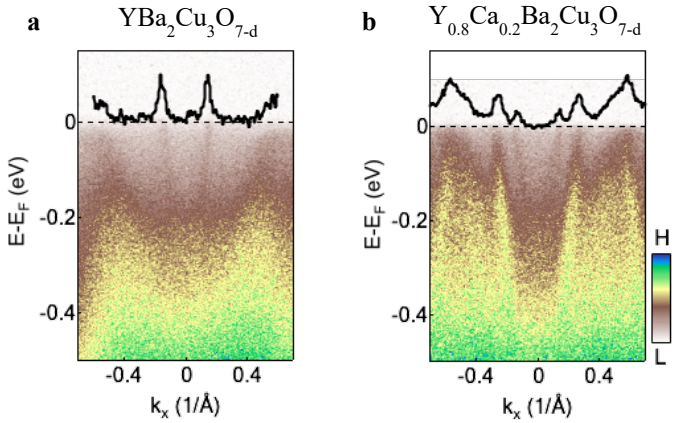

Figure 1. (a) ARPES intensity image of a near-optimally doped YBCO and (b) 20% Ca-doped thin film at the antinodal region obtained at 15 K, with a laboratory-based He-II light source (40.8 eV). The film was grown on a $LaAlO_3$(001) substrate.

In this work, we present an *in-situ* ARPES study on the calcium doping evolution of electronic states on the surface of YBCO epitaxial films grown by pulsed laser deposition. The ARPES of undoped YBCO shows the typical electronic structure of an optimally doped CuO_2 plane and a series of one-dimensional bands originating from the CuO chains, while the 20% Ca-doped YBCO thin film additionally shows a second chain state as shown in Figure (1 b). When YBCO is partially doped with Ca, we also observe

the appearance of band folding due to possible surface reconstructions. The careful tuning of the surface electronic states, together with a high Tc, as well as a larger coherence length along the c-axis, thus makes YBCO a good candidate as an HTSC substrate for *in-situ* heterostructures.

References:

[1]. H. Iwasawa *et al.*, *Phys. Rev. B.* 99 (14), 140510 (2019).
[2]. H. Iwasawa *et al.*, Ultramicroscopy, Volume 182, Pages 85-91 (2017).
[3]. Wu, Z.-B. *et al*., *Phys. Rev. Mater.* 4, 124801 (2020).
[4]. Y. Sassa et.al*., Phys. Rev. B* 83, 140511(R) (2011).

20AU018, 22AG005, 22BG004 BL-9A & μ-Laser ARPES

Symmetry reduction in the electronic structure of heavily overdoped Pb-Bi2201 detected by ARPES

Y. Miyai[a], T. Kurosawa[b], M. Oda[c], M. Arita[d], S. Ideta[d], and K. Shimada[d]

[a]*Graduate School of Science, Hiroshima University, Kagamiyama 1-3-1, Higashi-Hiroshima 739-8526, Japan*
[b] *Fuculty of Science and Engineearing, Muroran Institute of Technology, 27-1 Mizumoto-cho, Muroran, Hokkaido, 050-8585, Japan*
[c] *Department of Physics, Hokkaido University, Sapporo 060-0809, Japan*
[d] *Hiroshima Synchrotron Radiation Center, Hiroshima University, Kagamiyama 1-3-1, Higashi-Hiroshima 739-8526, Japan*

Keywords: High-T_C superconductor, ARPES

High transition-temperature (T_C) cuprate superconductors have attracted much interest since their discovery in 1986 for their high superconducting transition temperature as well as unusual physical properties such as a pseudogap state and a nematic phase [1,2]. Superconductivity occurs in the CuO_2 plane and the Cu $3d_{x^2-y^2}$ state forms the Fermi surface. One can expect a four-fold symmetry of the Fermi surface because the CuO_2 plane is tetragonal. However, symmetry reduction of the electronic structure has been reported in Bi-based cuprate superconductors recently [2,3]. Similar symmetry reduction or *nematicity* was found in the Fe-based superconductor, the electronic states break the four-fold rotational symmetry of the lattice [4]. Although nematicity in electron liquids has attracted much interest, the rotational symmetry breaking in the electronic states for high-T_C cuprate superconductors has not been clarified yet.

Here, we have examined the symmetry of the electronic structure of heavily overdoped $(Bi,Pb)_2Sr_2CuO_{6+\delta}$ (Pb-Bi2201) (T_C = 6 K) using high-resolution angle-resolved photoemission spectroscopy (ARPES). We selected Bi2201 because it has a single CuO_2 plane and one can exclude the complexity of the electronic structure such as bilayer splitting derived from plural CuO_2 planes. Furthermore, the heavily overdoped sample is favorable because the pseudogap is vanishing and one can clearly detect the Fermi surface in the normal state.

Figures 1(a) and (b) show the Fermi surface measured at $h\nu$ = 22 eV, *s*-polarization, and T = 20 K along two orthogonal nodal directions. We found a clear difference in the nodal distances; $d_1 = (7.948 \pm 0.003) \times 10^{-1}$ Å^{-1} (Fig. 1(a)) and $d_2 = (8.340 \pm 0.003) \times 10^{-1}$ Å^{-1} (Fig. 1(b)). These distances are temperature independent for the temperature range from T = 20 K up to 260 K (Fig. 1(c)). In addition, we have conducted MDC analysis along these two nodal directions and find different quasiparticle lifetime broadening as shown in Fig. 1(d), which is persistent up to 260 K. The situation is similar for the samples with T_C = 4, 6, and 10 K. Our results indicate the reduction of the four-fold symmetry in the electronic states.

In the heavily overdoped region, a charge density wave (CDW) is observed by resonant inelastic X-ray scattering and its onset is well above 250 K [5]. In addition, previous Raman scattering measurements suggest the Pomeranchuk instability and the nematic phase [6]. The previous reports are in line with our findings. Further study is required to reveal how symmetry reduction in the electronic state occurs in the heavily overdoped region. To investigate this issue, we are planning to examine the electronic structure at the endpoint of the hole concentration in the pseudogap state and at the onset of the Lifshitz transition that occurs between the hole-like and electron-like Fermi surfaces.

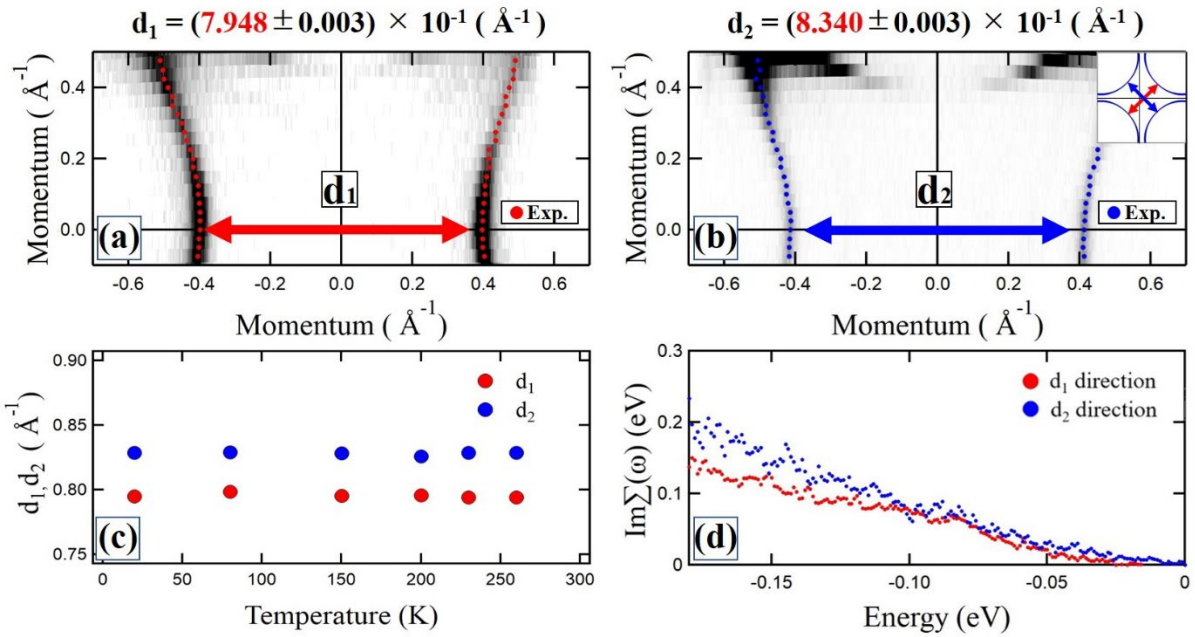

FIGURE 1. (a), (b) Fermi surface observed at $h\nu = 22$ eV, *s*-polarization and $T = 20$ K along the nodal directions shown in the inset of panel (b). The inset displays the Fermi surface centered at the $\bar{\Gamma}$ point. Red and blue dots indicate the Fermi surface points determined from the peaks of the momentum distribution curves. d_1 and d_2 indicate the distance between nodes. (c) Temperature dependence of d_1, d_2. (d) $Im\Sigma$ of the self-energy along d_1 and d_2 nodal directions.

1. M. Hashimoto *et al*., *Nature Physics* **10**, 483-495 (2014).
2. S. Nakata *et al*., *npj Quantum Materials* **6**, 86 (2021).
3. Y. He *et al*., *Scientific Reports* **7**, 8059 (2017).
4. H. C. Xu *et al*., *Physical Review Letters* **117**, 157003 (2016).
5. Y. Y. Peng *et al*., *Nature Materials* **17**, 697 (2018).
6. N. Auvray *et al., Nature Communications* **10**, 5209 (2019).

Recent upgrades and activities of HiSOR BL-1

S. Ideta[a,b], S. Kumar[a], Y. Miyai[b], Y. Kumar[b], A. Kumar[b], M. Arita[a], H. Iwasawa[c], and K. Shimada[a,b]

[a] *Hiroshima Synchrotron Radiation Center (HiSOR), Hiroshima Univ., Japan*
[b] *Graduate School of Advanced Science and Engineering, Hiroshima Univ., Japan*
[c] *National Institutes for Quantum Science and Technology (QST), Japan*

Keywords: Synchrotron radiation beamline, angle-resolved photoemission spectroscopy (ARPES), condensed-matter physics

The Hiroshima Synchrotron Radiation Center (HiSOR) is a compact race-track electron storage ring. As a linear undulator beamline, BL-1, one of the HiSOR beamlines, is operated for high-resolution angle-resolved photoemission spectroscopy (ARPES) in the VUV and soft X-ray regions [1], and many interesting studies have been reported [2-5]. In recent years, the necessity to measure the fine electronic structure in a wide variety of samples, for example, microscale samples, has led to a demand for ARPES experiments with energy resolution of a few meV using synchrotron radiation and controlling fine sample positions.

For these purposes, we have improved the endstation and beamline of BL-1 (Fig. 1): Beam sizes focused by a mirror, fast measurement by a newly installed electron analyzer, etc. To test the performance of the instruments, we measure the energy resolution using the evaporated Au sample. The total energy resolution which is determined by the monochromator, new hemispherical electron analyzer (MBS-A1), and resolution of synchrotron radiation including the thermal broadening at 10 K shows ~ 4.5 meV ($h\nu = 40$ eV). In the poster presentation, we will show details of the present status of BL-1 and upgrades in near future.

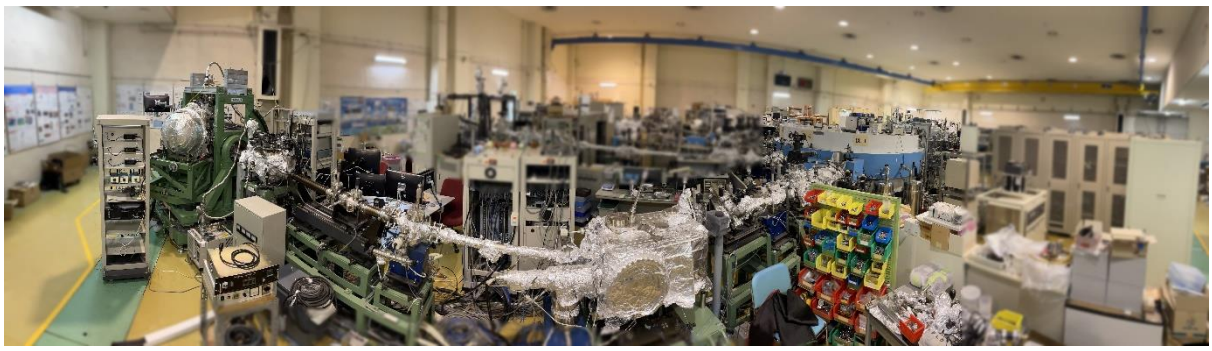

Figure 1. Beamline 1 (BL-1) (linear undulator beamline) for high-resolution angle-resolved photoemission spectroscopy (ARPES). The light polarization is changed by rotating the endstation (*s*- and *p*-polarization are available).

REFERENCES

1. H. Iwasawa *et al.*, J. Synchrotron Rad, **24**, 836-841 (2017).
2. Y. Wang *et al.*, Nano Lett. **15**, 4013-4018 (2015)
3. H. Ishii *et al.*, Nature **426**, 540-544 (2003).
4. K. Kuroda *et al.*, Phys. Rev. Lett. **105**, 076802 (2010).
5. Yu-Jie Hao *et al.*, Phys. Rev. X **9**, 041038 (2019).

2022AG005, 2022BG004 BL-1,9A

Re-examination of the phase diagram of the high-T_c cuprate superconductor $Bi_2Sr_2CaCu_2O_{8+\delta}$ studied by ARPES

Y. Tsubota[a], Y. Miyai[b], S. Nakagawa[e], S. Ishida[d], S. Kumar[b], K. Tanaka[c], H. Eisaki[d], T. Kashiwagi[e], M. Arita[b], K. Shimada[b], and S. Ideta[b]

[a] *Graduate School of Advanced Science and Engineering, Hiroshima Univ., Higashi-Hiroshima 739-0046, Japan*
[b] *Hiroshima Synchrotron Radiation Center (HiSOR), Hiroshima Univ., Higashi-Hiroshima 739-0046, Japan*
[c] *UVSOR-III Synchrotron, Institute for Molecular Science, Okazaki, Aichi 444-8585, Japan*
[d] *National Institute of Advanced Industrial Science and Technology (AIST), Tsukuba, Ibaraki 305-8560, Japan*
[e] *Division of Materials Science, Tsukuba University, Tsukuba, Ibaraki 305-8577, Japan*

Keywords: high-T_c cuprate superconductors, ARPES, electronic structure, strongly correlated electron materials

In high-T_c cuprate superconductors, superconductivity occurs upon hole doping into the CuO_2 plane. The electronic phase diagram of hole-doped high-T_c cuprate superconductors plotted as a function of temperature and carrier concentration has been reported as an empirical and universal phase diagram which is a dome-like shape centered at ~0.16 of hole concentration [1]. However, previous ARPES experiments suggest that its empirical phase diagram may not be universal and shifted toward overdoped region [2-4].

In this study, we have performed angle-resolved photoemission spectroscopy (ARPES) measurements systematically to directly investigate the electronic structure of the underdoped, optimally doped, and overdoped double-layer cuprates $Bi_2Sr_2CaCu_2O_{8+\delta}$ (Bi2212). We have estimated the hole concentration of each sample from the Fermi-surface area and compared them quantitatively. Figure 1 shows the Fermi surface of the optimally doped Bi2212 with T_c = 92 K and we determine the Fermi momentum (red dots in Fig. 1) from the ARPES spectra.

In this poster presentation, we will show the results of hole concentration estimated from the Fermi surfaces in Bi2212 for each sample and the result is compared with the previous study to investigate the relationship between the hole concentration and T_c (phase diagram). As a result, the phase diagram in the present study is different from the previous one reported by Tallon *et al* [1]. Based on the present ARPES study, we will show the new phase diagram in Bi2212 and discuss the physical properties compared with the other studies.

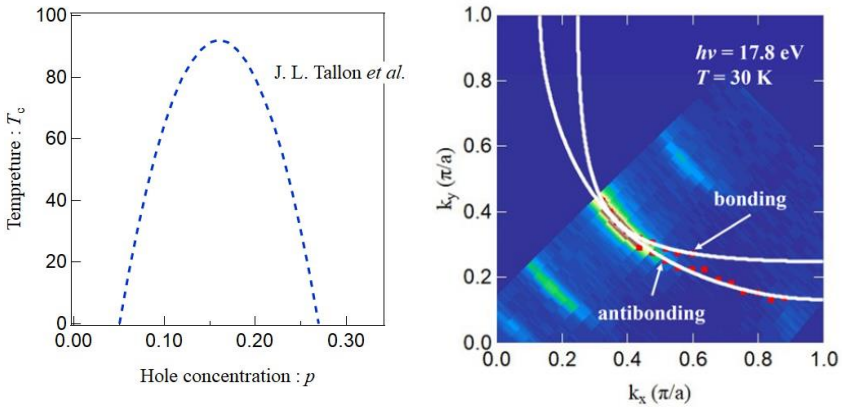

FIGURE 1. Schematic phase diagram of the double-layer cuprate Bi2212 (left) from Ref. [1]. Fermi surfaces of Bi2212 observed by ARPES (right). Red dots are the Fermi momentum estimated from momentum-distribution curves near the Fermi level. White curves are the Fermi surfaces obtained by tight-binding approximation and the bonding and antibonding bands are fitted by calculation.

REFERENCES

1. J. L. Tallon, C. Bernhard, H. Shaked, R. L. Hitterman and J. D. Jorgensen, *Phys. Rev. B* **51**, 12911 (1995).
2. I. K. Drozdov, I. Pletikosić, C.-K. Kim, K. Fujita, G. D. Gu, J. C. Séamus Davis, P. D. Johnson1, I. Božović and T. Valla, *Nat. Commun.* **9**, 5210 (2018).
3. R. Sodota, N. Kudo, M. Matsunami, and T. Takeuchi, *J. Phys. Soc. Jpn.* **88**, 064711 (2019).
4. H. Sakamoto, K. Ogawa, T. Kondo, S. Shin, M Matsunami, H. Ikuta, and T. Takeuchi, *J. Phys. Soc. Jpn.* **85**, 104710 (2016).

22AG001, 22AU002 BL-1 (HiSOR)

Exploration of Novel Topological Semimetal and Evolution of the Electronic Structure Using High-Resolution ARPES

Yogendra Kumar[a], Shiv Kumar[b], Kenya Shimada[a,b]

[a]*Graduate School of Advanced Science and Engineering, Hiroshima University, Japan 739-0046*
[b]*Hiroshima Synchrotron Radiation Centre (HiSOR), Hiroshima University, Japan 739-0046*

Keywords: Weyl semimetal, superconductivity, ARPES study, DFT calculation

Topological semimetals (TSMs) with the non-trivial topology of the band structure have been the focus of recent theoretical and experimental studies [1]. Depending on the shape and degeneracy of the band crossings around the Fermi level, TSMs can be mainly classified into the Dirac semimetals (DSMs), Weyl semimetals (WSMs) and topological nodal-line semimetals (NLSMs). In particular, WSMs represent a novel quantum state of matter, characterized by the presence of massless chiral particles acting as magnetic monopoles in the bulk (Weyl Fermions), and the discontinuous Fermi arcs in the topological surface states [2]. WSMs also offer interesting prospects for applications because they have the ultrahigh mobility of charge carriers and very high negative magnetoresistance due to the Adler-Bell-Jackiw anomaly [3]. The WSM concept was theoretically proposed by Wan *et al.* in 2011 [4], and one can realize it by breaking either time-reversal symmetry or spatial inversion symmetry. The WSMs are classified as either Type-I or Type-II. Type-I WSMs such as TaAs respect the Lorentz symmetry, whereas Type-II WSMs such as WTe_2 and $MoTe_2$ do not. In contrast to Type-I WSMs, the main magneto-transport feature of Type-II WSMs is the anisotropic chiral anomaly [5].

Here we examine the type-II Weyl semimetal PdSeTe and $PdTe_2$ with the CdI_2-type crystal structure [6] which is the trigonal family of the lattice with the space group $P\bar{3}m1$ (164) [7,8]. PdSeTe is non-symmorphic because it has screw axis and glid plane. PdSeTe and $PdTe_2$ are superconductors with a transition temperature of T_C ~2.74 K [8] and T_C ~1.78 K [9], respectively. We have grown high-quality PdSeTe single crystals by a two-step modified Bridgman method. We characterized the samples by the powder and single crystal X-ray diffraction (XRD) of the as-grown PdSeTe sample using a Rigaku SmartLab X-ray diffractometer with CuK_α radiation (λ =1.5406 Å). To determine the lattice parameters, we have performed Rietveld refinement using FullProf software of the XRD patterns for PdSeTe powder sample as shown in Fig. 1(a). The XRD results showed the reduction in unit cell volume from $PdTe_2$ by 10% due to Se substitution. Previous study indicated T_C of $PdTe_2$ was increased by applying pressure [10]. Since PdSeTe has slightly less unit cell volume to $PdTe_2$, we assume that the T_C was enhanced by the chemical pressure. Another possibility for the T_C enhancement could be lattice disorder or structural defects caused by Se doping. Recent study indicated that the T_C of the TaS_2 superconductor was enhanced from 2.89 K to 3.61 K due to the disorder arising from the structural defects [11].

Fig. 1(c) shows PdSeTe ARPES spectrum taken at BL-1, HiSOR. We obtained (001) clean surface by cleaving in ultrahigh vacuum. Near the Fermi level, one can see electron-like band at the $\bar{\Gamma}$ point and hole-like band at ~0.5 $Å^{-1}$. Based on the photon energy dependent measurements, we found that the band dispersion was highly two dimensional. Therefore, we have done the density functional theory (DFT) calculation for a five PdSeTe layers with the spin-orbit coupling as shown in Fig. 1(a). One can see some correspondence between the ARPES and DFT results though there are many bands in the calculation. In order to simulate ARPES spectral features we should take into account the mean-free-path of photoelectron and lifetime effect.

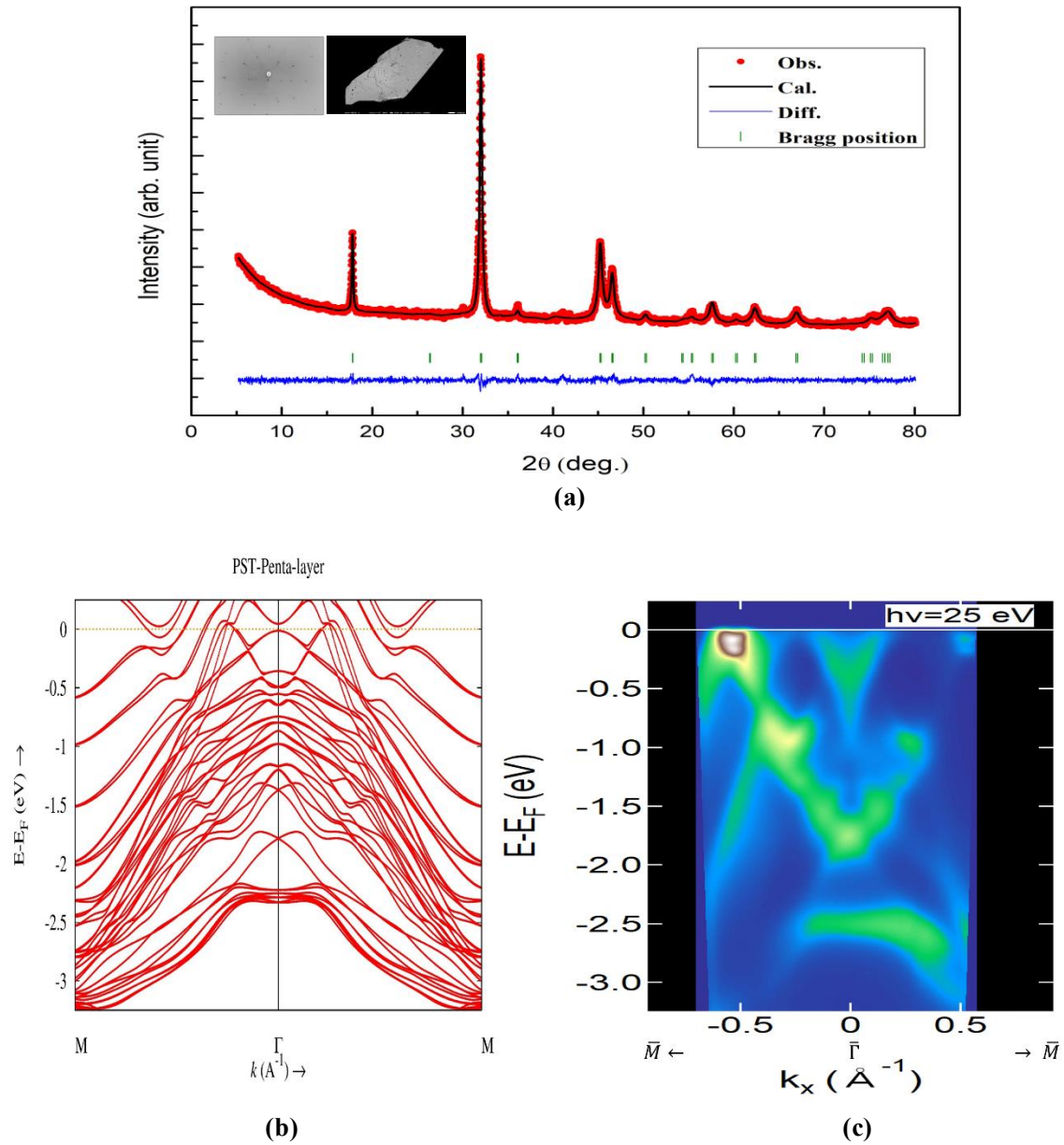

FIGURE 1. *(a) Rietveld refinement profiles of X-ray diffraction data of the PdSeTe powder sample. Insets show the Laue's diffraction pattern for (001) surface and image of the as-grown PdSeTe crystal. (b), (c) represents the simulated bands for slab (5 atomic layers) and measured ARPES spectrum along M-Γ-M direction.*

REFERENCES

[1] M. Z. Hasan and C. L. Kane, *Rev. Mod. Phys.* **82**, 3045–3067 (2010).
[2] S. Jia, S-Y. Xu and M. Z. Hasan, *Nature Materials* **15**,1140–1144 (2016).
[3] H. B. Nielsen and M. Ninomiya, *Phys. Lett. B* **130**, 389–396 (1983).
[4] X. Wan, A. M. Turner, A. Vishwanath, and S. Y. Savrasov, *Phys. Rev. B* **83**, 205101 (2011).
[5] T. Nag and S. Nandy, *J. Phys.: Condens. Matter* **33** 075504 (2021).
[6] L. Thomassen, *Z. Phys. Chem. B* **2**, 349 (1929).
[7] E. McCarron, R. Korenstein, A. Wold, *Materials Research Bulletin* **11**, 1457-1462 (1976).
[8] W. Liu, S. Li, H. Wu, N. Dhale, P. Koirala, and B. Lv, *Phys. Rev. Materials* **5**, 014802 (2021).
[9] J. Guggenheim, F. Hulliger, and J. Müller, *Helvetica Physica Acta* **34**, 408 (1961).
[10] H. Leng, A. Ohmura, L. N. Anh, F. Ishikawa, T. Naka, Y. K. Huang and A. de Visser, *J. Phys. Condens. Matter* **32**, 025603 (2020).
[11] J. Peng, Z. Yu, J. Wu, Y. Zhou, Y. Guo, Z. Li, J. Zhao, C. Wu, and Y. Xie, *ACS Nano* **12**, 9461 (2018).

20AU018 BL-1

Development of ARPES analysis method using Bayesian Inference and application to cuprates

K. Ishiba[1], Y. Miyai[1], S. Kumar[2], T. Kurosawa[3], M. Oda[4], S. Ideta[2], K. Shimada[2]

[1]*Graduate School of Advanced Science and Engineering, Hiroshima Univ., Japan*
[2]*Hiroshima Synchrotron Radiation Center, Hiroshima Univ., Japan*
[3]*Faculty of Science and Engineering, Muroran Institute of Technology, Japan*
[4]*Department of Science, Hokkaido Univ., Japan*

Keywords: Baysian inference, Many-body interaction, Self-energy, ARPES, Cuprates,

High-Tc cuprate superconductors exhibit unique physical properties such as high superconducting transition temperatures, density wave formation, and bad metallic states. To understand their physical properties, it is necessary to quantitatively evaluate the many-body interactions that give rise to them. Since high-resolution angle-resolved photoemission spectroscopy (ARPES) spectra correspond to the imaginary part of the single-particle Green's function, quantitative analysis of the ARPES spectral shape allows us to experimentally extract the self-energy (Σ) that reflects information on many-body interactions. In conventional self-energy analysis methods, the self-energy is extracted by assuming some form of a one-electron band and checking whether the real part of the self-energy (ReΣ) and imaginary part of the self-energy (ImΣ) satisfy the Kramers-Kronig relation. However, this method cannot eliminate arbitrariness in determining the one-electron band, and the parameters cannot be optimized in a single step. It is required, therefore, to optimize all the parameters directly from an image plot of the ARPES spectrum without arbitrariness. In this study, we applied Bayesian inference [1] to analyze ARPES image plots of heavily overdoped $(Bi,Pb)_2Sr_2CuO_{6+\delta}$ ($T_C \sim 6$ K) to extract all parameters simultaneously.

We applied a new analysis method to the ARPES spectra shown in Fig. 1(a). Fig. 1(b) shows the simulated ARPES spectrum using optimized parameters. One can see experimental ARPES spectral features are well reproduced by the simulation. It is noted that the suppression of the ARPES spectral intensity below -0.4 eV which is known as waterfall structure is well reproduced by the self-energy due to the electron-electron interaction. It indicates that the waterfall structure mainly originated from many-body interactions but not from the matrix element effect. Solid blue lines in Fig. 1(c) show evaluated ReΣ and ImΣ, being compared with those obtained from the conventional method (red dots). The deviation is mainly from the transition matrix element effect which is included in the new method but not in the conventional method. This indicates how the transition matrix element affects the self-energy extraction.

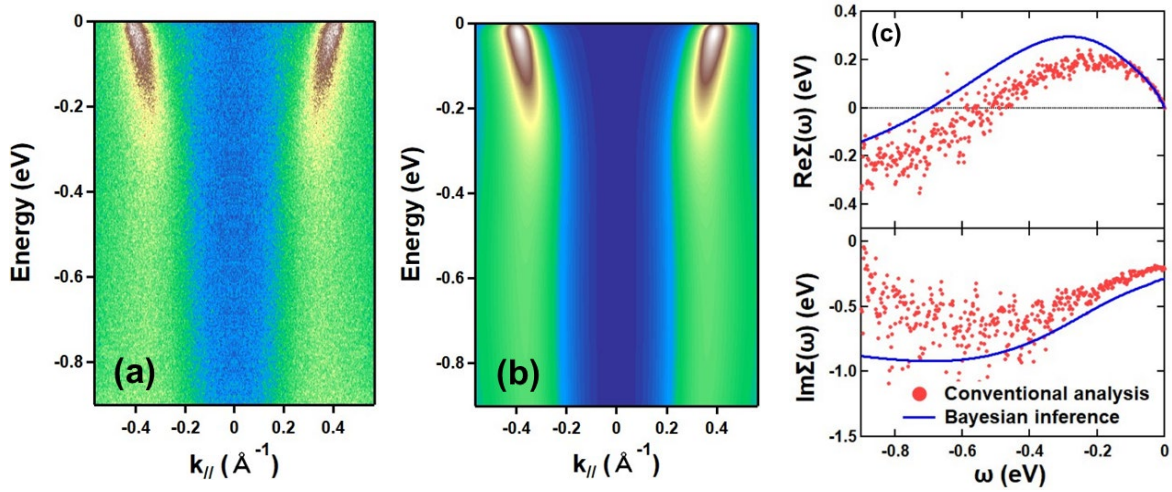

FIGURE 1. (a) Experimental data. (b) ARPES image plot simulated by the Bayesian inference method. (c)

Blue lines indicate evaluated total self-energy. Red dots show self-energy obtained from the conventional analysis method.

REFERENCES

1. S. Tokuda, S. Souma, K. Segawa, T. Takahashi, Y. Ando, T. Nakanishi & T. Sato, *Communications Physics,* **4**, 170 (2021).

22BG006 BL-9A

Momentum dependence of the spectral weight in the single layer high-T_c cuprate $Bi_2Sr_2CuO_{6+\delta}$ studied by ARPES

Y. Onishi[1], Y. Miyai[1], Y. Tsubota[1], S. Kumar[2], M. Atira[2], H. Eisaki[3], S. Ishida[3], K. Shimda[1,2], and S. Ideta[1,2]

[1]*Graduate School of Advanced Science and Engineering, Hiroshima Univ., Japan*
[2]*Hiroshima Synchrotron Radiation Center (HiSOR), Hiroshima Univ., Japan*
[3]*National Institute of Advanced Industrial Science and Technology (AIST), Japan*

Keywords: high- T_c superconductors, ARPES, strongly correlated electron materials, superfluid density

High-transition temperature (T_c) cuprate superconductors have attracted a lot of academic researchers because of their high T_c above ~40 K, which cannot be explained by the BCS theory [1]. The high-T_c superconductivity in cuprates has not been clear so far regardless of extensive studies. To understand the mechanism of high T_c in cuprate superconductivity, one of the essential physical parameters is superfluid density (ρ_s) which plays an important role in determining T_c [2].

In this study, we have performed an angle-resolved photoemission spectroscopy (ARPES) study to reinvestigate the relation between coherent spectral weights (SW) on the Fermi surface directly, which seem to correspond to the magnitude of ρ_s and T_c [3]. We measure the electronic structure of the single-layer Bi-based high-T_c cuprate superconductor, $Bi_2Sr_2CuO_{6+\delta}$ (Bi2201), which has one CuO_2 layer in the unit cell and shows a high T_c of 35 K at optimal doping [4]. In this poster, we present the doping and temperature dependence of SW in Bi2201 by using ARPES. In Fig. 1, we show the observed Fermi surface in the superconducting states. By the detailed comparison of Energy-distribution curves at Femri momentum above and below T_c, we have successfully estimated the momentum dependence of SW on the entire Fermi surface. Unexpectedly, the present result is in contrast with the previous ARPES study [3]. From our study, we will discuss the intrinsic momentum dependence of SW in Bi2201 and the origin of the high T_c in cuprates.

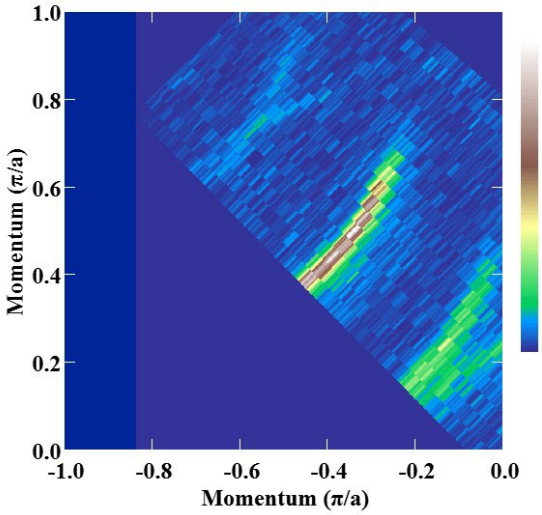

Figure. 1 Fermi surface mapping of Bi2201 taken at $h\nu$ = 17 eV, T = 10K in the superconducting state from the node to the antinode. We clearly see the main Fermi surface which shows the highest ARPES intensity. The other Fermi surfaces are so-called replicas and shadow.

REFERENCES

1. W. L. McMillan, *Phys. Rev.* **167**, 331 (1968).
2. Y. J. Uemura *et al*., *Phys. Rev. Lett.* **66**, 2665 (1991).
3. T. Kondo *et al*., *Nature* **457**, 296 (2009).
4. A. Iyo *et al*., *J. Phys. Soc. Jpn.* **76**, 094711 (2007).

22BG002 BL-14

Characterization of amorphous carbon films by X-ray magnetic circular dichroism

Yuji Muraoka[a], Taishi Kanayama[a], Sho Enomoto[a], Takanori Wakita[a], and Masahiro Sawada[b]

[a]*Research Institute for Interdisciplinary Science, Okayama University, Japan*
[b]*Hiroshima Synchrotron Radiation Center, Hiroshima University, Japan*

Keywords: Amorphous carbon, sp^3, Pulsed laser annealing, XAS

Upon pulsed laser annealing (PLA) with a laser energy density above threshold value, amorphous carbon films are melted and then transformed into allotropes such as Q-carbon, nanodiamond, and reduced graphene oxide, depending on the quench rate during liquid-phase regrowth [1, 2]. Q-carbon, which was recently discovered, has a high sp^3 contents of about 80% and shows excellent physical properties such as hardness superior to that of diamond, room-temperature ferromagnetism, and even high-temperature superconductivity when boron is doped with Q-carbon. Since it has peculiar physical properties, Q-carbon is of interest in terms of both fundamental and application viewpoints [3].

Q-carbon is prepared by irradiating ArF and KrF excimer lasers to the amorphous carbon films. A challenging study is to prepare the Q-carbon by using a YAG solid-state laser with a wavelength of 355 nm. This is because the wavelength of 355 nm is longer than those of excimer lasers (193 nm for ArF laser and 248 nm for KrF laser) and is close to visible light. The successful preparation of Q-carbon by using the 355 nm YAG laser will help expand the preparation condition and accelerate the research for Q-carbon. In this experiment, the 355 nm YAG laser was applied to the PLA treatment for amorphous carbon films and X-ray absorption and X-ray photoemission spectroscopies were employed for characterization of the obtained films .

Amorphous carbon films were prepared using a YAG laser with a wavelength of 355 nm. The same laser was employed for PLA treatments. X-ray absorption spectroscopy measurements were performed at HiSOR BL14. Photoemission spectroscopy measurements were conducted at Spring-8 BL25 SU. All measurements were performed at room temperature.

Figure 1(a) shows XAS spectra at C *K*-edge for amorphous carbon films before and after PLA. A signal related to the sp^3 state was seen at 290 eV. A decrease in the intensity at 290 eV was observed for the film after PLA, suggesting the reduction of sp^3 contents in the film after PLA. Figure 1 (b) shows the photoemission C 1s core-level spectra of the films before and after PLA. Clearly seen was the decrease in the intensity at 285.3 eV which corresponds to the binding energy of sp^3 states in carbon. The sp^3 content was estimated from the area ratio of the sp^2 and sp^3components to be approximately 40% for the film before PLA and 20% for the film after PLA. The sp^3 content in the film is reduced by PLA, which is consistent with the result of XAS measurements.

The sp^3 content in the films is decreased by PLA. The estimated sp^3 content for the film after PLA is smaller than that of Q-carbon. The results show that the quenching rate required for Q carbon formation is insufficient, and suggest that a higher quench speed is needed for obtaining the Q-carbon. Laser energy density for PLA and/or film thickness are effective experimental parameters to improve the quench speed. We believe that Q carbon can be prepared using a YAG laser with a 355 nm wavelength by optimizing experimental conditions.

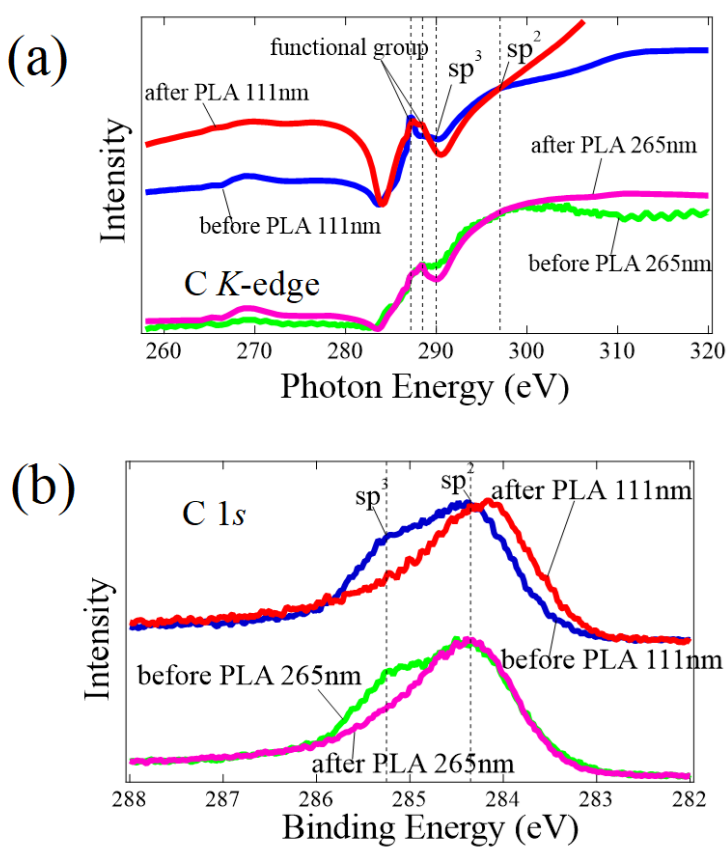

FIGURE 1. (a) XAS spectra at C *K*-edge for amorphous carbon films before and after PLA. The spectral intensity is normalized at 298 eV which corresponds to the signal related to the sp^2 states. (b) Photoemission spectra of C 1s core-level for amorphous carbon films before and after PLA. Photon energy of 1330 eV was used for measurements.

REFERENCES

1. S. Gupta *et al.*, *Appl. Nano Mater.* **3**, 5178 (2020).
2. S. Gupta *et al.*, *JOM.* **70**, 450 (2018).
3. J. Narayan, and A. Bhaumik, *J. Appl. Phys.* **118**, 215303 (2015).

BL-5

Photoemission spectroscopy measurements for phase-separated TiO_2-VO_2 films on mica substrates

Yuji Muraoka[a], Takanori Wakita[a] and Takayoshi Yokoya[a]

[a]*Research Institute for Interdisciplinary Science, Okayama University, 3-1-1 Tsushima-naka, Tsushima, Kita-ku, Okayama 700-8530, Japan*

Keywords: Photoemission spectroscopy, TiO_2, VO_2, Film, Phase separation, Mica substrate

Spinodal decomposition is a phase-separation process in which a material spontaneously decomposes into two phases with distinct composition [1]. This results in the spontaneous formation of microstructures with nanosized compositional fluctuations that have been observed in many oxide systems. A rutile-type TiO_2-VO_2 system is known to exhibit spinodal decomposition in bulk [2], where VO_2 exhibited a metal-insulator transition (MIT) at 340 K upon cooling, accompanied by a structural change from a high-temperature rutile-type tetragonal form to a low-temperature monoclinic form (M1). The TiO_2-VO_2 system showed a characteristic phenomenon, that is, anisotropy in decomposition. Solid solution of $Ti_{0.4}V_{0.6}O_2$ bulk was firstly prepared and annealed below 800 K. The system showed spinodal decomposition along the *c*-axis direction, and a nanometer-scale lamellar structure with alternating stacking of tetragonal Ti-rich and monoclinic V-rich phases was formed while retaining a coherent interface.

The anisotropy in decomposition has been applied to form multilayer structures in TiO_2-VO_2 films, and horizontally, diagonally, and vertically aligned multilayer films have been obtain by using single crystal and glass substrates [3-5]. Such self-organized multilayer structures via phase separation are attracted interest as a bottom-up technology for the fabrication of nanostructured devices. A, challenging research for the self-assembled multilayer structures is to form them on flexible substrates such as a mica substrate. The obtained multilayered films could be used as flexible electronics for applications. So far there is no repot on the formation of multilayer structures via the phase decomposition in TiO_2-VO_2 films on flexible substrates. In this study we prepare the spinodally decomposed TiO_2-VO_2 films on mica substrates and study the electronic states by using photoemission spectroscopy in order to examine the occurrence of the phase decomposition in the films.

The TiO_2-VO_2 films were fabricated on mica substrates using a pulsed laser deposition technique with a YAG laser (λ = 355 nm). To induce spinodal decomposition, thermal annealing was performed at 673 K under an oxygen pressure of 1.3 Pa for 24 h. Photoemission spectroscopy (PES) measurements were carried out on the beamline BL-5, at the Hiroshima Synchrotron Radiation Center in Hiroshima University. The excitation photon energy $h\nu$ of 150 eV was used for measurements and valence band spectra were taken at 300 K and 370 K to examine the occurrence of metal-insulator transition. Before measurements, the films were annealed at 393 K under ultrahigh vacuum (~10^{-6} Pa) for 10 min to clean the film surface.

Figure 1(a) shows the valence band spectra of annealed TiO_2-VO_2 films on mica substrates taken at 300 K. No intensity at the Fermi level was seen, indicating that the film is insulating. On the other hand, the finite intensity at the Fermi level is observed in the spectrum taken at 400 K, showing that the film is metallic. This clearly shows that the annealed film exhibits a metal-insulator transition as increasing temperature from 300 to 400 K. Since the metal-insulator transition originates from the V-rich phase, the PES results indicate the emergence of spinodal decomposition in the annealed TiO_2-VO_2 films on mica substrates.

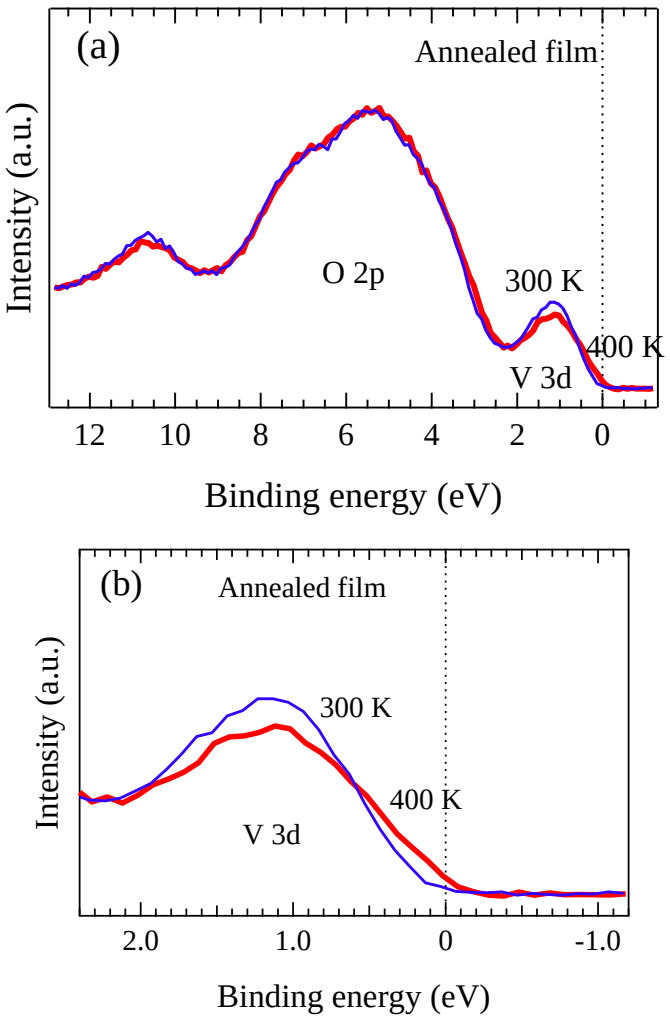

FIGURE 1. (a) Valence band spectra and (b) Near Fermi level spectra of the annealed TiO_2-VO_2 films measured at 300 and 400 K.

REFERENCES

1. J.W. Cahn, *Acta Met.* **9,** 795 (1961).
2. Z. Hiroi *et al.*, *Chem. Mater.* **25,** 2202 (2013).
3. Z. Chen *et al.*, *ACS Nano* **10,** 10237 (2016).
4. G. Sun *et al.*, Sci. Rep. **8,** 5342 (2018).
5. Y. Muraoka *et al.*, *Thin Solid Films* (2023) accepted.

22AG035 BL-5

Current Activities of Research and Education on BL-5 (FY2022)

T. Yokoya[a,b], T. Wakita[a] and Y. Muraoka[a,b]

[a]*Research Institute for Interdisciplinary Science, Okayama University*
[b]*Research Laboratory for Surface Science, Okayama University, Okayama 700-8530, Japan*

Keywords: Photoemission spectroscopy, photoelectron emission microscopy

We present an overview of our resent research and educational activities on beamline 5 (BL5) in the fiscal year 2022. Our beamline has two experimental stations in a tandem way. The first station is equipped with an angle-resolved photoemission spectrometer (ARPES), a low energy electron diffraction (LEED) apparatus and an X-ray source. The hemispherical analyzer of ARPES spectrometer (HA54, VSW) has a mean radius of 50 mm and is mounted on a twin axis goniometer in ultra-high vacuum chamber. Using this goniometer, one can perform ARPES and photoelectron diffraction (PED) measurements. It is also possible to perform resonant photoemission spectroscopy (RPES) measurements by using photon energy tunability of synchrotron radiation with X-ray absorption spectroscopy (XAS) measurement. With the X-ray source (XR2E2, FISONS), we can perform an X-ray photoelectron spectroscopy (XPS) measurement for the chemical state analysis and the PED. At the second station, we have installed a photoelectron emission microscope (PEEM, 'PEEM III', Elmitec). PEEM provides a magnified image of lateral intensity distribution of photo-emitted electrons from a sample surface. The spatial resolutions are several ten nanometers with Hg lamp and a few micrometers with synchrotron radiation. The sample is transferred between the ARPES and the PEEM chamber in-situ, and one can perform measurements at both stations for the same sample.

In the recent researches on BL-5, we have studied the electronic structure of potassium doped aromatic molecule (K_x picene) [1], iron-based superconductor ($FeSe_xTe_{1-x}$) [2], transition metal di-oxide films such as VO_2 thin films which exhibits a first-order metal-to-insulator transition at 340 K [3], CrO_2 thin films which are known as a half-metallic material [4], TaO_2 film which is stabilized with a new technique developed in our group [5], and phase-separated TiO_2-VO_2 films on mica substrates. We have also studied the electronic structures of a high-quality boron-doped diamond film which shows a signature of the highest superconducting transition temperature of 25 K [6] and a high quality single crystal of $YbFe_2O_4$ which is one of multiferroic materials [7], by utilizing RPES at B *K*- and Fe $M_{2,3}$- edges, respectively. In addition, we have studied the sp^3 content in diamond-like carbon films by using photoemission spectroscopy in order to optimize the conditions to produce Q-carbon (quenched carbon) which is a newly discovered amorphous phase of carbon with several exotic properties [8]. In this fiscal year, we have performed PEEM and TEY measurements at BL5 in HiSOR for a B-doped carbon nano wall film on a Si substrate and a micro-droplet of solidified L-boronophenylalanine on a Si substrate in order to investigate microscopic chemical states of trace B atoms in them from fine structures in local- and wide-area-XAS spectra near B *K*-edge and to visualize B distributions on their surfaces.

Recently, we have prepared an auto-measurement system and an X-ray focusing capillary lens for photoemission holography (PEH). PEH is a method that has been greatly developed in Japan in recent years as a measurement method for elucidating the local structure of materials with an atomic resolution [9]. In particular, various results have been reported in the study of the three-dimensional atomic configurational structure around the dopants in crystals [10]. However, the opportunity to use state-of-the-art apparatuses (for example, DA30 analyzer and RFA of BL25SU at SPring-8) are limited. Although our photoelectron energy analyzer is an old model and it is difficult to separate and observe small shifts in core levels because of the energy resolution of 1-2 eV of the system, preliminary experiments on undoped materials can be carried out with our apparatus before the experiment using the latest ones. It can also be used for educational purposes such as experiencing photoelectron holography experiments and learning the analysis methods.

We have used the BL-5 for education activity as well, for example, practical education for undergraduate students of Okayama University. The students have an opportunity to study the synchrotron radiation mechanism and to experience XPS measurement which is very useful for the surface science research. We accepted more than 100 students from 2006 to 2012. From 2014, we have started to join the practical lecture for experiments using the beamline end stations in HiSOR for both graduate school students of Hiroshima and Okayama Universities. In 2018, we have had a new project for education under a Japan-Asia youth exchange program in science supported by Japan Science and Technology Agency (JST), "Sakura Exchange Program in Science". We have accepted six students from Changchun University of Science and Technology in China.

REFERENCES

1. H. Okazaki *et al*., *Phys. Rev* **82**, pp. 195114 (5 pages) (2010).
2. Y. Yoshida *et al*., *J. Phys. Soc. Jpn* **78**, pp. 034708 (4 pages) (2009).
3. K. Saeki *et al*., *Phys. Rev* **80**, pp. 125406 (5 pages) (2009).
4. Y. Muraoka *et al*., *MRS Proceedings* **1406** (2012).
5. Y. Muraoka *et al*., *Thin Solid Films* **599**, pp. 125-132 (2016).
6. H. Okazaki *et al*., *Appl. Phys. Lett* **106**, pp. 052601 (5 pages) (2015).
7. K. Fujiwara *et al*., *Trans. Mater. Res. Soc. Jpn.* **41**, pp. 139-142 (2016).
8. H. Yoshinaka *et al*., *Carbon.***167**, pp. 504-511 (2020).
9. T. Matsushita *et al*. *Europhys. Lett*. **71**, 597 (2005). *Phys. Status Solidi B* **255**, 1800091 (6 pages) (2018).
10. K. Hayashi, T. Matsushita, *SPring-8 Research Frontiers* **2020**, pp. 12 -15 (2021).

22AG035 BL-5

Visualization of boron distributions on inorganic and organic material surfaces by PEEM

Takanori Wakita[a], Kazuyo Igawa[b], Miyu Kaneda[c], Naoshi Ikeda[c], Hiroaki Terato[d], Yuji Muraoka[a,c], Takayoshi Yokoya[a,c]

[a]*Research Institute for Interdisciplinary Science, Okayama University*
[b]*Neutron Therapy Research Center, Okayama University*
[c]*Graduate School of Natural Science and Technology, Okayama University*
[d]*Advanced Science Research Center, Okayama University*

Keywords: Photoemission electron microscopy, local X-ray absorption spectroscopy, elemental distributions

Visualization of microscopic elemental distributions for a small amount of ingredients in inorganic and organic materials has an essential role in developing new functional features for them, especially where their distributions are inhomogeneous. Electron probe micro analyzer (EPMA) has been widely used in visualization of microscopic elemental distributions on various material surfaces as one of the most popular techniques, by means of combination of a scanning electron microscope and an X-ray fluorescence analyzer [1]. X-ray fluorescence is produced via relaxation of core-holes excited, in this case, by an electron beam, which is therefore element specific in nature. For light elements such as boron (B), however, Auger transition rates are more than 99.9% in their core-hole relaxation processes, which means that detection of trace light elements by X-ray fluorescence has difficulty. In contrast, X-ray absorption spectroscopy (XAS) with total electron yield (TEY) is suitable to detect trace light elements because TEY is proportional to the amount of secondary electrons generated mainly by Auger electrons [2]. The intensity of photoemission electron microscope (PEEM) is also proportional to the TEY intensity when it is used with X-ray as a light source and without both an energy filter and an energy analyzer [3]. One can obtain a local XAS spectrum by plotting intensities in a certain area on a series of PEEM images as a function of X-ray energies. In addition, an elemental distribution image can be obtained as a difference image of two PEEM images measured at X-ray energies of (1) a pre-edge and (2) a peak position above a certain absorption edge.

In this study, we have performed PEEM and TEY measurements at BL5 in HiSOR for inorganic and organic samples in order to investigate microscopic chemical states of trace B atoms in them from fine structures in local- and wide-area-XAS spectra near B *K*-edge and to visualize B distributions on their surfaces. The experimental station of BL5 is equipped with a PEEM III (Elmitec GmbH) and with a manipulator connected to a digital amperemeter for a TEY measurement. As a light source, the second-order X-rays from the monochromator were used because they have higher intensity and energy resolution around B *K*-edge than the first-order X-ray from the monochromator with the same entrance and exit slit widths. All the measurements were performed at room temperature.

As an inorganic sample, we have used a B-doped carbon nano wall (CNW) film on a Si substrate which are newly grown by using a plasma CVD method with a mixture of carbon and B_4C powders. For an estimation of the B concentration of the sample, we have performed photoemission spectroscopy (PES) measurements of C 1s and B 1s core-levels with an angle-resolved PES (ARPES) apparatus at BL5 (the ARPES and the PEEM III chambers have been installed tandemly in the experimetal station). The X-ray energy was set to 634 eV for C 1s and 534 eV for B 1s, respectively, as intending that the kinetic energies of both signals have the same values (about 340 eV) and therefore the probing depth of the photoelectrons the same values (about 0.8 nm [4]). The B concentration was estimated by using the integrated intensities of the core-level spectra (not shown) as about 4 %.

Figure 1 (a) shows that a PEEM image of a B-doped CNW film surface on a Si substrate measured with Hg lamp, showing 2 dimensional local work function distribution for it. The field of view is 150 μm. The PEEM image has flat area and small protrusions. Figure 1 (b) shows plots of averaged intensities per a pixel in squares A (red, protrusion area) and B (green, in flat area) as a function of X-ray energy around B K-edge,

where both squares have a side length of about 21.5 μm. The red and green curves in figure 1 (b) show noisy jagged shapes, probably due to the effect of repeated charging and discharging caused by the (weak) insulating nature of the film (a strong insulating nature will produce just a strong charging effect). Despite of the noisy jagged shapes, strikingly, the blue curve in figure 1 (c) obtained after division of the red one by the green one in figure 1 (b) shows a clear near edge structure which closely resembles the XAS spectrum reported for B_4C bulk [5], revealing existence of B_4C-rich regions on a B-doped CNW film surface. In contrast, XAS spectrum measured by TEY (black curve in figure 1 (c)) has a different spectral shape from the local XAS spectrum for the protrusions and is similar with ones for B-rich boron carbide thin films and B crystalline powders [5], where the TEY-XAS spectrum provides an averaged information of the sample surface from a wide area illuminated by X-ray (the size of X-ray is about 1 x 5 mm^2 on the sample surface). Figure 1 (d) shows a difference image of PEEM images measured with X-rays of 188 and 191 eV. We consider that the bright areas indicate B_4C-rich regions, which seem to roughly correspond to protrusions.

As an organic sample, we are proceeding measurements for a micro-droplet of solidified L-boronophenylalanine (BPA) on a Si substrate which is one of boron delivery drugs developed to use for boron neutron capture therapy (BNCT, a type of radiation therapy for cancer treatment [6]). In addition, we are addressing visualization of boron distribution in cancer cells dosed with BPA in order to obtain useful information for development of a new boron delivery agent which possesses advantages over BPA.

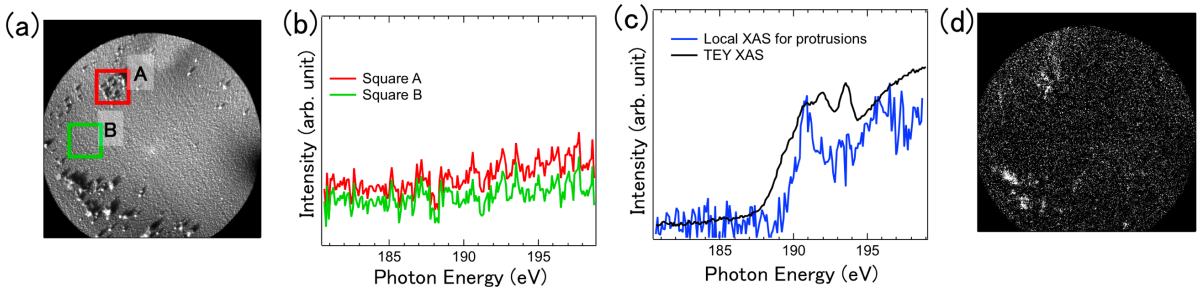

FIGURE 1. (a) PEEM image of a B-doped CNW film surface on a Si substrate measured with Hg lamp. The field of view is 150 μm. (b) Plots of averaged intensities per a pixel in squares A (red, protrusion area) and B (green, in flat area) in (a) as a function of X-ray energy around B *K*-edge, where both squares have a side length of about 21.5 μm. (c) Local XAS spectrum (blue) for the protrusions obtained after division of the red one by the green one in (b) and XAS spectrum (black) measured by TEY where the size of X-ray is about 1 x 5 mm^2 on the sample surface. (d) Difference image of PEEM images measured with X-rays of 188 and 191 eV.

REFERENCES

1. J. I. Goldstein *et al*., *Scanning electron microscopy and X-ray microanalysis 4th ed.*, Springer (2017).
2. A. Erbil *et al*., Phys. Rev. B **37**, 2450 (1988).
3. A. Locatelli and E. Bauer, J. Phys.: Condes. Matter **20**, 093002 (2008).
4. A. Zangwill, *Physics at surfaces*, Cambridge university press (1988).
5. I. Jiménez *et al*., J. Electron Spectrosc. Relat. Phenom. **101-103**, 611 (1999).
6. H. Nakashima, YAKUGAKU ZASSHI **142**, 155-164 (2022)

21BU007 BL-6

X-ray absorption spectroscopy of photodamaged polyimide film

○Osamu Takahashi[a,d] , Takuma Ohnishi[a,d], Ryosuke Yamamura[a,d], Eiichi Kobayashi[b], Kenta Kubo[c,d], Mayako Okazaki[c,d], Yuka Horikawa[c,d], Masaki Oura[d], and Hiroaki Yoshida[a,e]

[a]*Basic Chemistry Program, Graduate School of Advanced Science and Engineering, Hiroshima University*
[b]*Kyushu Synchrotron Light Research Center, 8-7 Yayoigaoka, Tosu, Saga 841-0005, Japan*
[c]*Department of Physics and Information Science, Yamaguchi University, Japan*
[d]*RIKEN SPring-8 Center, Kouto, Sayo-gun, Hyogo 679-5148, Japan*
[e]*Hiroshima Synchrotron Radiation Center, Hiroshima University, Kagamiyama, Higashi-Hiroshima, 739-0046, Japan*
Continue Here

Keywords: XAS, Polyimide, theoretical calculation

Polyimide, Capton, is a kind of organic polymers including imide bonds, and it has high electrical insulation and mechanical strength, and is used in a variety of applications such as insulating films. It is also known that it has gradually a damage due to light irradiation, but the mechanism is still controversial and the details are not well understood.

In the present study, photo-damaged mechanism is examined by visible light using X-ray absorption spectroscopy (XAS). Photo-damaged polyimide films for 24 – 96 hours are prepared in advance. Then XAS spectra are obtained XAS spectra at C, N, and O K-edges. XAS of polyimide film at the O K-edge is shown in Figure 1. Light irradiation for 48 hours or more shows broadening of the peak at 533 eV derived from the product oxidized by C-N bond cleavage. And by theoretical calculations using density functional theory, XAS spectra of monomer model and corresponding dissociated products are produced.

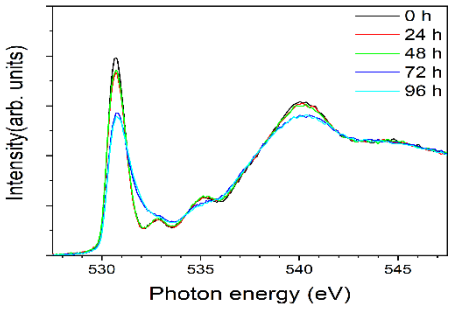

FIGURE 1. XAS spectra of polyimide film at O K-edge.

22AG002, 22BU007 BL-7

Investigating the possibility of creating a "pure" p-type Bi_2Se_3

Yuki Higuchi[a], Ryota Itaya[a], Mito Tomita[a], Harutaka Saito[b], Katsuhiro Suzuki[b], Hitoshi Sato[c], Kazunori Sato[b,d], and Kazuyuki Sakamoto[a,d]

[a] *Department of Applied Physics, Osaka University, Osaka 565-0871, Japan*
[b] *Division of Materials and Manufacturing Science, Osaka University, Osaka 565-0871, Japan*
[c] *Hiroshima Synchrotron Radiation Center, Hiroshima University, Higashi-Hiroshima 739-0046, Japan*
[d] *Spintronics Research Network Division, OTRI, Osaka University, Osaka 565-0871, Japan*

Keywords: Topological insulator, Bi_2Se_3, ARPES, QSGW calculation

Three-dimensional topological insulators (TIs), which hold spin-polarized Dirac cone type metallic bands on the surface while the bulk is insulating, are promising materials to realize next-generation spintronics devices. For example, controlling the Fermi level by, *e.g.,* charge doping, and making both n-type and p-type from a single TI sample will allow to create p-n topological junction [1-4], a device that has a great possibility to solve the problem of processing the explosive volume of information, which cannot be solved by the existing electronics technology based solely on the charge degrees of freedom. Bi_2Se_3 is a typical n-type TI whose bulk valence band maxima (BVBM) was predicted to located close to the Dirac point (DP) both theoretically and experimentally [5-8]. This means that even by doping the sample and tuning the Fermi level below the DP, it is impossible to create a "pure" p-type Bi_2Se_3, because the bulk band crosses the Fermi level simultaneously. This situation makes the spin-polarized surface electrons diffusing into the bulk, and therefore difficult to generate a highly efficient spin current in practical applications.

In this study, we performed state-of-the-art ARPES measurements and DFT calculations to obtain precise information on the bulk band behavior to have a proper understanding on the electronic structure of Bi_2Se_3, and to discuss the feasibility of this TI for spintronics devices. ARPES measurements were performed at the beamline BL-7 of HiSOR. The bulk band along the $\bar{\Gamma}-\bar{\mathrm{M}}$ direction, the direction where the BVBM was predicted to be above the DP, was measured using photon energies ($h\nu$) from 33 eV to 89 eV. This $h\nu$ range covers more than a single Brillouin zone along the $k_\perp$ direction. Fig. 1(a) shows the band structure obtained at $k_\perp = 4.10\ \text{Å}^{-1}$ and Figs. 1(b)-(d) are the $k_\perp$-dependent EDCs measured at different $k_\parallel$. The band structure in Fig. 1(a) shows that the BVBM is located at the $\bar{\Gamma}$ point and below the DP, and a saddle-like-valence band (SVB) to be present along the $\bar{\Gamma}-\bar{\mathrm{M}}$ direction. Furthermore, the EDCs in Figs. 1(b)-(d) show that the BVMBs are located below the DP throughout the entire 3D Brillouin zone, and the SVB to show a $k_\perp$ dependence. In order to confirm these experimental results, we have performed DFT calculations using the Quasiparticle Self Consistent GW (QSGW) [9-11], a method that has the property of showing the band gap more accurately than the DFT calculations used in former studies. Two types of projected bulk band are shown in Fig. 2 (a) and(b). The theoretically obtained results using QSGW indicates the BVBM to be located at the Γ point, and therefore strongly support our experimental results. The present results also suggest that it is possible to make a "pure" p-type Bi_2Se_3 by hole-doping, and therefore the possibility of using this TI as a material to realize novel spintronics devices.

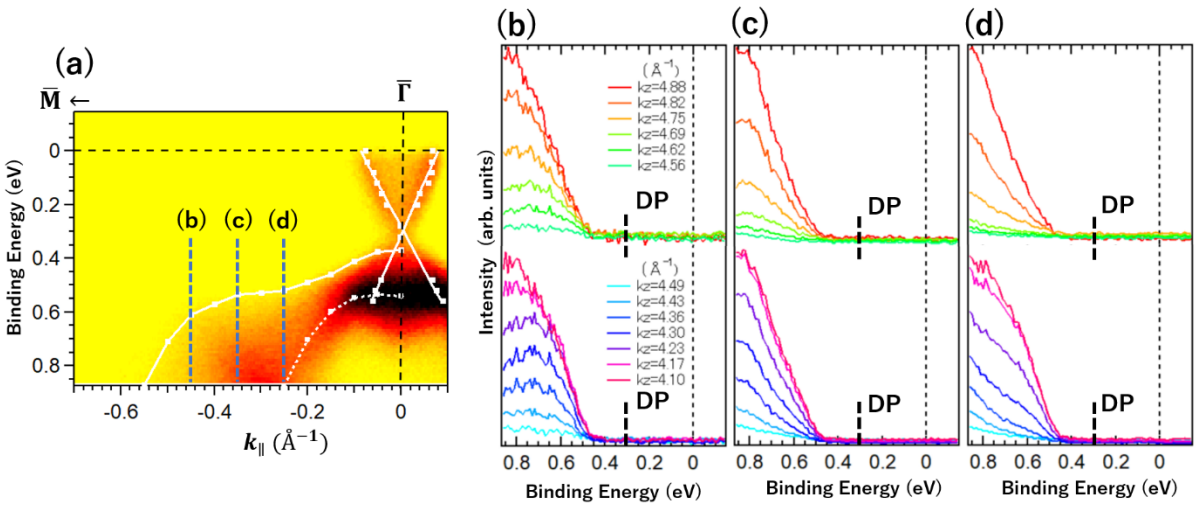

Figure 1. (a) Band structure of Bi_2Se_3 along $\bar{\Gamma} - \bar{M}$ at $k_\perp = 4.10$ Å^{-1}, and (b)-(d) $k_\perp$-dependent EDCs at different $k_\parallel$. $k_\perp = -0.45$ Å^{-1} in (b), -0.35 Å^{-1} in (c), and -0.25 Å^{-1} in (d). The range of $k_\perp$ is larger than that of single Brillouin zone.

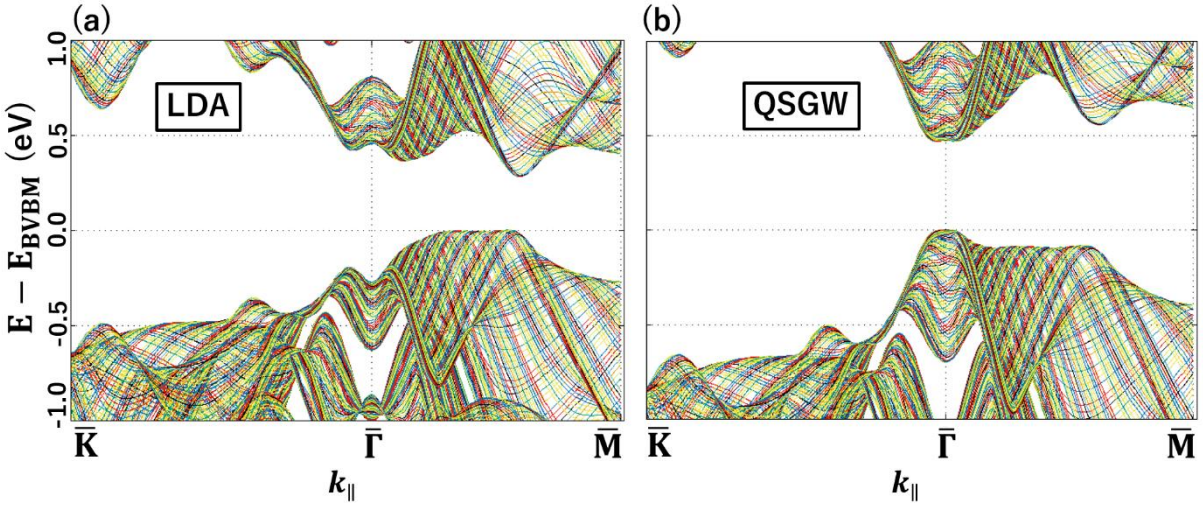

Figure 2. Theoretical projected bulk band structure along the $\bar{K} - \bar{\Gamma} - \bar{M}$ direction of the 2D Brillouin zone obtained using (a) LDA and (b) QSGW.

REFERENCES

1. J.-L. Mi, M. Bremholm, M. Bianchi, K. Borup, S. Johnsen, M. Søndergaard, D. Guan, R. C. Hatch, P. Hofmann, B. B. Iversen, *Adv. Mater.* **25**, 889 (2013).
2. N. H. Tu, Y. Tanabe, Y. Satake, K. K. Huynh, K. Tanigaki, *Nat. Commun.* **7**, 13763 (2016).
3. S. H. Kim, H.-H. Jin, B. W. Kho, B.-G. Park, F. Liu, J. S. Kim, and H. W. Yeom, *ACS Nano* **11**, 9671 (2017).
4. K. Sakamoto, H. Ishikawa, T. Wake, C. Ishimoto, J. Fujii, H. Bentmann, M. Ohtaka, K. Kuroda, N. Inoue, T. Hattori, T. Miyamachi, F. Komori, I. Yamamoto, C. Fan, P. Krueger, H. Ota, F. Matsui, F. Reinert, J. Avila, and M. C. Asensio, *Nano Lett.* **21**, 4415 (2021).
5. H. Chang, C.-X. Liu, X.-L. Qi, X. Dai, Z. Fang, and S.-C. Zhang, *Nature Phys.* **5**, 438 (2009).
6. Y. Xia, D. Qian, D. Hsieh, L. Wray, A. Pal, H. Lin, A. Bansil, D. Grauer, Y. S. Hor, R. J. Cava and M. Z. Hasan, *Nature Phys.* **5**, 398 (2009).
7. S. Kim, M. Ye, K. Kuroda, Y. Yamada, E. E. Krasovskii, E. V. Chulkov, K. Miyamoto, M. Nakatake, T. Okuda, Y. Ueda, K. Shimada, H. Namatame, M. Taniguchi, and A. Kimura, *Phys. Rev. Lett.* **107**, 056803(2011).
8. O. V. Yazyev, J. E. Moore, and S. G. Louie, *Phys. Rev. Lett.* **105**, 266806(2010).
9. T. Kotani, M. v. Schilfgaarde and S. V. Faleev, *Phys. Rev. B* **76**, 165106 (2007).
10. I. A. Nechaev, R. C. Hatch, M. Bianchi, D. Guan, C. Friedrich, I. Aguilera, J. L. Mi, B. B. Iversen, S. Blugel, Ph. Hofmann, and E. V. Chulkov, *Phys. Rev. B* **87**, 121111(R) (2013).
11. I. Aguilera, C. Friedrich, and S. Blügel, *Phys. Rev. B* **100**, 155147(2019).

22AG010/22BG014 BL-1/BL-9A

Observation of electron structure of chiral magnet $Yb(Ni_{1-x}Cu_x)_3Al_9$ by ARPES

Y. Tanimoto[a], M. Sugimoto[b], R. Kamimori[a], H. Sato[c], M. Arita[c], S. Kumar[c], K. Shimada[c], S. Nakamura[d], S. Ohara[d]

[a]*Graduate School of Advanced Science and Engineering, Hiroshima University, Higashi-Hiroshima 739-8526, Japan*
[b]*Faculty of Science, Hiroshima University, Higashi-Hiroshima 739-8526, Japan*
[c]*Hiroshima Synchrotron Radiation Center, Hiroshima University, Higashi-Hiroshima 739-0046, Japan*
[d]*Graduate School of Engineering, Nagoya Institute of Technology, Nagoya 466-8555, Japan*

Keywords: chiral magnetic crystal, helical magnetism, angle resolved photoemission spectroscopy

Trigonal $YbNi_3Al_9$ has a chiral crystal structure belonging to space group of *R*32 (No. 155) and is of interest as the first chiral magnetic alloy discovered in 4*f* electron compounds [1]. The localized Yb 4*f* spins are magnetically ordered below T=3.4 K, ferromagnetic in the *ab*-plane, and exhibit left-handed or right-handed helical magnetism with period q_z=0.8 in the *c*-axis direction [2]. Substitution of Ni with Cu significantly alters the magnetic interaction and shortens the helical period to q_z=0.4 for $Yb(Ni_{0.94}Cu_{0.06})_3Al_9$. Spin-polarized conduction electrons are thought to be responsible for this phenomenon. In this study, angle-resolved photoemission spectroscopy (ARPES) was performed on $YbNi_3Al_9$ and $Yb(Ni_{0.94}Cu_{0.06})_3Al_9$ to investigate the band structure of conduction electron bands near the Fermi level (E_F). Single crystals used for the ARPES measurements were synthesized by the flux-method [3]. The experiments were performed at BL-1 and BL-9A of Hiroshima Synchrotron Radiation Center (HSRC), Hiroshima University.

Figures 1(a) and (b) show the ARPES intensity plots of $YbNi_3Al_9$ measured at $h\nu$=24 eV with *p*-polarized geometry along the $\bar{\Gamma}$-$\bar{M}$ and $\bar{\Gamma}$-$\bar{K}$ directions of the surface Brillouin zone, respectively. Some hole-like bands around the $\bar{\Gamma}$ point and an electron-like band around the $\bar{M}$ point cross E_F. The bands located at around E_B=2.0~3.0 eV are due to the Ni 3*d* states. A parabolic band with a top of E_B~3.0 eV centered at the $\bar{\Gamma}$ point is also observed.

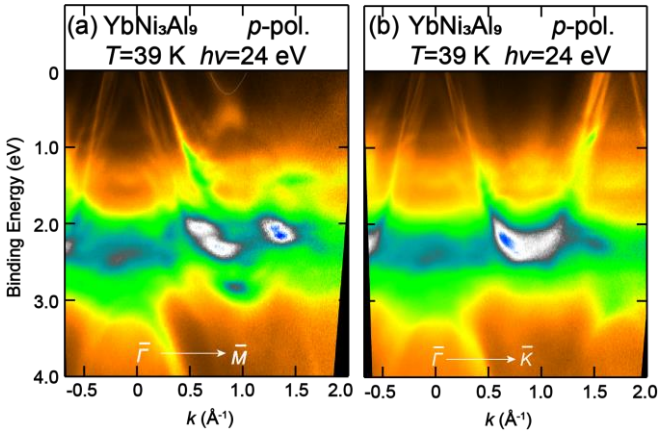

Fig. 1. ARPES intensity plots of $YbNi_3Al_9$ measured along (a) $\bar{\Gamma}$-$\bar{M}$ and (b) $\bar{\Gamma}$-$\bar{K}$ directions measured at $h\nu$=24 eV with *p*-polarized geometry.

Figures 2(a) and (b) represent the Fermi surfaces of $YbNi_3Al_9$ measured at $h\nu$=24 eV with *p*- and *s*-polarized geometries. The horizontal and vertical axes are the wavenumbers (k_x, k_y) along $\bar{\Gamma}$-$\bar{K}$ and $\bar{\Gamma}$-$\bar{M}$ directions, respectively. In Fig. 2(a), five hole-like Fermi surfaces, (a)~(e), were observed around the $\bar{\Gamma}$

point. The bands (b)~(e) in Fig. 2(a) correspond to the bands (b')~(e') in Fig. 2(b). The band (b) appears three-fold symmetric, reflecting the trigonal crystal structure with the three-fold symmetry. On the other hand, the (f) band at k_x=0.6~0.9 Å^{-1} and k_y=0.3~0.6 Å^{-1} in Fig. 2(a), which is not detected in Fig. 2(b), is an electronic-like Fermi surface. The (f) band has six-fold symmetry.

The Fermi surfaces of $Yb(Ni_{0.94}Cu_{0.06})_3Al_9$ becomes smaller in comparison with that of $YbNi_3Al_9$, although the feature is almost unchanged. This observation indicates the electron doping due to the substitution of Ni ion with Cu. The spin-resolved ARPES measurements for $YbNi_3Al_9$ are in progress.

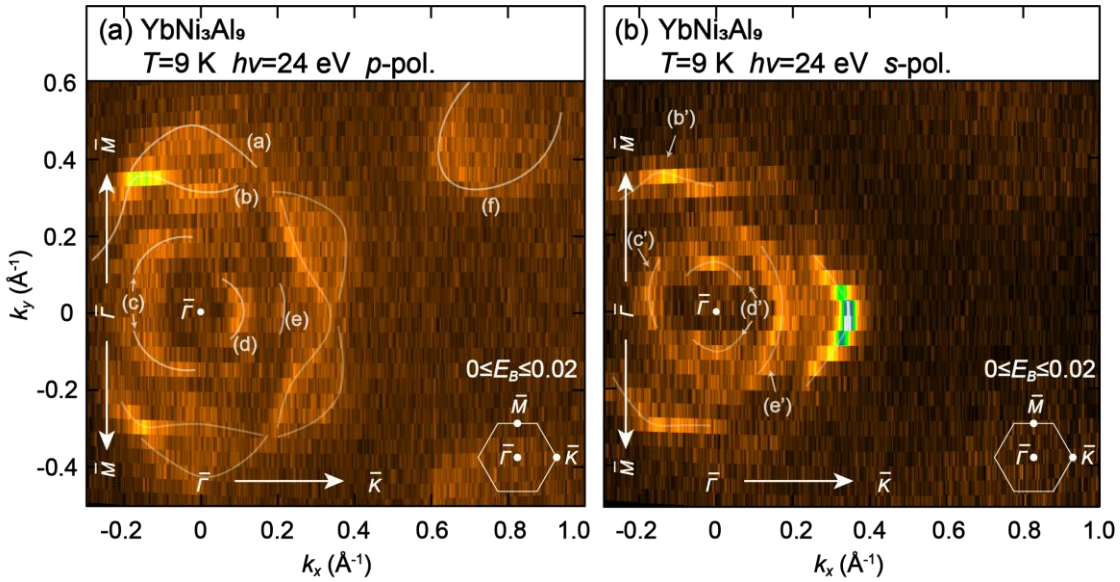

Fig. 2. Fermi surfaces of $YbNi_3Al_9$ measured at $h\nu$=24 eV with (a) *p*- and (b) *s*-polarized geometries.

REFERENCES

1. S. Ohara, S. Fukuta, K. Ohta, H. Kono, T. Yamashita, Y. Matsumoto and J. Yamaura, JPS Conf. Proc. **3**, 017016 (2014).
2. T. Matsumura, Y. Kita, K. Kubo, Y. Yoshikawa, S. Michimura, T. Inami, Y. Kousaka, K. Inoue and S. Ohara, J. Phys. Soc. Jpn. **86**, 124702 (2017).
3. T. Yamashita, R. Miyazaki, Y. Aoki and S. Ohara, J. Phys. Soc. Jpn. **81**, 034705 (2012).

22BU001, 22BU002, 21BG014, 21BG015, 21AU001, 21AU007, 20AG023, 20AG024 BL-7, RIPES

Changes in Electronic States in Gd-TM metallic glasses Rejuvenated by Temperature Cycling

Shinya Hosokawa and Kentaro Kobayashi

Institute of Industrial Nanomaterials, Kumamoto University, Kumamoto 860-8555, Japan

Keywords: Metallic glasses, Rejuvenation effect, Temperature cycling, Electronic structures, Core levels

Rejuvenation in glasses is defined as an excitation to a higher energy state by an external stress, the opposite of the usual relaxation by thermal annealing. A rejuvenation effect by a temperature cycling in metallic glasses (MG) was recently reported by Ketov *et al*. on a $La_{55}Ni_{10}Al_{35}$ bulk MG [1]. They found such a rejuvenation effect by cycling between liquid N_2 and room temperatures in several macroscopic properties. According to their interpretation, the thermal expansion coefficient has a distribution over a glass sample if it is not elastically homogeneous. By repeated temperature changes, the different magnitudes of thermal expansion at different positions in a glass induces shearing forces, and as a result, a rejuvenation effect occurs in the glass. They called this 'Rejuvenation of metallic glasses by non-affine thermal strain' [1]. The validity of this picture is the subject of intensive debate.

Hufnagel reviewed thermal cycling rejuvenation effect, named as 'cryogenic rejuvenation', and suggested that non-affine deformation must be caused on an atomistic length scale [2]. The extent of the heterogeneity of glasses can be judged by the magnitude of so-called β-relaxation peak in dynamical mechanical analysis (DMA) spectra, and large peaks were detected in Gd-transition metal (TM) glasses by Yamasaki [3]. By referencing these ideas and results, we recently measured high energy x-ray diffraction (HEXRD) and anomalous x-ray scattering (AXS) on a $Gd_{65}Co_{35}$ metallic glass by comparing before and after the temperature cycling, and the structural data were analyzed by reverse Monte Carlo modeling [4]. Tiny but clear structural changes are observed by HEXRD in the nearest neighboring region of the real space pair distribution function. Partial structural information obtained by AXS reveals that slight movements of the Gd and Co atoms occur in the first- and second peaks in the nearest neighboring shells around the central Gd atom. We expect that electronic structures may be largely affected by these structural changes by the cryogenic rejuvenation.

In this series of experiments, we carried out photoemission and inverse-photoemission spectroscopies (PES and IPES) on $Gd_{65}TM_{35}$ (TM = Co and Ni) metallic glasses to clarify the rejuvenation effects in the valence- and conduction band densities of states (DOSs) in these glasses, respectively. Master $Gd_{65}TM_{35}$ ingots were manufactured by arc-melting a mixture of pure Gd and TM metals in an Ar atmosphere. The purities of Gd, Co, and Ni were 99.95, 99.999, and 99.999 at.%, respectively. Glassy foils with a thickness of about 20 μm and width of about 2 mm were prepared by melt spinning with a single Cu roll in a pure Ar atmosphere. The concentration was confirmed to be within 0.5 wt.% of the nominal values by electron-probe micro-analysis. A thermal cycling treatment was made between liquid N_2 and room temperatures 40 times, and all the experiments were performed for the same sample foils before and after the above temperature cycling.

The PES spectra were measured using a spectrometer installed at BL-7 of Hiroshima Synchrotron Radiation Center (HSRC). Ultraviolet photons generated from a compact electron-storage ring (HiSOR) were monochromatized with a Dragon-type monochromator, covering the incident photon energy, $h\nu$, values from 20 to 450 eV. A PES spectrometer with a hemispherical photoelectron energy-analyzer (GAMMA-DATA, SCI- ENTA SES2002) attached to the analyzer chamber under the ultrahigh vacuum below 1×10^{-8} Pa at the end-station of BL-7, was used for the PES experiments. The overall energy resolution, ΔE, of the spectrometer was about 0.1-0.5 eV depending on the $h\nu$ values of 20-450 eV. All the PES spectra were collected at room temperature. Clean surfaces were in situ obtained by sputtering the samples with Ar^+ ions in a sample preparation chamber with the base pressure below 1×10^{-8} Pa. The energies of all spectra were defined with respect to the Fermi energy, E_F, of the sample or a freshly evaporated Au film.

The IPES experiments were carried out at the resonant IPES spectroscopy (RIPES) station in the HSRC. The self- developed IPES spectrometer is equipped with a low-energy electron gun, a non-periodic spherical grating, and a one-dimensional photon detector. The total energy resolution was ~0.5 eV at the electron gun energy E_k of 50 eV. The energy of the IPES spectra is referred to E_F, determined from the Fermi edge of the IPES spectra of a Au film. All the IPES experiments were also carried out at room temperature. Clean surfaces were in situ obtained by scraping the samples with a diamond filer in a sample preparation chamber attached with the analyzer one, both of which were kept under ultrahigh vacuum below 1×10^{-8} Pa.

Left panel of Fig. 1 shows the valence-band PES spectra on the $Gd_{65}Co_{35}$ glass at $h\nu$ of 40-230 eV before (blue curves) and after (red curves) the cryogenic rejuvenation. The spectral features drastically change with varying $h\nu$. Right panel of Fig. 1 shows the $h\nu$ dependence of photoionization cross-sections of Gd 4*f*, 5*d*, and 6*s*, and Co 3*d* and 4*s* electrons. By taking this figure into account, the peaks in the ranges around -5 and -8 eV are mainly composed of the Co 3*d* and Gd 4*f* electrons, respectively. By the cryogenic rejuvenation, only the Co 3*d* peak largely decreases.

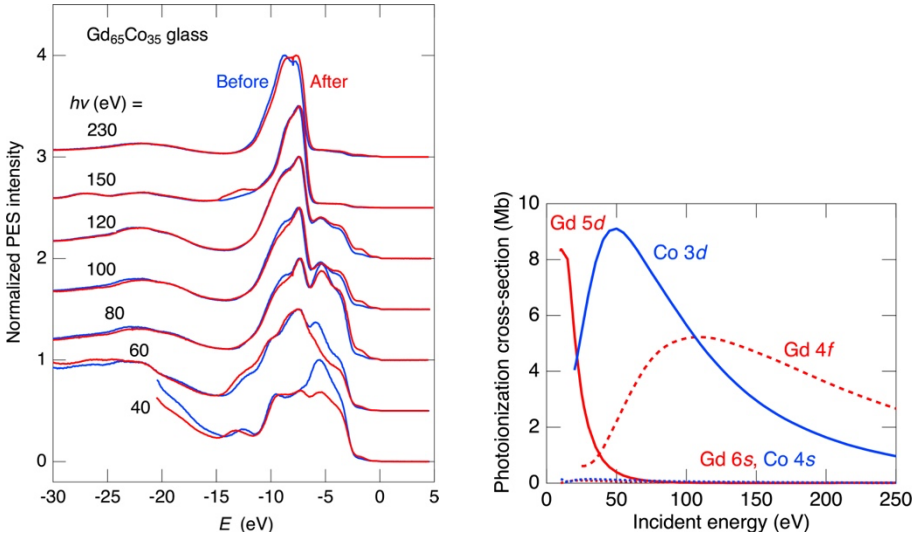

FIGURE 1. (Left) Valence-band PES spectra on $Gd_{65}Co_{35}$ glass before (blue curves) and after (red curves) the cryogenic rejuvenation. (Right) Incident photon energy dependence of the photoionization cross-sections of Gd 4*f*, 5*d*, and 6*s*, and Co 3*d* and 4*s* electrons.

Left and right panels of Fig. 2 show the Gd 4*d* and Co 3*p* core-level PES spectra on the $Gd_{65}Co_{35}$ glass measured at $h\nu$ = 230 eV. By the temperature cycling, the peak in the Gd 4*d* spectrum at about -142 eV slightly shifts towards the shallower energy direction, while the peak in the Co 3*p* spectrum at about -60 eV looks mostly unchanged, suggesting the chemical mature of the Gd atoms may be slightly changed reflecting the structure changes by the rejuvenation.

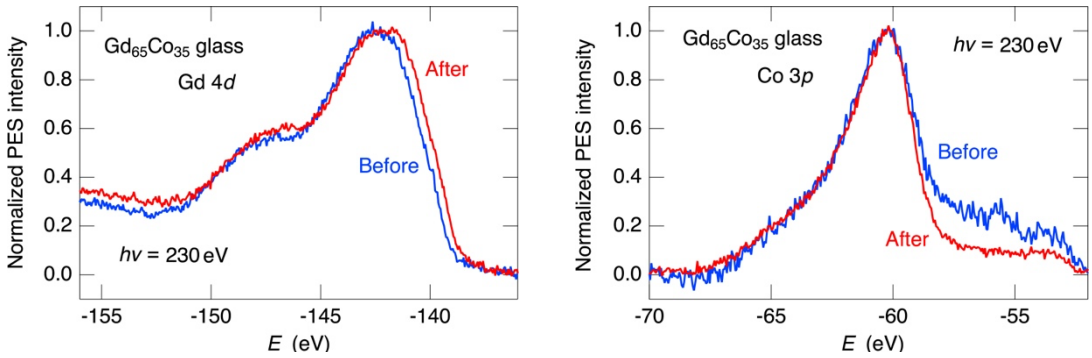

FIGURE 2. Gd 4*d* (left) and Co 3*p* (right) core-level PES spectra on $Gd_{65}Co_{35}$ glass before (blue curves) and after (red curves) the cryogenic rejuvenation.

Left and right panels of Fig. 3 show the conduction-band IPES spectra on the $Gd_{65}Co_{35}$ and $Gd_{65}Ni_{35}$ glasses before (blue curves) and after (red curves) the cryogenic rejuvenation, respectively. As clearly seen in the figures, the empty-state spectra of $Gd_{65}Co_{35}$ and $Gd_{65}Ni_{35}$ glasses resemble each other. The prominent peak at about 7 eV shifts to about 5.5 eV and becomes sharper and higher in the height. Since the spectra of these glasses are very similar, the origin of this peak may be the Gd atoms.

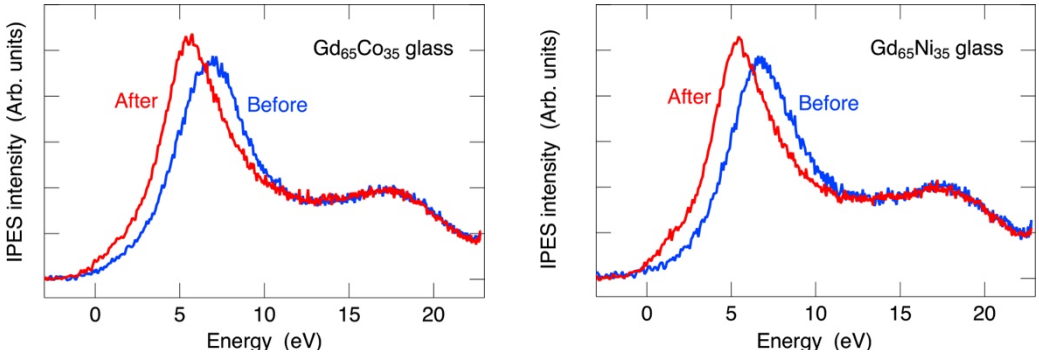

FIGURE 3. Conduction-band IPES spectra on $Gd_{65}Co_{35}$ (left) and $Gd_{65}Ni_{35}$ (right) glasses before (blue curves) and after (red curves) the cryogenic rejuvenation.

In addition to these works, we measured soft x-ray absorption and emission spectroscopies near the Co and Ni 2*p*-3*d* resonances, and the 3*d* partial DOS are obtained. The results are under analyzing. Moreover, an *ab-initio* molecular dynamics simulation is planned to obtain further on the atomic and electronic changes by the cryogenic rejuvenation on the Gd-TM glasses.

This work was supported by the Japan Society for the Promotion of Science (JSPS) Grant-in-Aid for Transformative Research Areas (A) 'Hyper-Ordered Structures Science' (Nos. 20H05878 and 21H05569), that for Scientific Research (C) (No. 22K12662), the Japan Science and Technology Agency (JST) CREST (No. JP-MJCR1861).

REFERENCES

1. S. V. Ketov, Y. H. Sun, S. Nachum, Z. Lu, A. Checchi, A. R. Beraldin, H. Y. Bai, W. H. Wang, D. V. Louzguine-Luzgin, M. A. Carpenter, and A. L. Greer, *Nature* 524, 200-203 (2015).
2. T. C. Hufnagel, *Nature Mater.* **14**, 867-868 (2015).
3. Y. Yamazaki, *Doctoral thesis* (Tohoku University, 2016).
4. S. Hosokawa, J. R. Stellhorn, L. Pusztai, Y. Yamazaki, J. Jiang, H. Kato, T. Hayashi, T. Ichitsubo, E. Magome, N. Blanc, N. Boudet, K. Ohara, S. Tsutsui, H. Uchiyama, and A. Q. R. Baron, *Nature Commun.*, submitted.

*21-A-U-013 BL-9B

Spiral Band Structure Hidden in the Bulk Chiral Crystal $NbSi_2$

Cheng Zhang[a], Koji Miyamoto[a], Tatsuya Shishidou[b], Ryoga Amano[c], Taisei Sayo[c], Chiho Shimada[c], Yusuke Kousaka[c], Michael Weinert[b], Yoshihiko Togawa[c], and Taichi Okuda[a]

[a]*Hiroshima synchrotron Radiation Center, Hiroshima University, Higashi-Hiroshima 739-0046, Japan.*
[b] *Department of Physics, University of Wisconsin-Milwaukee, Wisconsin 53201, USA.*
[c] *Deparment of Physics and Electronics, Osaka Metropolitan University, Osaka 599-8531, Japan.*

Keywords: Chiral crystal, Spiral band structure, ARPES, DFT.

Recently, so-called chirality induced spin selectivity effect (CISS) has been observed in the chiral crystal $NbSi_2$ through electrical conductivity measurement [1], CISS effect refers to a phenomenon that a spin-polarized current is generated when a current is passed through a material with a chiral structure [2,3].

To investigate the electronic structure of $NbSi_2$, we performed synchrotron-radiation angle resolved photoemission spectroscopy for both right-($P6_222$) and left-handed ($P6_422$) samples. Since the $NbSi_2$ crystal is difficult to cleave, the clean surface was obtained by mechanical polishing, Ar ion sputtering and annealing. We found not only the clear energy bands, but also spiral-shaped constant energy contours (CEC) at specific binding energies (E_B). The fact that the helicity of this pattern is reversed in the crystal having opposite chirality indicates that the observed intriguing pattern has its origin in the structural chirality. Our density functional theory (DFT) calculations confirmed this point. This result demonstrates that a photoemission experiment can be a new way to distinguish the chirality of crystals.

Figure 1 (a) and (b) show energy band structure of the right-handed $NbSi_2$ observed by ARPES along the high-symmetry lines $\bar{M}$-$\bar{\Gamma}$-$\bar{M}$ and $\bar{K}$-$\bar{\Gamma}$-$\bar{K}$. Figure 1 (c) and (d) show the bulk and surface calculated energy band structure, respectively. Bulk bands and surface states of ARPES data can be distinguished. Figure 2 (a) and (b) are CEC patterns for the right- and left-handed $NbSi_2$, respectively. Figure 2 (c) and (d) are the bulk calculated results without the showing spiral patterns. By comparing the surface calculated results, as shown in Figure 2 (e) and (f), we can confirm that the spiral structure is a surface effect.

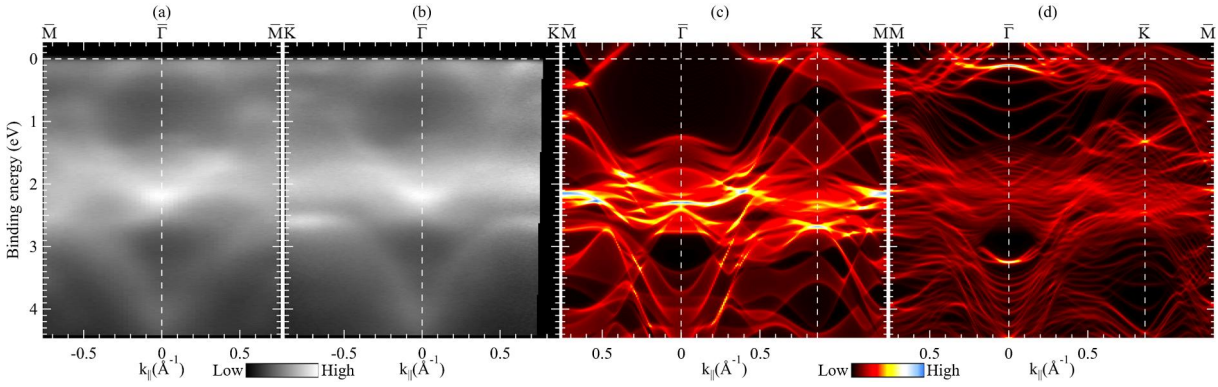

Figure 1. (a), (b) ARPES band structures of right-handed $NbSi_2$ crystal ($P6_222$) along lines $\bar{M}$-$\bar{\Gamma}$-$\bar{M}$ and $\bar{K}$-$\bar{\Gamma}$-$\bar{K}$. (c), (d) Bulk and surface calculated energy band structures by DFT along the high-symmetry lines.

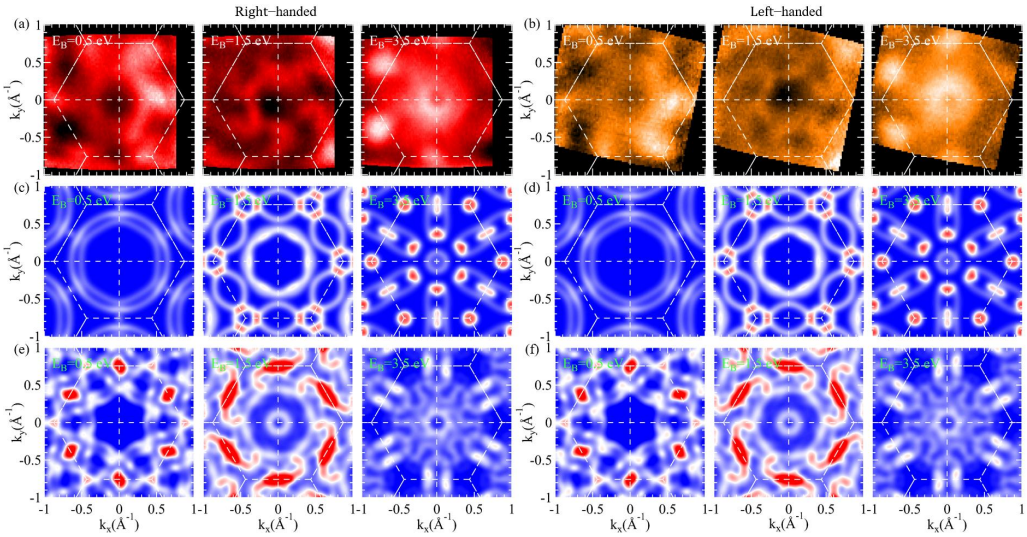

Figure 2. (a), (b) ARPES CEC patterns for the right-handed ($P6_222$) and left-handed $NbSi_2$ ($P6_422$) at some typical E_B, respectively, which are constant energy cut at E_B through a $E(k_x, k_y)$ data set obtained at a photon energy of 50 eV. (c), (d) Bulk calculated results for some corresponding E_B. (e), (f) Surface calculated results.

REFERENCES

[1] Kohei Shiota, Akito Inui et al., Chirality-Induced Spin Polarization over Macroscopic Distances in Chiral Disilicide Crystals, Phys. Rev. Lett. ,127, 126602 (2021).

[2] R. Naaman and D. H. Waldeck, Chiral-induced spin selectivity effect, J. Phys. Chem. Lett. 3, 2178 (2012).

[3] R. Naaman and D. H. Waldeck, Spintronics and chirality: Spin selectivity in electron transport through chiral molecules, Annu. Rev. Phys. Chem. 66, 263 (2015).

BL-9B

Investigation of Perpendicular Anisotropy in FeCo Alloy Films Covered with Oxygen for Development of Multi Spin Detecting Target

K. Kunitomo [a], K. Miyamoto[b] and T. Okuda [b]

[a]*Graduate School of Advanced Science and Engneering Hiroshima University, 1-3-1 Kagamiyama, Higashi-Hihiroshima 739-8526, Japan*
[b]*Hiroshima Synchrotron Radiation Center (HSRC), Hiroshima University 2-313 Kagamiyama, Higashi-hiroshima 739-0046, Japan*

Keywords: FeCo alloys, oxygen adsorption, spin polarization, perpendicular magnetic anisotropy (PMA)

At Hiroshima Synchrotron radiation center, we have been developing a spin- and angle-resolved photoemission spectroscopy (SARPES) machine using a reflection-type multichannel Very Low Energy Electron Diffraction (VLEED) detector. A current single-channel VLEED spin detection target is Fe(001)p(1×1)-O which possesses in-plane magnetic anisotropy. Therefore, we can observe only in-plane spin polarization. In order to observe all three components of spin polarization (Px, Py, Pz) in VLEED detector, we need a target with perpendicular magnetic anisotropy (PMA) in addition to Fe(001)p(1×1)-O.

We focused on FeCo alloys as potential targets for out-of-plane spin detection. In the case of thin films of the specific substrate, the crystal structure of FeCo alloy changes from the bcc structure to the bct structure due to the chemical pressure applied, which results in PMA [1-4]. Therefore, if we use such thin films it might be possible to observe out-of-plane spin polarization with a VLEED detector. On the other hand, it is also important that PMA is kept stably for a long time for practical use as a target. Current VLEED detector target Fe(001)p(1×1)-O has an oxide overlayer that acts as a protective film, and the lifetime of the target can be extended from several hours to several weeks (several months or more with flash annealing)[5,6]. We supposed it is possible that oxygen can form an effective protective film in FeCo film similar to Fe(001)p(1×1)-O because the crystal structure of FeCo is the same as Fe though half of the Fe atoms are replaced by Co. However, it was not obvious whether PMA was preserved after oxygen termination.

Thin FeCo films were deposited on single crystal Rh(001). LEED and Auger Electron Spectroscopy (AES) were used for sample evaluation. Fig.1 shows LEED patterns of FeCo/Rh(001) and FeCo-O/Rh(001) prepared by oxygen-termination of the FeCo/Rh(001). We observed sharp spots in either film and confirmed that high-quality epitaxial thin films were obtained. Fig.2 shows the results of out-of-plane SARPES of FeCo/Rh(001) and FeCo-O/Rh(001) films. Distinct out-of-plane spin polarization was observed even in FeCo-O surface, indicating that the FeCo-O film retained PMA. Fig.3 shows the change over time of the spin polarization. It was found that the speed of the spin-polarization change, i.e., the lifetime of the spin-polarized film is quite slow in both FeCo and FeCo-O films. In this system, the lifetime of FeCo film is longer than those of FeCo-O film, which is different from the case of Fe and Fe(001)p(1×1)-O surface.

From these results, it was found that FeCo and FeCo-O film has a high possibility of being used as a perpendicular spin detection target.

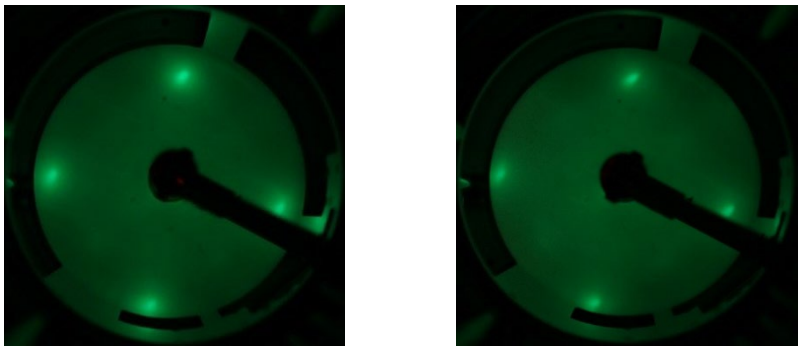

FIGURE 1. LEED patterns of (a) FeCo/Rh(001) films and (b) FeCo-O/Rh(001) films. Both images are 1 × 1 spot.

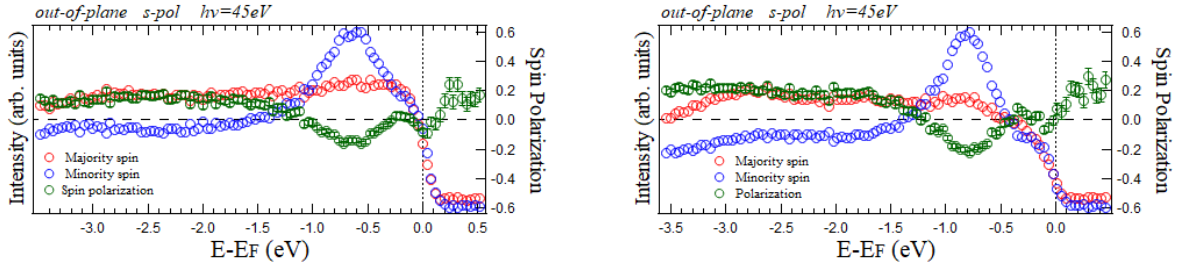

FIGURE 2. Out-of-plane SARPES of (a) FeCo film, and (b) FeCo-O film.

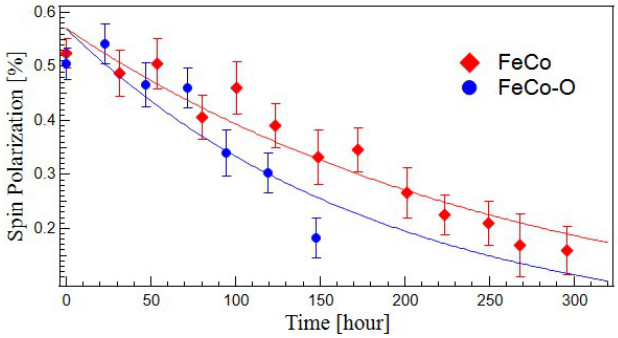

FIGURE 3. Life time of FeCo film (Red, τ =268 hour) and FeCo-O film (Blue, τ =186 hour). The vertical axis is the spin polarization, and the horizontal axis is time. The FeCo-O film was prepared by oxygen annealing the surface-contaminated FeCo film in the oxygen atmosphere.

REFERENCES

1. F. Yildiz, *et al*., Phys. Rev. B **80**, 064415 (2009).
2. Y. Kota and A. Sakuma, J. Magn. Soc. Jpn., 37, 17-23 (2013).
3. L I. Turek, J. Kudrnovsky, K. Carva., J Supercond Nov Magn **26**,1581 (2013).
4. T. Burkert, L. Nordström, O. Erikssonm, and O. Heinonen: Phys. Rev. Lett., **93**, 027203 (2004).
5. T. Okuda *et al.*, Rev. Sci. Instrum. **79**, 124117 (2008).
6. M. Zheng, E. F. Schwier, H. Iwasawa and K.shimada. Chin. Phys. B **29**, 067901 (2020).

21AG045 BL-11

Cluster Distortions in Amorphous Organotin Sulfide Compounds by EXAFS Measurements

Jens R. Stellhorn[a,b], Shinjiro Hayakawa[b], Benedict Paulus[c], Jonathan Link Vasco[c], Benjamin D. Klee[d], Stefanie Dehnen[c], Wolf-Christian Pilgrim[c]

[a] *Department of Physics, Nagoya University, Nagoya 464-8602, Japan*
[b] *Department of Applied Chemistry, Graduate School of Advanced Science and Engineering, Hiroshima University, Higashi-Hiroshima, Hiroshima 739-8527, Japan*
[c] *Department of Chemistry, Philipps University of Marburg, Marburg 35032, Germany*
[d] *Complex Fluid Research Department, Wigner Research Centre for Physics, Budapest 1121, Hungary*

Keywords: non-linear optical properties, white-light generation, amorphous compound, local structure, EXAFS.

Tailored light sources have greatly advanced technological and scientific progress by optimizing colour and brilliance, improving energy efficiencies or the quantum properties of light. So called supercontinuum generators are premier examples for media with nonlinear optical (NLO) effects – far superior in some respects to other sources such as phosphorescent white light-emitting diodes (LEDs). However, unlike LEDs, most of these advanced light sources are only used for scientific purposes, as they require extreme electric field strengths which are commonly realized by high-power pulsed lasers. In contrast, the materials of interest for this research project represent a new generation of supercontinuum emitters that are readily obtained from ubiquitous resources in a simple synthesis.

Our recent studies [1-4] investigated the local structure of 4 different amorphous organotin sulfide [$(R\text{-}Sn)_4S_6$] compounds by X-ray absorption spectroscopy and X-ray scattering measurements. These compounds exhibit a non-linear optical response upon irradiation with a continuous-wave near-infrared laser.[5-7] Their basic structural motif is a hetero-adamantane cluster with different organic substituents R. The nature of the NLO response depends strongly on the morphology of the material, which is influenced by the choice of the organic substituents, leading to either a second harmonic generation or the generation of a supercontinuum, potentially appearing as white light.

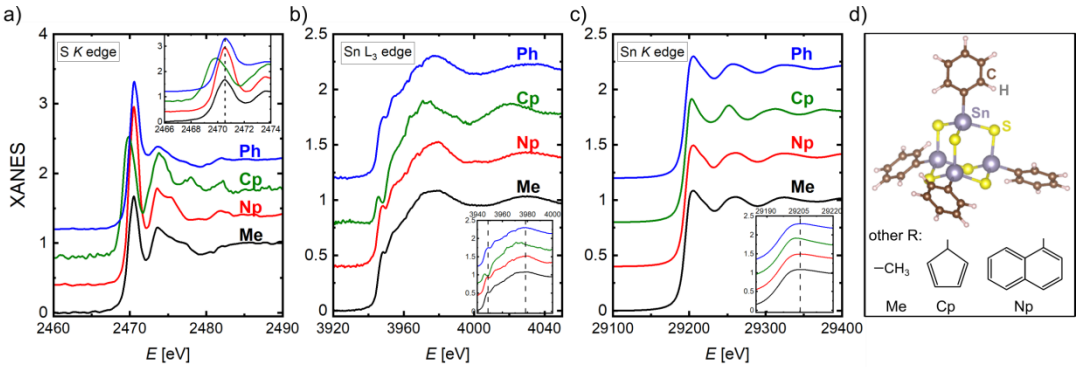

Fig. 1: XANES data for the 4 organotin sulfide samples (Me: black, Np: red, Cp: green, Ph: blue, shifted upwards for clarity) at the S *K* (a), the Sn L_3 (b) and the Sn *K* edge (c). The insets highlight the regions close the first maxima of the respective edges. A model of the Ph-Cluster from a DFT simulation[5] is illustrated in (d), along with schematic illustrations of the other organic substituents.

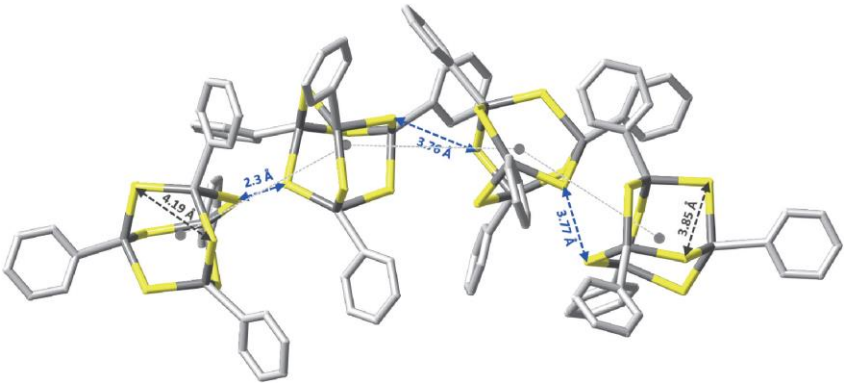

Fig. 2: Fourfold linear chain of $\{Sn_4S_6\}$ clusters from a dynamic molecular Reverse Monte Carlo simulation ensemble.[2] H-atoms have been omitted to retain clarity. Molecules in chains prefer a staggered mutual configuration with respect to the organic ligands. Also shown are some intramolecular and intermolecular distances, indicating similarity between intra- and intermolecular sulfur-sulfur spacings.

Due to the amorphous nature of the materials, their structural properties, and thereby the apparent origin of this effect, is difficult to determine [6]. Despite these difficulties, our results provide experimental evidence that the nature of the NLO properties is tied to distortions occurring at the cluster core, with almost ideal clusters in compounds that show second harmonic generation, and strongly distorted clusters in the case of compounds that generate a supercontinuum. These distortions may enable a closer proximity of the cluster cores, and thereby influence the NLO response by altering the intermolecular order.

As an example, Figure 1 illustrates the near-edge structure of the absorption spectrum (XANES) around the S *K*, Sn L_3 and Sn *K* edges (the latter was measured at P65 of the PETRA-III synchrotron). In all datasets, the edge of the cluster with R=Cyclopentadienyl (Cp) is shifted to lower energies (see insets in Fig. 1), indicating a change in the oxidization state of the cluster core. As we will show in the analysis of the XAFS data, this leads to a significant distortion of the cluster relative to the other compounds.

To conclude, the XAFS experiments at the S *K* edge performed at BL11 of HiSOR provide key information about the interaction of neighboring clusters, which determine the intermolecular order of the system and can be regarded as the origin of the differences of the non-linear optical properties.

REFERENCES

[1] J.R. Stellhorn et al., Adv. Optical Mater. 2201932 (2022)

[2] B. D. Klee et al, Scripta Materialia 219, 114851 (2022)

[3] W.-C. Pilgrim et al., J. Phys. Soc. Jpn. 91, 091004 (2022)

[4] J. R. Stellhorn et al., Phys. Status Solidi B 202200088 (2022)

[5] N.W. Rosemann et al., Science 6291, 1301 (2016)

[6] B. D. Klee, et al., Phys. Stat. Solidi B 255, 1800083 (2018)

[7] K. Hanau et al., Angew.Chem. Int. Ed. 60, 1176-1186 (2021)

22AG032 BL-11

First results of phase transformation from vaterite to calcite observed by Ca K-edge XAFS and XRD.

Yujie MA [1], Jens R. STELLHORN[1,3], Naomi KAWATA[2], Shinjiro HAYAKAWA[1].

[1]*Graduate School of Advanced Science and Engineering, Hiroshima University, Japan*

[2] *Natural Science Center for Basic Research and Development, Hiroshima University, Japan*

[3]*Department of Physics, Nagoya University, Japan*

Keywords: calcium carbonate, XAFS, phase transformation, XRD.

Insoluble calcium carbonate can be synthesized by mixing two aqueous solutions for calcium source and carbonate source, and calcium carbonate is precipitated under a condition of supersaturation (**FIG.1**) [1]. The initial precipitation is vaterite, and it will be transformed into more stable phase like calcite. We are interested in the mechanism of phase transformation, and X-ray absorption spectroscopy is utilized to obtain local structural information around Ca in an aqueous environment.

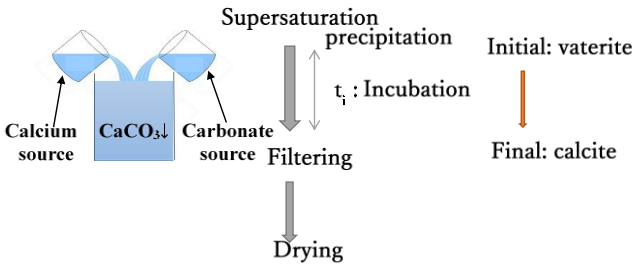

FIGURE 1. A schematic synthesis process of calcium carbonate.

The supersaturation was realized by mixing solutions of $CaCl_2$ and $NaHCO_3$, and the typical concentration of the solution was from 30 mM to 300 mM. Selective synthesis of the phase was carried out by changing the incubation time, t_i, before filtering the precipitation with a membrane filter (pore size 0.45 μm). The obtained calcium carbonate was identified by powder X-ray diffraction measurements (XRD). **FIG. 2** shows XRD patterns obtained from reagent (pure) calcite, pure vaterite

(t_i=16 mins for 30 mM solutions [1]), and the mixture of them as a function of the incubation time. The fraction of vaterite in a mixed sample can be determined by using normalized peak intensity with that of pure phase. The fraction of vaterite, f_V was estimated by the following equation by using the normalized peak intensities of 112 reflection of vaterite and 104 reflection of calcite.

$$f_v = V_{112n}/(V_{112n} + C_{104n}) \qquad (1)$$

XAFS (X-ray absorption fine structure) measurements were carried out by using a transmission mode, and a sample was attached to a Scotch tape and was placed in a helium filled chamber.

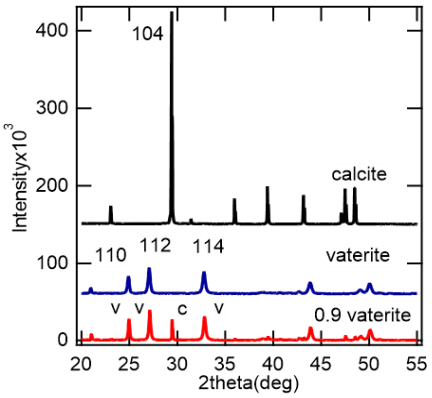

FIGURE 2. XRD patterns of calcium carbonates. Reagent calcite (black), synthesized vaterite (blue) and a mixture of them t_i=16 mins for 90 mM solutions, f_V =0.9).

XAFS data were processed with Athena and Artemis, and extracted EXAFS oscillations, χ(k) and Fourier transform of them were shown in **FIG. 3**, and the obtained data were almost identical to those reported previously [2]. It was also confirmed that the XAFS spectrum from a sample with t_i of 520 mins was identical to that of reagent calcite. FT spectra showed main peak corresponding to neighboring oxygens (Ca-O). Moreover, new peaks corresponding to Ca-Ca might be obtained. They were not observed when EXAFS spectra of calcium acetate in an aqueous solution were investigated [3]. Possibilities of observing the phase transformation in the aqueous solution will be discussed in this presentation.

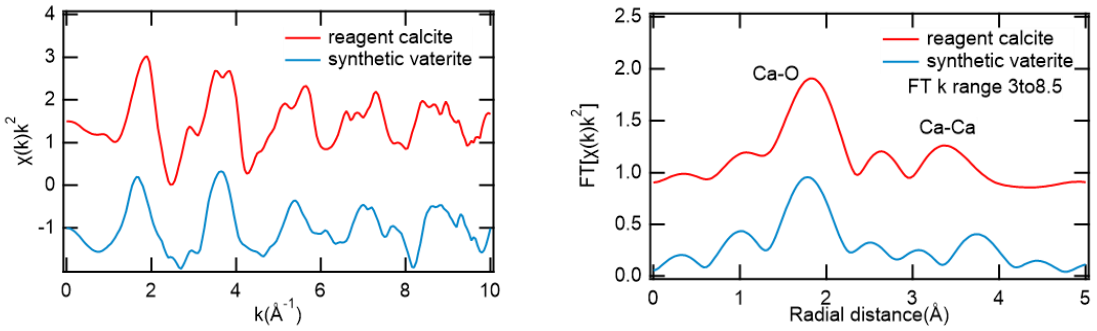

FIGURE 3. χ(k) spectra and their Fourier transform of χ(k), FT k range was 3 to 8.5. Reagent calcite (red line) and vaterite (blue line) Red line was reagent calcite, blur line was synthetic vaterite.

REFERENCES

1. S. Hayakawa et al., Anal. Sci. 24, 835-837 (2008). : 2. Li Qiao et al., Crystals 10,750 (2020). : 3. A. Munoz-Noval et al., J. Mol. Struct., 1161, 512-518 (2018).

22AG031 BL-12

Hydration Structure of Acetone Studied with Concentration-Dependent Absorption Spectra in the Ultraviolet Region

Chika Sugahara[a], Koichi Matsuo[b], and Kazumasa Okada[a,b]

[a] *Graduate School of Advanced Science and Engineering, Hiroshima University, 1-3-1 Kagamiyama, Higashi-Hiroshima 739-8526, Japan*
[b] *Hiroshima Synchrotron Radiation Center, Hiroshima University, 2-313 Kagamiyama, Higashi-Hiroshima 739-0046, Japan*

Keywords: UV absorption spectra, chemometric analysis, hydration structure

Hydration structure plays a fundamental role in our understanding of physical properties and chemical reactions of solutes. One of the typical aqueous solutions is acetone solution, but the physicochemical properties still need to be studied. Acetone is miscible with water in any ratio. The mixture has a negative excess enthalpy in the dilute region [1], indicating an attractive interaction between acetone and water. The interaction is a hydrogen-bond type, with an additional weak C–H···O bond in a very dilute region [2]. The purpose of this study is to explore the hydration structure of acetone using UV absorption spectroscopy.

The experiments were performed on the beamline for vacuum-ultraviolet circular dichroism spectroscopy, BL-12. The sample chamber [3] was filled with the nitrogen gas. The sample cell consisted of two CaF_2 windows and a Teflon spacer with a thickness of 200 μm. The measurement range was 170–320 nm, and the spectrum of liquid water was used as a reference. The sample acetone–water binary mixture was prepared with molar fraction of acetone ranging from 0.05 to 0.50. Acetone was obtained commercially from FUJIFILM Wako Pure Chemicals Corp., Japan.

The peak of $\pi^* \leftarrow n$ absorption band non-linearly shifts to the longer wavelength with the molar fraction of acetone, x_A. The absorption band and the peak shift are shown in Fig. 1. All the spectra have a tail toward the shorter wavelength. This implies that the spectra consist of some components. The components include hydrated acetone. The hydration structure depends on x_A. Judging from the shift of the peak position, there are three regions: Region 1; $x_A =$ 0.05–0.10; Region 2, $x_A =$ 0.15–0.35; and Region 3, $x_A =$ 0.40–0.50.

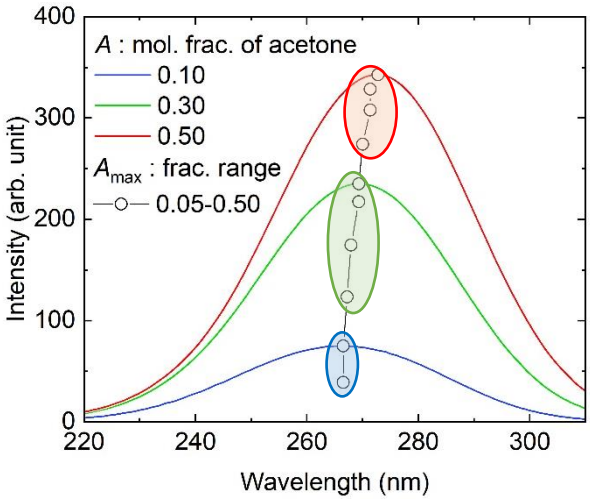

FIGURE 1. The $\pi^* \leftarrow n$ absorption band of acetone aqueous solution at different molar fractions.

Quantitative analysis of the change of the band has been carried out by the principle component analysis (PCA). The result of PCA is shown in Fig. 2. The measurement spectra are well explained by two components (total 99.99%). The primary component (PC1) has a peak at 270.70 nm and the secondary component (PC2) has a peak at 252.64 nm and a valley at 287.36 nm. The vector of PC1 corresponds to the average spectrum, and the score of PC1 is almost proportional to x_A. The score of PC2 increases in $x_A = 0.05$–0.20, reduces in $x_A = 0.25$–0.35, and is negative in $x_A = 0.40$–0.50. The PC1 is similar to the spectrum for $x_A = 0.35$. This indicates that the dominant hydration structure is the 1:1 acetone–water complex. Additional hydration structures are analyzed as PC2.

The physical meaning of PC2 is made clearer if we plot the difference spectra from PC1. The difference spectra have a sinusoidal-like shape. The behavior of peak shift is reproduced by the difference spectra. Peaks come at shorter wavelengths in the spectra for Region 1, suggesting an additional attractive interaction with water. A possible interaction model is shown in Fig. 3(a): The acetone molecule interacts with two water molecules. This kind of hydration model is the same as that proposed in an IR and NMR spectroscopic study [2]. In Region 2, two acetone molecules are hydrated with one water molecule like in Fig. 3(b). In Region 3, there are not enough water molecules for hydration due to the large x_A: The solution contains non-hydrogen-bonded acetone molecules. The presence of the non-hydrogen-bonded molecules is supported by the coincidence of the peak of PC2 with the absorption peak position of gaseous acetone [4].

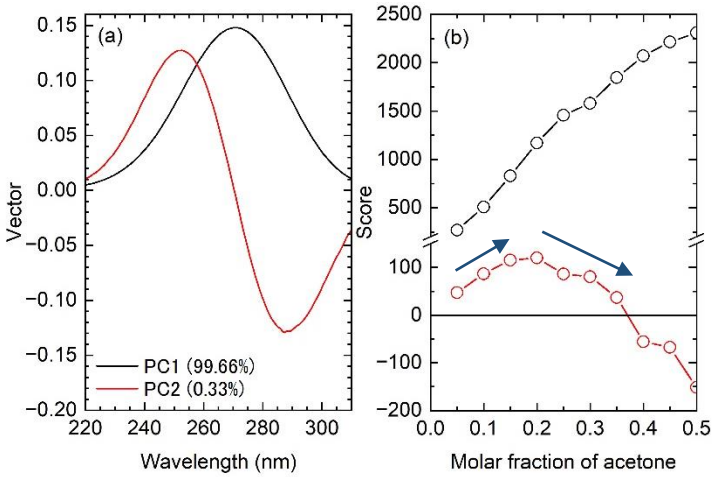

FIGURE 2. Spectral components (a) and scores (b) obtained by PCA for the UV absorption data presented in Fig. 1.

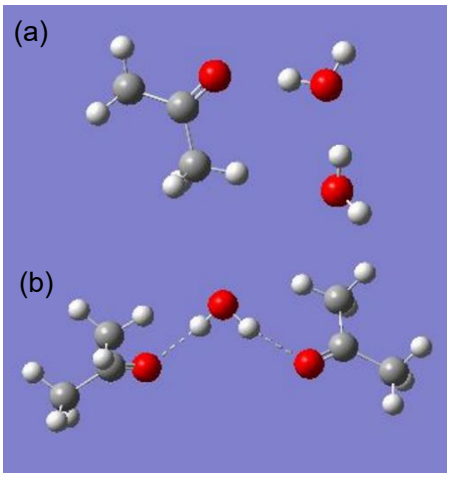

FIGURE 3. Plausible hydration structures of acetone; (a) 1:2 complex, (b) 2:1 complex.

REFERENCES

1. B. Löwen and S. Schultz, *Thermochim. Acta* **262**, 69–82 (1995).
2. K. Mizuno, T. Ochi, and Y. Shindo, *J. Chem. Phys.* **109**, 9502–9507 (1998).
3. K. Matsuo, T. Fukuyama, R. Yonehara, H. Namatame, M. Taniguchi, and K. Gekko, *J. Electron Spectrosc. Relat. Phenom.* **144–147**, 1023–1025 (2005).
4. M. Nobre, A. Fernandes, F. Ferreira da Silva, R. Antunes, D. Almeida, V. Kokhan, S. V. Hoffmann, N. J. Mason, S. Eden, and P. Limão-Vieira, *Phys. Chem. Chem. Phys.*, **10**, 550–560 (2008).

22AG013 BL-12

Dynamic Observation of Interaction Process between β-Lactoglobulin and Membrane by Time-Resolved Vacuum-Ultraviolet Circular Dichroism

Satoshi Hashimoto[a], Koichi Matsuo[b]

[a]*Graduate School of Advanced Science and Engineering, Hiroshima University, 1-3-1 Kagamiyama, Higashi-Hiroshima, Hiroshima 739-8526, Japan*
[b]*Hiroshima Synchrotron Radiation Center, Hiroshima University, 2-313 Kagamiyama, Higashi-Hiroshima 739-0046, Japan*

Keywords: Circular dichroism, β-Lactoglobulin, Membrane interaction, Secondary structures, Time-resolved measurement

Membrane-bound proteins closely relate to various biological functions such as drag delivery into the membrane, stabilization of myelin in central nervous system, and antibacterial properties. Although it is difficult to observe the conformation change of protein due to the membrane interaction, a vacuum-ultraviolet circular dichroism (VUVCD) spectroscopy has a great advantage to monitor the protein structure in the presence of membrane and has been applied to characterize the conformation of membrane-bound protein such as myelin basic protein (MBP) [1] and α_1-acid glycoprotein (AGP) [2]. However, this synchrotron radiation CD technique can only obtain the structural information before and after membrane interaction, requiring the necessity of the dynamic parameters in the processes of membrane interaction. Recently, we constructed a microchannel cell [3, 4] with sequential flow method and installed into VUVCD system to measure the time-resolved (TR) CD spectra. In this study, this system was applied to observe the structural dynamics of β-lactoglobulin (bLG) interacting with two types of membrane (LysoDMPG and sodium dodecyl sulfate: SDS). TR-CD spectra of bLG were measured between 1 and 60 s for the interaction of LysoDMPG and between 0.1-90 s for the interaction of SDS. The global fitting analysis was conducted for all CD values from 235 to 205 nm and then two rate constants were obtained for each membrane interaction, indicating the existence of at least one intermediate state. Further the CD spectra of intermediate states in each membrane interaction were also estimated from the all TR spectra considering the two rate constants. Secondary structural contents and positions of native, intermediate, and membrane-bound states are obtained using SELCON3 program and VUVCD-NN method, revealing the step-by-step conformation changes in the both membrane interactions. TR-CD system is an excellent experiment tool to disclose the conformation dynamics of protein during the interaction. In addition to the static observations of concentration- and temperature-dependence, the observations of structural dynamic of proteins from TR system would be helpful for elucidating the unique and important functions of membrane-bound proteins.

REFERENCES

1. K. Matsuo and K. Gekko (2009) Biochemistry, 48:9103–9111.
2. M. Kumashiro, Y. Izumi, and K. Matsuo (2021) Proteins, 89:1251–1261.
3. A. S. Stroock, S. K. W. Dertinger, A. Ajdari, I. Mezic, H. A. Stone, G. M. Whitesides (2002) Science, 295:647-651.
4. T. J. Kwak, Y. G. Nam, M. A. Najera, A. W. Lee, J. R. Strickler, W. J. Chang (2016) PLOS ONE, e0166068

22BG017 BL-12

Optical Activity Measurement of Amino-acid Films Irradiated with Circularly Polarized Lyman-α Light

Jun-ichi Takahashi[a], Masahiro Kobayashi[b], Gen Fujimori[a], Kensei Kobayashi[a]
Hiroshi Ota[c], Koichi Matsuo[d], Masahiro Katoh[c,d], Yoko Kebukawa[a]
Shinji Yoshimura[b], Hiroaki Nakamura[b]

[a]*Faculty of Engineering, Yokohama National University, 79-5 Tokiwadai, Hodogaya-ku, Yokohama 240-8501, Japan*
[b]*Department of Helical Plasma Research, National Institute for Fusion Science, 322-6 Oroshi-cho, Toki 509-5292, Japan*
[c]*UVSOR Facility, Institute for Molecular Science, 38 Nishigo-Naka, Myodaiji, Okazaki 444-8585, Japan*
[d]*Hiroshima Synchrotron Radiation Center, Hiroshima University, 2-313 Kagamiyama, Higashi-Hiroshima 739-0046, Japan*

Keywords: Homochirality, Amino Acid, Optical Activity, Circularly Polarized Light, Circular Dichroism.

The origin of homochirality in terrestrial biomolecules (L-amino acid and D-sugar dominant) remains one of the most mysterious problems in the research for the origins of life. Rational explanations for the chiral asymmetry introduction into biomolecules are required through interdisciplinary collaborations. One of the most attractive hypotheses in the context of astrobiology is “Cosmic Scenario” as below [1, 2]; (1) Asymmetric reactions of prebiotic molecules on interstellar dust surfaces in molecular cloud circumstances were introduced by polarized quantum radiation sources in space, that is “chiral radiations”. (2) The chiral products were transformed into the complex organic materials including amino-acid precursors as “chiral seeds”. (3) The complex organic materials as “chiral seeds” were transported with meteorites or asteroids to primitive Earth and resulting in terrestrial biomolecular homochirality by some “chiral amplification” effect.

Among the polarized quantum radiation sources, circularly polarized light (CPL) in the space environment is thought to be one of the most likely causes of the enantiomeric excesses of terrestrial bioorganic molecules. A cosmogenic scenario has attracted attention, which proposes that the radiation fields of CPL induce new optical activity in organic molecules produced in the interstellar environment, leading to the enantiomeric excesses. The radiation fields of CPL are assumed to exist in the scattered light by magnetic field-aligned dust in massive star-forming regions [3] and in synchrotron radiation (SR) or gamma-ray bursts from neutron stars with strong magnetic fields [2]. Ultraviolet light with a wavelength shorter than 230 nm is highly absorbed by bioorganic molecules such as amino acids. Furthermore, this is in the region where the optical response to left- (L-) and right- (R-) CPL is of opposite sign, that is, optical activity is prominent.

To validate the cosmogenic scenario, several ground simulating experiments have been investigated using ultraviolet CPL from high-energy particle accelerators. We have already carried out irradiation experiments of ultraviolet CPL with different wavelengths (215, 180 and 155 nm) to investigate the photon energy dependence of chiral asymmetric reactions by using UVSOR beam lines [4, 5]. Photon absorption bands correspond with the chromophores from the characteristic electronic transitions of carboxyl and amino groups (n-π^*, π-π^* and n-σ^*, respectively) of alanine molecule [6, 7]. The results of circular dichroism (CD) measurements strongly suggested that optical activity emergence depends on photon energy of the irradiated CPL.

In this study, we focused on a hydrogen Lyman-α wavelength of 121.6 nm, where strong emission lines are observed in star-forming regions. Furthermore, it is predicted by recent theoretical calculations that the hydrogen Lyman-α light is circularly polarized by the magnetic field-aligned dust scattering in massive star-forming regions. We have carried out irradiation experiments by using circularly polarized hydrogen Lyman-α light to investigate the further photon energy dependence of chiral asymmetric reactions. We formed thin solid film samples of racemic mixture of alanine (DL-alanine) on quartz substrates from crystal powders of

DL-alanine by using a thermal-crucible vacuum-evaporation system. The samples were irradiated with L- or R-CPL in hydrogen Lyman-α wavelength of 121.6 nm using the undulator beam line BL1U of UVSOR-III. The irradiated CPL wavelength are corresponding to photon absorption bands with the chromophores from the electronic transitions of carboxyl and amino groups (π -σ*) of alanine molecule [6, 7]. The samples were set in a vacuum sample chamber preventing attenuation by air absorption. The 121.6 nm wavelength radiation from the undulator is reflected by a gold-coated mirror located in the mirror chamber directly beam upstream of the sample chamber and then enters the sample chamber. On the beam entrance side of the vacuum sample chamber, a gate valve with an MgF_2 vacuum sealing window (0.5 mm in thickness) was mounted. The use of gold-coated mirror reflections has made it possible to suppress high-energy higher-order light from the undulator source expecting to reduce the transmittance loss of the MgF_2 window due to high-energy radiation induced defects. The sample substrate was set in the sample holder, in which magnetic and electric fields can be applied to perpendicularly to the sample surface. The total photon beam intensity irradiated on the sample was monitored with photoelectron current of a silicon photodiode settled at the beam downstream side of the sample holder.

CD spectra of the CPL irradiated films were measured using the SR-CD beam line BL-12 of HiSOR to clarify the optical activity emergence by CPL irradiation. CD spectroscopy can detect optical activity with a high accuracy because CD spectra sensitively reflects the steric structures of chiral molecules. Figure 1(a) shows spectra of DL-alanine films irradiated for 30 min with L- or R-CPL at 121.6 nm in wavelength. To delete the effects of linear dichroism components, the CD spectra at sample rotation angles (0, 45, 90, and 135 degrees) from both back and front directions of each were individually measured and averaged them. Comparing with CD spectra of irradiations at 215, 180 and 155 nm in wavelength, the observed optical activity emergence strongly depends on the irradiated CPL wavelength and the polarization helicity (L- or R-CPL). In addition, we have also examined the additional effect of applying a magnetic field to the sample to investigate the effect of the magnetic field in interstellar space (Fig. 1(b) and (c)). Detailed analysis of CD spectra is in progress supported by quantum chemical calculations. The clarification of full mechanism of the optical activity emergence potentially has relevance to the origin of terrestrial bioorganic homochirality stimulated by “chiral photon radiation”.

This work is supported by the Astrobiology Center Program of National Institutes of Natural Sciences (NINS) (Grant Number AB041014) and Frontier Photonic Sciences Project of National Institutes of Natural Sciences (NINS) (Grant Number 01212202).

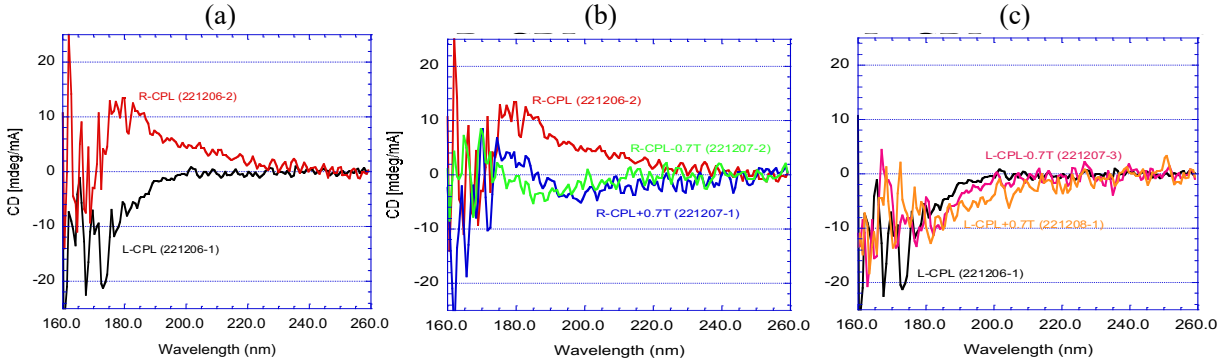

FIGURE 1. (a) CD spectra after right (R-) and left (L-) circularly polarized Lyman-α (121.6 nm) irradiation on DL-alanine films without magnetic field, (b) right (R-) circularly polarized Lyman-α irradiation with magnetic field (±0.7 T), and (c) left (L-) circularly polarized Lyman-α irradiation with magnetic field (±0.7 T).

REFERENCES

1. W. A. Bonner, *Orig. Life Evol. Biosph.* **21**, 407 (1991).
2. J. Takahashi and K. Kobayashi, *Symmetry* **11**, 919 (2019).
3. H. Fukushima, et al., *Month. Notices Roy. Astron. Soc.* **496** 2762 (2020).
4. J. Takahashi et al., *Int. J. Mol. Sci.* **10**, 3044 (2009).
5. T. Sakamoto et al., in Proceedings of 25th Hiroshima Int. Conf. Synchrotron Radiation (2021).
6. M. Tanaka et al., *Enantiomer* **7** 185 (2002).
7. F. Kaneko et al., *J. Phys. Soc. Jpn.* **78** 013001 (2009).

21AU011 BL-12

Interaction Mechanism between the Antimicrobial Peptide Magainin2 and Lipid Membrane Revealed by Synchrotron-Radiation Circular- and Linear-Dichroism Spectroscopy

Ryoga Tsuji[a], Munehiro Kumashiro[b], Koichi Matsuo[c]

[a]*Physics Program, Graduate School of Advanced Science and Engineering, Hiroshima University, 1-3-1 Kagamiyama, Higashi-Hiroshima, Hiroshima 739-8526, Japan*
[b] *Institute of Advanced Medical Sciences, Tokushima University, 3-18, Kuramoto-cho, Tokushima 770-8503, Japan*
[c]*Hiroshima Synchrotron Radiation Center, Hiroshima University, 2-313 Kagamiyama, Higashi-Hiroshima, Hiroshima 739-0046, Japan*

Keywords: Antimicrobial Peptide, Circular dichroism, Lipid membrane

Magainin2 (M2), is one of the antimicrobial peptides and composed of 23 amino acids, induces the permeabilization of membranes for numerous gram-negative and gram-positive bacteria, by interacting with membrane followed by forming an amphipathic helix. We have investigated the effects of some physical characteristics of membranes such as spontaneous curvature [1] and fluidity [2] etc. on the membrane interaction of M2 using four types of lipid molecules and found that in the membrane with the positive spontaneous curvature (dilauroyl phosphatidylcholine, dimyristoyl phosphatidylcholine, and dipalmitoyl phosphatidylcholine), M2 could adsorb onto the membrane surface when its fluidity was increased and decreased (annealing), forming the helical structure, while in the membrane with the negative spontaneous curvature (distearoyl phosphatidylcholine), M2 could not access the membrane surface even after annealing procedure, retaining its random coil structure. In this study, to further confirm the effects of the spontaneous curvature and fluidity on the membrane interaction, we analyzed the membrane-bound conformation of M2 in the presence of the lipid membrane composed of dipentadecanoyl phosphatidylcholine (15:0PC), which has negative spontaneous curvature and phase transition temperature of 35ºC, using a synchrotron-radiation circular-dichroism (CD) and linear-dichroism (LD) spectroscopy. The results showed that M2 mostly retained a random coil structure in the presence of 15:0PC membrane at 25ºC but the CD spectrum of M2 showed the formation of helical structure after the annealing. These are very similar phenomena to those observed in the presence of DPPC membrane, suggesting that as mentioned above, M2 could clearly adsorb onto the membrane surface with the positive spontaneous curvature and the change of fluidity due to phase transition is necessary for M2-membrane interaction. The LD spectrum of M2 in the presence of 15:0PC lipid membrane showed the positive sign around 200 nm. The analytical results indicated that there are two hypotheses, one is that all M2 peptides form the helical orientation with a single angle against the membrane surface and second is that M2 peptides form the mixtures of perpendicular (transmembrane) and parallel helical structures against the membrane surface. The results under the first assumption showed that the LD spectrum could be interpreted as the angle between the helix axis and the membrane normal would be 46°, while those under the second assumption showed that the ratio of M2 helix axes perpendicular and parallel to the membrane surface was 1: 1.1. We need further characterizations to understand the effect of the spontaneous curvature and fluidity on the membrane interaction, but the M2 conformation and orientation on the membrane obtained here would be helpful for disclosing the details of interaction mechanism between lipid membranes and M2.

REFERENCES

1. E. Strandberg, J. Zerweck, P. Wadhwani, and A. S. Ulirich, *Biophysical Journal*, March 2013, pp. L09-L011
2. L. Ma, Y. Luo, Y-H. Ma and X. Lu, *Langmuir,* 2021, 37, 1613-1621

22AG022 BL-12

Membrane-bound conformation of the non-amyloid-β component of α-synuclein characterized by vacuum-ultraviolet circular dichroism and molecular-dynamics simulation

Ryota Imaura[a], Koichi Matsuo[b]

[a]*Graduate School of Advanced Science and Engineering, Hiroshima University*
[b]*Hiroshima Synchrotron Radiation Center, Hiroshima University,*

Keywords: Synchrotron radiation circular dichroism; MD simulation; α-Synuclein; non-amyloid-β component; Membrane; Protein-membrane interaction; Secondary structures.

α-synuclein (αS) interacts with synaptic vesicle membranes in neurons to forms amyloid fibrils, which are involved in the pathogenesis of neurodegenerative diseases [1]. αS is composed of 140 amino acid residues and is divided into three regions: N-terminal region (residues 1-60), non-amyloid β-component (NAC) region (residues 61-95), and C-terminal region (residues 96-140) [2]. Among them, the NAC region has been proposed as a core region of amyloid fibril formations on the membrane in vivo [3]. In this study, synchrotron radiation vacuum-ultraviolet circular dichroism (VUVCD) [4] and molecular dynamics (MD) simulation were applied to characterize the membrane-bound structures of the peptides (αS_{57-102}) including the NAC region.

The VUVCD spectrum of αS_{57-102} was measured in the absence of membrane (native state) and in the presence of liposome membrane composed of DMPG lipid molecules. The native state exhibited the characteristic peaks of the random structure, while the spectrum in the presence of liposome showed the characteristic ones of α-helix structure as the L/P (DMPG lipid/αS_{57-102} peptide) ratio increased (L/P = 0 ~ 100), giving the two isoelliptic points at 201 and 202 nm and the saturated CD intensity around L/P=100. From the plots of CD values at 222 nm, we found that αS_{57-102} formed an intermediate structure around L/P =50~60 and formed the membrane-bound state around L/P=100.

To characterize the interaction mechanism between αS_{57-102} and membrane, MD simulation was conducted for the system composed of αS_{57-102} and DMPG membrane. During the simulation, some parts of αS_{57-102} were inserted into the membrane, disclosing that the V70-V95 region of αS_{57-102}, where several hydrophobic residues are localized, formed the hydrophobic interactions with the membrane interior, and the K96 and K97 residues formed the electrostatic interactions with negatively charged lipid head groups on the membrane surface. These unique hydrophobic and electrostatic interactions would induce the intermediate state of αS_{57-102} peptide.

The intermediate structure of αS_{57-102}, which would be partially folded in the membrane, is expected to influence the amyloid fibril formation. The peptide with L/P =50~60 was incubated for about 12 hours (37°C, shaking at 2000 rpm) and it was found that the β-strand structure increased only these L/P ratios, suggesting an intermediate structure of αS_{57-102} in the membrane is important factor for the aggregation or amyloid fibrils formation process.

REFERENCES

1. D. J. Selkoe, *Nature,* vol. 426, pp. 900-904, 2003.
2. Aaron D. Gitler, Brooke J. Bevis, James Shorter, Katherine E. Strathearn, Shusei Hamamichi, Linhui Julie Su, Kim A. Caldwell, Guy A. Caldwell, Jean-Christophe Rochet, J. Michael McCaffery, Charles Barlowe, Susan Lindquist, *Proceedings of the National Academy of Sciences,* vol. 105, no. 1, pp. 145-150, 2008
3. Ueda, K., Fukushima, H., Masliah, E., Xia, Y.U., Iwai, A., Yoshimoto, M., Otero, D.A., Kondo, J., Ihara, Y. and Saitoh, T., *Proceedings of the National Academy of Sciences*, vol.*90*, no. 23, pp.11282-11286, 1993.
4. Koichi Matsuo, Kunihiko Gekko, *Methods in Molecular Biology,* vol. 974, pp. 253-279, 2013.5.

22AG025, 22BG044 BL-13

Torsional Angle Dependence of Ultrafast Charge Transfer in Biphenyl Monolayers

K. Yoshioka[a], J. Yamada[a], A. Niozu[a], and S. Wada[a,b]

[a]*Department of Physical Science, Hiroshima University, Higashi-Hiroshima 739-8526, Japan*
[b]*Hiroshima Synchrotron Radiation Center, Hiroshima University, Higashi-Hiroshima 739-0046, Japan*

Keywords: π-conjugated system, core-hole clock.

Introduction

In recent years, the application of organic molecules in the field of molecular electronics, such as organic semiconductors and molecular devices, has attracted considerable interest [1]. The evaluation of the conductivity of organic molecules is an important issue for their use in those applications. Among organic molecules, aromatic systems with π-electrons exhibit excellent electrical conductivity [2]. Therefore, the purpose of this study is to investigate the effect of the degree of π-conjugation of the molecules on the electrical conductivity. To investigate this, we evaluated the molecular conductivity by observing the charge transfer process that occurs when inner-shell electrons are excited by soft X-ray irradiation.

Experiment

In this study, Auger electron spectroscopy (AES) measurements were performed at HiSOR BL-13 to observe charge transfer processes. The experimental chamber is equipped with a circular hemisphere electron energy analyzer, and the pressure is ~10^{-10} torr at room temperature.

The samples are self-assembled monolayers (SAMs) of biphenyl thiol molecules on Au substrates. The molecular structures are shown in Figure 1. The molecules have different torsional angles by the introduction of methyl groups, which result in different degrees of π-conjugation. As a reference system, MHDA molecule composed of a highly insulating aliphatic chain was employed. The molecules have methyl ester groups as the tail group, which are resonantly excited in the AES measurements.

In observing the charge transfer process, we focus on the oxygen atom in the methyl ester group at the end group. For the characterization of the prepared SAMs, we evaluated the orientation of the molecules by soft X-ray absorption spectroscopy varying X-ray incidence angles.

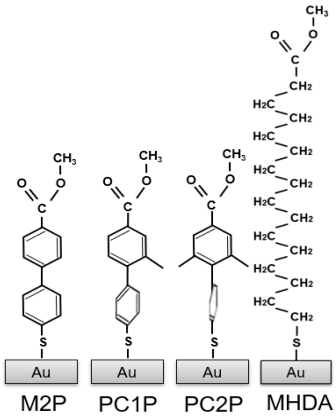

Figure 1. Overview diagram of each sample molecule.

Results and Discussion

We compared soft X-ray absorption spectra at different incidence angles. As an example, the spectra of M2P SAM is shown in Figure 2. A clear polarization dependence was observed in the absorption intensities of the peaks for the transitions of π^*(C=C) orbital (about 285 eV) and the π^*(C=O) orbital (about 289 eV). The intensities of those peak increases with increasing incident angle, indicating that the molecules in the SAMs are arranged in nearly upright orientations.

We investigated the charge transfer process that occurs when the oxygen atoms at the tail group are inner-shell excited to the π^*(C=O) orbital. The charge transfer

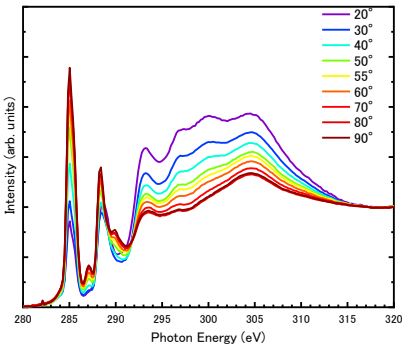

Figure 2. The soft X-ray absorption spectra of M2P SAM at different incidence angles.

process competes with the pure-resonant Auger decay, and Auger electrons with different kinetic energies are emitted in those processes. Therefore, by decomposing the measured AES spectra into the charge transfer component and the resonant Auger component, the charge transfer time can be evaluated. The fitting results are shown in Figure 3. Here, for the spectra of the pure-resonant Auger electrons, we used the data of the MHDA SAM at the photon energy of the π^*(C=O) transition. For the spectra of the normal Auger electrons emitted when charge transfer occurs, the data at the energy of the σ^*(C－O) transition was used.

An evident admixture of the normal Auger electrons was observed in the case of M2P SAM, indicating that a charge transfer occurred within the core-hole lifetime. Table 1 shows the charge transfer time τ_{CT} calculated with the following equation [3] using the normal Auger electron yield ratio P_{CT} obtained from there fitting results and the core-hole lifetime τ_{CH} (O: about 4 fs).

$$\tau_{CT} = \tau_{CH} \frac{P_{CT}}{1-P_{CT}}. \quad (1)$$

The results show that M2P SAM has the highest yield ratio of normal Auger electrons and the shortest charge transfer time. For, PC1P and PC2P SAMs, the yield ratio of normal Auger electrons decreased due to torsion, and the charge transfer times were PC1P: 52 fs and PC2P: 63 fs. These results suggest that torsion decreases the degree of π-conjugation, making the charge transfer less likely to occur.

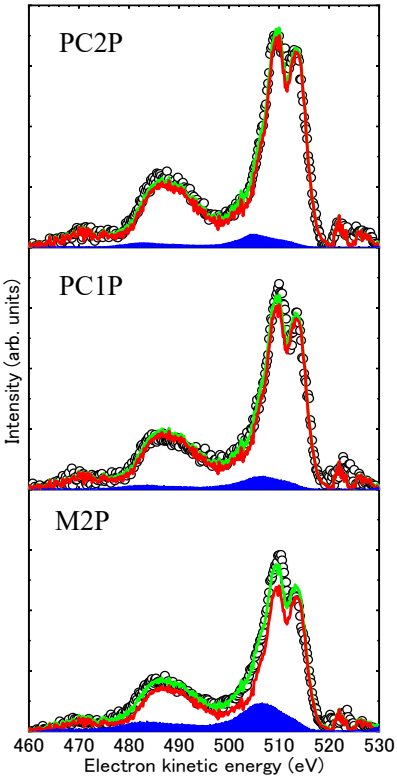

Figure 3. The fitting results of AES spectra for each sample SAMs. (The black dot: The experimental data, The green line: The fitting results, The red line: The data of pure-resonant Auger electrons, The blue area: The data of normal Auger electrons.)

Table 1. The yield ratio of normal Auger electrons and the charge transfer times obtained from AES spectra.

	M2P	**PC1P**	**PC2P**
The yield ratio of normal Auger electrons P_{CT}	0.18	0.07	0.06
Charge-transfer time τ_{CT}	19 fs	52 fs	63 fs

Conclusion

In this study, we observed the charge transfer that occurs when SAMs of biphenyl molecular systems with different torsion angles due to the addition of methyl groups by Auger electron spectroscopy with soft X-rays. The charge transfer time was evaluated by using the core-hole clock method for the Auger spectra. The obtained charge transfer times are M2P: 19 fs, PC1P: 52 fs, and PC2P: 63 fs. The results indicate that torsion decreases the π-conjugation and slows down the charge transfer between the molecule and the substrate.

REFERENCES

1. A. Asyuda, R. O. de la Morena, E. Sauter, K. Turner, K. McDonald, M. Buck, M. Zharnikov: J. Phys. Chem. C, **124**, 25107 (2020).
2. A. Asyuda, A. Wiesner, X. Wan, A. Terfort, M. Zharnikov: J. Phys. Chem. C, **124**, 24837 (2020).
3. P. A. Bruhwiler, O. Karis, N. Martensson: Rev Mod Phys, **74**, 703 (2002).

22AG026, 22BG043 BL-13

Measurements of Work Functions of Organic Monolayers Adsorbed on Gold Surfaces

Junna Yamada[a], Kakuto Yoshioka[a], Akinobu Niozu[a,b], and Shin-ichi Wada[a,b,c]

[a] *Faculty of Science, Hiroshima University, Higashi-Hiroshima, 739-8526 Japan*
[b] *Graduate School of Advanced Science and Technology, Hiroshima University, Higashi-Hiroshima, 739-8526 Japan*
[c] *Hiroshima Synchrotron Radiation Center, Hiroshima University, Higashi-Hiroshima, 739-0046 Japan*

Keywords: Work function, self-assembled monolayers (SAMs), X-ray photoelectron spectroscopy

Electronic devices based on organic thin films are expected to realize device forms that are difficult to realize with conventional inorganic semiconductors due to the versatility of their molecular design. One of the characteristics of such excellent performance of organic compounds is the importance of delocalized π-electrons in the molecules. In general, organic compounds are insulating materials that are unsuitable for the development of conductivity, but by making extremely thin films of 100 nm or less, the transport of holes and electrons between electrodes and organic semiconductor layers becomes possible, making it possible to treat organic materials as semiconductors. Thus, the processes that hold the key to the operation of organic devices occur at the interface, and understanding the interface structure and electronic structure is essential for device development. The work function, which is the focus of this study, has been determined and evaluated as one of the important parameters that describe the interface.

The work function is the minimum energy required to extract electrons from the Fermi level into the vacuum and is intrinsic to the material. Even the presence of trace amounts of adsorbed molecules on a metal surface can change the electronic structure of the interface and significantly affect the work function. For example, the work function of a thin film of polycrystalline gold is 4.4~4.7 eV when exposed to air, 5.0~5.1 eV when cleaned at the atomic level under ultrahigh vacuum, and the largest value of 5.3~5.4 eV for a thin film sputtered and vacuum deposited with argon gas or so. These findings can also be used to evaluate the charge transport capability of organic monolayers (SAMs), which is the subject of our research work.

In this study, we measured in detail the secondary electron cut-off region in the photoelectron spectrum using synchrotron radiation in order to determine the change in work function of organic monolayers on gold surfaces due to differences in molecular backbones. Among the electrons emitted from the sample surface by light irradiation, those that reach the vacuum level are detected as photoelectron spectra. The electrons with zero kinetic energy are detected in large quantities as secondary electrons at the rising edge of the spectrum, and this region is called the secondary electron cut-off (SECO). On the other hand, photoelectrons with the highest kinetic energy are detected on the high-energy side of the spectrum as photoelectrons originating from the Fermi level. The relationship between the Fermi level E_{Fermi}, the energy of the SECO E_{SECO}, the energy of incident light $h\nu$, and the work function ϕ is expressed as follows.

$$E_{Fermi} - E_{SECO} = h\nu - \phi \quad (1)$$

The Fermi level of each sample is coincident with that of a single molecule adsorbed on Au, so that the change in the work function ϕ appears in the spectrum as a change in E_{SECO}. In this study, we investigate the relative change of the work function by measuring the E_{SECO} region of photoelectrons in detail by X-ray irradiation.

The experiments were performed using X-ray photoelectron spectroscopy (XPS) measurements at the beamline BL-13 of HiSOR, Hiroshima University. The cut-off region with zero kinetic energy was precisely measured by applying a negative voltage (typically -10 V) to the sample and shifting the photoelectron spectrum toward the high energy side. The SAMs used are shown in Fig. 1: MP0, MP1, and M2P composed of conductive aromatic rings in their molecular chains. On the other hand, MHDA and HD are aliphatic-chain SAMs with high insulating properties, and HD was used as a reference sample with a known work function.

Fig. 2 shows the photoelectron spectrum in the secondary electron region measured for MHDA SAM under the conditions of this experiment. Since a sample bias of -10 V is applied, the SECO is detected around 7 eV. A detailed measurement of this cut-off region for each sample is shown in Fig. 3. It can be seen that the SECO position varies greatly from sample to sample. The E_{SECO} was determined by linearly approximating the slope of this SECO. The work functions 4.37 eV for MHDA, 4.90 eV for MP0, and 5.00 eV for M2P were determined based on the work function of HD, 4.32 eV [1]. The work function of the Au surface deposited on a Si substrate at a deposition rate of 1 Å/s under high-vacuum was also determined to be in the range of 4.8-5.1 eV, lower than the value of 5.2 eV for a polycrystalline (111) clean surface [2]. This indicates that the surface is contaminated by exposure to air after deposition and that a perfectly clean surface cannot be maintained even if cleaned just prior to measurement.

Compared to HD and MHDA with aliphatic chains, M2P and MP0 with aromatic chains have work functions about 0.5~0.7 eV higher. This may be due to the push back effect. In this model, the interfacial electric bilayer (δ^- and $^-\delta^+$) that originally exists on the metal surface is reduced by molecular adsorption, resulting in a decrease in the work function. Since aromatic-chain SAMs have delocalized π-electrons in the ring, when they are adsorbed on the substrate, electrons in organic molecules are added to the δ^- side of the metal surface, and the apparent decrease in δ^- is considered to be smaller than that of aliphatic-chain SAMs. Therefore, the polarization of aromatic-chain SAMs is expected to be larger than that of aliphatic-chain SAMs, and the work function is also expected to be larger than that of aliphatic-chain SAMs.

REFERENCES

1. O. M. Cabarcos, S. Schuster, I. Hehn, P. P. Zhang, M. M. Maitani , N. Sullivan, J.-B. Giguère, J.-F. Morin, P. S. Weiss, E. Zojer, M. Zharnikov, and D. L. Allara, *J. Phys. Chem. C* **121**, 15815 (2017).
2. G. N. Derry et al., *J. Vac. Sci. Technol. A* **33**, 060801 (2015).

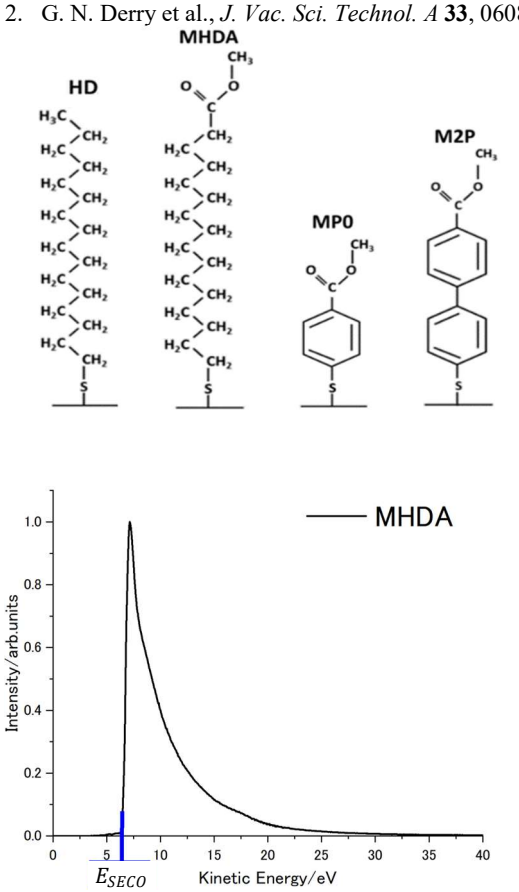

FIGURE 1. Self-assembled monolayers used in this experiment.

FIGURE 2. Photoelectron spectrum in the secondary electron region measured for MHDA SAM

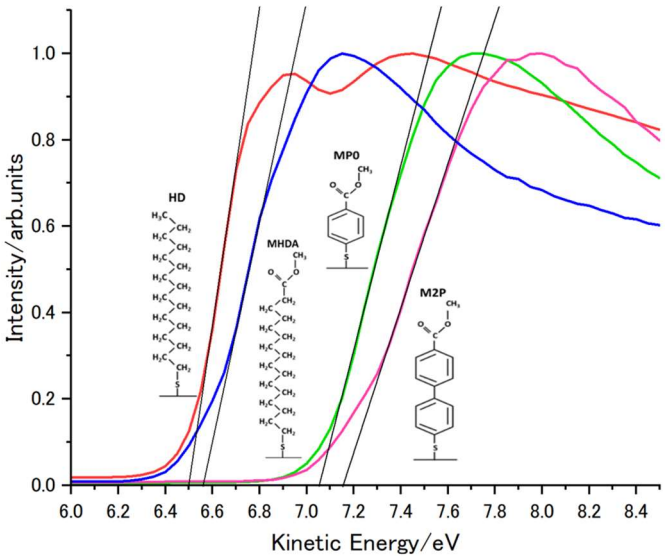

FIGURE 3. Photoelectron spectrum in the secondary electron cut-off (SECO) region measured for aliphatic and aromatic SAMs.

22BG008 BL-14

XMCD study of magnetic thin-films of FeMn alloys grown on h-BN/Ni(111)

Wataru Nishizawa[a] and Masahiro Sawada[b]

[a]*Graduate School of Science, Hiroshima University*
[b]*Hiroshima Synchrotron Radiation Center, Hiroshima University*

Keywords: XMCD, ultrathin films, hexagonal boron nitride, FeMn alloys

Magnetic tunneling junction (MTJ) structures, where ferromagnetic electrode layers sandwich an insulating barrier layer, show tunnel magnetic resistance (TMR) effect that is widely applied for spintronics devices such as magnetic random-access memory. One of important performance factors of TMR element is magnetic resistance (MR) ratio, which is sensitive to both of interfacial structure and magnetic state. Conventionally, metal oxide layers have been utilized for the barrier layer in the device structures. However, further improvement of MR ratio is difficult in MTJ with such oxide-based barriers, because of crystal disorder arises from lattice mismatch and defect formation at the interface. In recent years, much attention and intensive studies have been devoted to hexagonal boron nitride (h-BN) whose structure is two-dimensional honeycomb formed by stable chemical bonding. Monolayer h-BN is one of good candidates for the ideal burrier layer of TMR devices because the h-BN layer is expected to form a pinhole-less and flat interface with magnetic layers. Recently, in Fe or Co layers grown on the monolayer h-BN uniformly established on a single crystal substrate of Ni(111), anti-ferromagnetic coupling has been found between the overlayer and Ni substrate. An effect of electron filling control in the 3d valence band of the overlayer is of great interest, to investigate the origin of unexpected magnetic coupling through the h-BN monolayer.

In this study, we have investigated interlayer magnetic coupling between the FeMn films and the Ni substrate by means of XMCD spectroscopy at $L_{2,3}$ absorption edges of Fe, Mn and Ni. Ultrathin films of FeMn alloys were fabricated on h-BN/Ni(111) in ultra-high vacuum condition, whose XMCD spectra were measured *in-situ*. In Fig.1(a) and (b), XAS spectra for $Fe_{84}Mn_{16}$/h-BN/Ni(11) are shown at Ni and Fe $L_{2,3}$ edge, respectively. The red (blue) curves are corresponding to excitation light with helicity parallel(antiparallel) to external magnetic field of 1.1 T along to the sample normal direction. XMCD signals of Ni and Fe are opposite each other at both L_2 and L_3 edge. That means anti-ferromagnetic coupling through h-BN monolayer. Overlayer thickness dependence of XMCD for the $Fe_{84}Mn_{16}$/h-BN/Ni(111) sample (shown in Fig.1(c)) indicates gradual change of magnetization direction from antiparallel into parallel to the applied magnetic field, with the thickness increasing. The critical thickness where the sign of XMCD recovers into positive, includes information on energetic stability of interlayer magnetic coupling. The concentration dependence of the critical thickness has also been found in our series of XMCD experiments for the alloy films with different concentration of Fe and Mn.

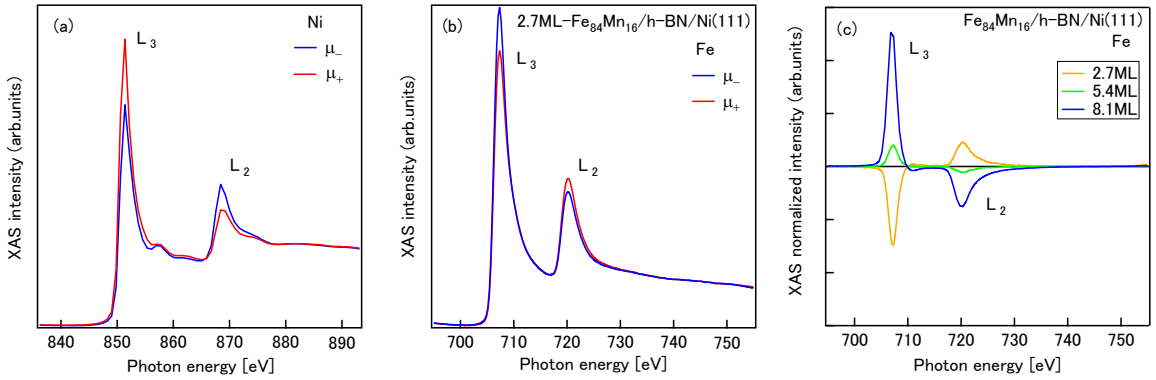

FIGURE 1. XAS spectra for (a) Ni substrate and (b) Fe atomic site in the FeMn alloy layer whose concentration of Fe is 84%. (c) Thickness dependence of the XMCD signals ($\mu_+ - \mu_-$) of Fe in the FeMn film on h-BN/Ni(111).

Design Study on HiSOR-II

Y. Lu[a], M. Shimada[c,a] , H. Miyauchi[c,a], and M. Katoh[a,b]

[a]*Hiroshima Synchrotron Radiation Center, Hiroshima University, Higashi-Hiroshima, Hiroshima 739-0046, Japan*
[b]*Institute for Molecular Science, Okazaki, Aichi 444-8585, Japan*
[c]*High Energy Accelerator Research Organization, Tsukuba, Ibaraki 305-0801, Japan*

Keywords: Accelerator lattice design, beam injection, Top-up operation

HiSOR is a compact racetrack-type light source in Hiroshima university, which has been operated stably from 1996 [1]. Although the energy is 700 MeV, HiSOR can provide synchrotron radiation from vacuum ultraviolet (VUV) to soft X-ray, which is due to the strong magnetic field (2.7 T) of the bending magnets. On the other hand, the brilliance is limited because of the large emittance, which is owning to the simple lattice configuration with two 18 degree bending magnets. To satisfy the demands of users for high brilliance undulator radiation, a new storage ring HiSOR-II is being designed.

Currently, two accelerator lattice designs shown in Figure 1 are under consideration. The parameters of two designs are summarized in Table 1. The emittance are both around 10 nm, and the brilliance of the synchrotron radiation can reach to 1×10^{17} ph/sec/mm^2/mrad^2/0.1%b.w which is 100 times higher than that of the present HiSOR. The first lattice (Design A) is compact and has a relatively small number of magnet elements. Therefore, a combined function magnet is required in this design for a chromaticity compensation. As for the second lattice (Design B), it is a double-bend achromat (DBA) lattice modified from the optics of ASTRID2 [2, 3]. Although the circumference is larger and the number of magnet elements is more than that of Design A, Design B is more general and has a better performance.

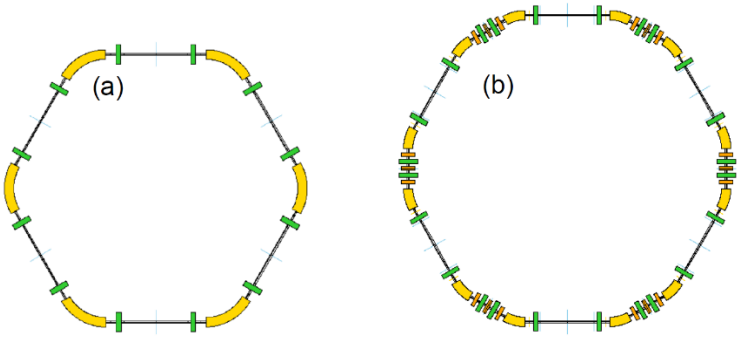

FIGURE 1. Schematic view of the magnet layout (a) Design A and (b) Design B.

TABLE 1. Storage ring parameters

	Design A	**Design B**
Energy [GeV]	0.5	
Circumference [m]	31.38	40.78
Emittance [nm]	17.43	8.92
Beam current [mA]	300	
RF frequency [MHz]	191	
Tunes: ν_x, ν_y	2.75/2.46	5.12/1.67
Number of undulators	4	

In this study, the dynamic Aperture (DA) survey and beam injection simulation are also performed. We have shown that the DA is relatively wide with simple sextupole correction scheme. For the beam injection, there are two schemes, pulsed multipole magnet injection [4, 5] and bump injection. A pulsed sextupole magnet can be installed in the Design A-ring, which injects the beam successfully by a three-turn kick. The

beam injection only needs one magnet and can save space for the injection system. For Design B, a bump orbit can be adjusted freely by three dipole kickers. The possibility of a pulsed multipole injection will be surveyed by a tune adjustment in the future.

A top-up operation is preferred for users' experiments. Therefore, a booster ring is necessary for a full energy beam injection. Figure 2 shows a one accelerator layout of HiSOR-II based on the building of the facility. A new experimental hall and Beam Transport (BT) line are needed for the main ring.

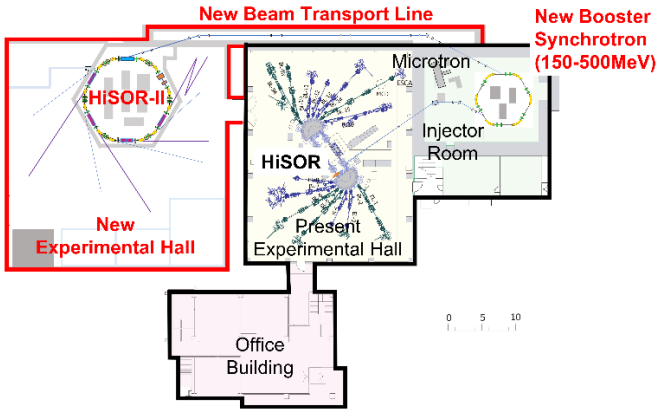

FIGURE 2. One accelerator layout of HiSOR-II.

REFERENCES

1. K. Yoshida, *et al*., *J. Synch. Rad*. vol. 5, pp. 345-347 (1998).
2. S.P. Møller, *et al*, in *Proc. 1st Int. Particle Accelerator Conf. (IPAC'10)*, Kyoto, Japan, May 2010, pp. 2489-2487.
3. S. Matsuba, *et al*, in *Proc. 10th Int. Particle Accelerator Conf. (IPAC'19)*, Melbourne, Australia, May 2019, pp. 200-202.
4. H. Takaki, *et al*, Phys. Rev. ST Accel. Beams 13, 020705 (2010).
5. C. Mitsuda, *et al*, Phys. Rev. ST Accel. Beams 25, 112401 (2022)

The order of flash poster session

Thursday, 9 March, 2023　13:40 - 14:40

The flash talk is about 2 min/person.

Order	Poster no.	Name	Poster title
1	P02S	A. Krishnadas	Evolution of Electronic States in Epitaxial YBCO Thin Films with Calcium Doping by AngleResolved Photoemission Spectroscopy
2	P03S	Y. Miyai	Symmetry reduction in the electronic structure of heavily overdoped Pb-Bi2201 detected by ARPES
3	P05S	Y. Tsubota	Re-examination of the phase diagram of the high-Tc cuprate superconductor $Bi_2Sr_2CaCu_2O_{8+\delta}$ studied by ARPES
4	P06S	Y. Kumar	Exploration of Novel Topological Semimetal and Evolution of the Electronic Structure Using High-Resolution ARPES
5	P07S	K. Ishiba	Development of ARPES analysis method using Bayesian Inference and application to cuprates
6	P08S	Y. Onishi	Momentum dependence of the spectral weight in the single layer high-T_c cuprate $Bi_2Sr_2CuO_{6+\delta}$ studied by ARPES
7	P14S	Y. Higuchi	Investigating the possibility of creating a "pure" p-type Bi_2Se_3
8	P15S	Y. Tanimoto	Observation of electron structure of chiral magnet $Yb(Ni_{1-x}Cu_x)_3Al_9$ by ARPES
9	P18S	K. Kunitomo	Investigation of Perpendicular Anisotropy in FeCo Alloy Films Covered with Oxygen for Development of Multi Spin Detecting Target
10	P20S	Y. Ma	First results of phase transformation from vaterite to calcite observed by Ca K-edge XAFS and XRD.
11	P21S	C. Sugahara	Hydration Structure of Acetone Studied with Concentration-Dependent Absorption Spectra in the Ultraviolet Region
12	P22S	S. Hashimoto	Dynamic Observation of Interaction Process between β-Lactoglobulin and Membrane by Time-Resolved Vacuum-Ultraviolet Circular Dichroism
13	P24S	R. Tsuji	Interaction Mechanism between the Antimicrobial Peptide Magainin2 and Lipid Membrane Revealed by Synchrotron-Radiation Circular- and Linear-Dichroism Spectroscopy
14	P25S	R. Imaura	Membrane-bound conformation of the non-amyloid-β component of α-synuclein characterized by vacuumultraviolet circular dichroism and molecular-dynamics simulation
15	P28S	W. Nishizawa	XMCD study of magnetic thin-films of FeMn alloys grown on h-BN/Ni(111)